

A HIGH THROUGHPUT PARYLENE MICROCHANNEL COULTER COUNTER FOR
CELL SIZING AND CELL COUNTING APPLICATIONS

A THESIS SUBMITTED TO
THE GRADUATE SCHOOL OF NATURAL AND APPLIED SCIENCES
OF
MIDDLE EAST TECHNICAL UNIVERSITY

BY

ÖZGEN SÜMER LAÇIN

IN PARTIAL FULFILLMENT OF THE REQUIREMENTS
FOR
THE DEGREE OF MASTER OF SCIENCE
IN
ELECTRICAL AND ELECTRONICS ENGINEERING

AUGUST 2014

Approval of the thesis:

**A HIGH THROUGHPUT PARYLENE MICROCHANNEL COULTER
COUNTER FOR CELL SIZING AND CELL COUNTING APPLICATIONS**

submitted by **ÖZGEN SÜMER LAÇIN** in partial fulfillment of the requirements for
the degree of **Master of Science in Electrical and Electronics Engineering**
Department, Middle East Technical University by,

Prof. Dr. Canan Özgen
Dean, Graduate School of **Natural and Applied Sciences**

Prof. Dr. Gönül Turhan Sayan
Head of Department, **Electrical and Electronics Engineering**

Assoc. Prof. Dr. Haluk Külâh
Supervisor, **Electrical and Electronics Eng. Dept., METU**

Examining Committee Members:

Prof. Dr. Nevzat Güneri Gençer
Electrical and Electronics Engineering Dept., METU

Assoc. Prof. Dr. Haluk Külâh
Electrical and Electronics Engineering Dept., METU

Assoc Prof. Dr. Yeşim Serinağaoğlu
Electrical and Electronics Engineering Dept., METU

Dr. Fatih Koçer
Electrical and Electronics Engineering Dept., METU

Dr. Ebru Özgür
METU MEMS Research and Application Center, METU

Date: **05.08.2014**

I hereby declare that all information in this document has been obtained and presented in accordance with academic rules and ethical conduct. I also declare that, as required by these rules and conduct, I have fully cited and referenced all material and results that are not original to this work.

Name, Lastname: Özgen Sümer LAÇIN

Signature:

ABSTRACT

A HIGH THROUGHPUT PARYLENE MICROCHANNEL COULTER COUNTER FOR CELL SIZING AND CELL COUNTING APPLICATIONS

Laçın, Özgen Sümer

M.Sc., Department of Electrical and Electronics Engineering

Supervisor: Assoc. Prof. Dr. Haluk Kulah

August 2014, 111 pages

In medical research, cell counting is of a great importance for the indication of the health status of the patients, diagnosis of the illness, and the detection of the progress of a disease. In clinics, cell counting and sorting is carried out by Coulter Counter devices, in which the electrical potential or resistance change is measured when the cells flow through the defined aperture. Coulter Counter devices perform rapid and accurate analysis of the biological particles in terms of their size and dielectric properties. However, traditional Coulter Counters are bulky and expensive requiring large sample volume. Therefore, miniaturizing this device, utilizing micro-electromechanical systems (MEMS) technology, simply reduces the cost and provides rapid analysis and ease of use.

In this study, two different MEMS-based Coulter Counter designs, employing single and double channels, were developed. The novel double channel Coulter Counter design allows the detection of the particles simultaneously by forming sub-channels inside a main channel, increasing the throughput and obviating the need for hydrodynamic focusing of the particles. Two different electrode geometries,

coplanar surface Au electrodes and 3D Cu-electroplated electrodes, were employed in the same microchannel, to compare the sensitivities and allow double counting in a single channel. Before fabricating each of these designs, simulations regarding the surface velocity field, electrical field change, and electrical resistance change were accomplished in COMSOL Multiphysics 4.3b. It was observed that designed channels do not face a turbulent flow or clogging problem at the detection points, where channels narrow down. Flow is stable and accurate. Electric field (E-field) simulations proved that when there is no particle in the sensing zone, E-field has the highest value; while when the particle starts to enter the sensing zone, this value decreases gradually and reaches to its minimum when the particle is at the center of the sensing zone or aperture. The existence of a particle in the sensing zone removes the amount of liquid in proportion to the volume of the particle; hence, decreases the area of the aperture. This leads to an increase in the electrical resistance. After getting satisfactory results from the simulations, both of the designs were fabricated. A four-mask fabrication protocol, including the electrode lithography, Cu-electroplating and channel lithography, was developed for the fabrication. Channels were formed of Parylene C, a biocompatible polymer, possessing excellent properties of the chemical resistance for biological analysis, and have long shelf life. Focusing of the particles is achieved by adjusting the channel dimensions relative to the particle diameter; hence, the additional inlet requirement for hydrodynamic focusing is eliminated. For our case, we aimed to sense polystyrene microbeads (10 μm) and K562 leukemia cancer cells (13-22 μm); therefore, a channel having a diameter of approximately 30 μm is adequate for sensing and counting. The excitation voltage (5 V_{pp} AC) and the frequency (55 kHz) were adjusted to prevent Electrical Double Layer (EDL) and electrode degeneration. A custom-made electrical detection circuit was built to filter out undesired frequencies and detect the passage of the particles. All results were recorded with a Data Acquisition Board (National Instruments 6337) and illustrated with LabVIEW SignalExpress software. An algorithm for counting the number of negative peaks was developed on MATLAB R2013b. A flow rate of 1 $\mu\text{l}/\text{min}$ was introduced to the main channel and this rate increased up to 7.5 $\mu\text{l}/\text{min}$ in single channel design and 4.5 $\mu\text{l}/\text{min}$ in double channel design. 10 μm polystyrene microbeads and 17 μm K562 cancer cells were

counted separately and in mixture, with different flow rates and frequencies. It was proven that both of the designs are capable of counting the particles larger than 10 μ m with a flow rate of maximum 75 μ l/min.

In conclusion, two different Coulter Counters were developed. Satisfactory results were obtained from both simulations and experiments. Different flow rates and frequencies were employed to investigate flow rate profile and electrical double layer effect on the measurements. Both of the devices sensed and counted the microparticles introduced in a conductive medium. With further improvements, granular analysis of the cell, in addition to the size based detection, and reaching faster detection rate are the ultimate goals of this study.

Keywords: High throughput parylene microchannel, Coulter Counter, cell counting, cell sizing, 3D and coplanar electrodes.

ÖZ

HÜCRE SINIFLANDIRMA VE SAYMA UYGULAMALARI İÇİN YÜKSEK VERİMLİ PARİLEN KANALLI COULTER SAYACI

Laçın, Özgen Sümer

Yüksek Lisans, Elektrik ve Elektronik Mühendisliği Bölümü

Tez Yöneticisi: Doç.Dr. Haluk Külah

Ağustos 2014, 111 sayfa

Medikal arařtırmalarda hücre ve parçacık sayımının önemi büyüktür çünkü kandaki hücre sayısı bir hastalığın teşhisinde, hastanın sağlık durumunun belirlenmesinde veya varolan bir hastalığın ilerlemesini gözlemlemekte kullanılabilir. Hücreler gözenekten geçişleri sırasında boyutlarıyla doğru orantılı olarak bir değişim meydana getirirler ve bu sayede sınıflandırılabilirler. Coulter sayaçları, hücrelerin sayımı ve sınıflandırılmasında hızlı ve güvenilir sonuçlar sağlamasına rağmen pahalı ve büyük boyutlarda olan cihazlardır. Bunun yanı sıra sayma işlemlerini gerçekleştirebilmek için 7ml civarında numuneye ihtiyaç duyarlar, ki bu miktar laboratuvar ortamı dışarısında elde edilmesi güç olan bir miktardır. Bu yüzden tezgah üstü Coulter Sayaçlarının küçültülmesine ihtiyaç vardır. Mikro elektromekanik sistemler (MEMS) teknolojisi sayesinde Coulter sayaçları bir çip boyutuna indirgenip, çok sayıda üretilebilir. Bu teknik sayesinde ucuzlayan cihazlar, kırsal yörelerdeki bir çok insanın da hizmetine sunularak yaşam kalitesini arttırabilir. Ayrıca küçülen cihaz boyutları sayesinde çok daha az bir örnek ile istenilen sayma işlemi de gerçekleştirilebilir. Literatürde MEMS tabanlı bir çok Coulter Sayacı bulunmaktadır. Fakat bu cihazların bir çoğu, az miktardaki numuneyi uzun sürede işleyerek, süreci uzatmakta ve böylece pratiklikten uzaklaşmaktadır.

Bu çalışmada MEMS tabanlı tek ve çift kanallı Coulter Sayaçları tasarlanmıştır. Her iki tasarımda da geniş başlayan kanal yapısı parçacık boyutuyla orantılı olacak şekilde daraltılmış böylece, parçacığın gözenekten geçisi sırasındaki algı kuvvetinin arttırılması amaçlanmıştır. Çift kanallı tasarımda ana kanal, silindirik bir yapı sayesinde ikiye bölünmüş ve akışın her iki dar kanala eşit olarak dağılması sağlanmıştır. Bu sayede, bir cihaz içerisinde iki tane birbirinden bağımsız cihaz yaratılmış ve tek kanallı sayaçlara göre daha hızlı analizler yapılmasına izin verilmiştir. Kanal genişliğinin ve derinliğinin parçacık boyutuyla orantılı olarak ayarlanması sonucunda, akış istikrarlı bir yol izlemiş ve fazladan giriş ağızlarına ihtiyaç duyulmadan hidrodinamik odaklanma sağlanmıştır. Yapılan tasarımların simülasyonları COMSOL yazılımı yardımıyla yapılmıştır. Bu simülasyonlar cihazların üretiminden önce herhangi bir sorunla karşılaşılıp karşılaşılmayacağını göstermenin yanında teorik sonuçlar hakkında da değerli bilgiler vermiştir. Başlıca yapılan simülasyonlar arasında, yüzey akış profili, elektrik alan ve elektrik direnç değişimini gösteren simülasyonlar yer almaktadır. Bu simülasyonlar sonucunda elektrik alanın parçacık gözenekteyken en düşük değere elektriksel direnç değerinin ise en yüksek değere ulaştığı gözlemlenmiştir. Beklenen değerlerin elde edilmesi üzerine, cihazlar 100 ve 1000 sınıfına sahip olan temiz alan ortamında üretilmiştir. Kanal yapıları, biyouyumlu bir polimer olan Parilen C maddesi yardımıyla oluşturulmuştur. Kanalların farklı yerlerine yerleştirilen üç boyutlu bakır ve düzlemdeş altın elektrotlar sayesinde, parçacıkların geçişi algılanmış ve sayımı yapılmıştır. Deneyler sırasında 10 mikron boyutunda polisitiren ham kauçuk parçacıklarlar, ve ortalama çapı 17 mikron olan K562 kan kanser (lösemi) hücreleri kullanılmıştır. Bu parçacıkların gözenekten geçisini algılayabilmek için bir elektrik devresi kurulmuş ve istenmeyen sinyaller bu devre sayesinde filtrelenmiş ve oluşan anlık değişim tespit edilmiştir. Tespit edilen bu değişimin sayımı ise başka bir yazılım olan MATLAB yardımıyla yapılmıştır. Yapılan testler sonucunda her iki tasarımın da farklı frekanslarda, farklı akış hızlarında çalıştığı gözlemlenmiş ve iki farklı parçacığı başarıyla tespit ettiği kanıtlanmıştır. Ayrıca sıvı içerisine degen elektrotlar üzerinde düşük frekanslarda iyonların birikmesiyle meydana gelen iki katmanlı elektrik yüzeyin de tasarlanan cihazları etkilemediği, 20 kHz düzeyindeki frekanslarla yapılan testlerde gösterilmiştir. Ölçümler genellikle 5V alternatif akım

potansiyeli ve 55 kHz sabit frekans kullanarak yapılmıştır. Yapılan tüm sonuçlar bilgi toplama kartıyla kaydedilip, LabVIEW yazılımıyla ekranda gözlemlenmiştir. Gözlenen bilgiler bu ortamdan alınıp MATLAB a aktarılmıştır ve parçacık sayımı yapılmıştır. Yapılan deneyler sonucunda, her iki cihazın da yüksek frekanslarda gürültüye mağruz kaldığı ve 75 μ l/dk dan yüksek hızlarda akış profilinin bozulduğu gözlemlenmiştir.

Sonuç olarak, grubumuz tarafından tasarlanan her iki cihazın da tatmin edici sonuçlar verdiği gözlemlenmiştir. Farklı akış hızları, farklı frekans aralıkları ve farklı boyuttaki parçacıkların sayımı gerçekleştirilmiş ve tüm bu senaryolardan olumlu sonuçlar alınmıştır. Kullanılan frekans aralığı gereği tüm ölçümler parçacıkların hacmi ile doğru orantılı sonuçlar vermiştir. İleride yapılacak çalışmalar için, çalışılan frekans artırılarak, parçacıkların ya da hücrelerin içsel yapısı hakkında da bilgi alınabilip, daha detaylı çalışmalar yapılabilir. Cihazların her ikisinde de görülen hava kabarcığı problemi ise, kanal içerisine T şeklinde engeller koymak yerine daha oval ya da Y şeklinde engeller konularak ortadan kaldırılabilir. Tüm bunlar yapıldığı takdirde, üretilecek Coulter Sayacı daha verimli çalışıp, detaylı sonuçlar sağlayabilir.

Anahtar Kelimeler: Yüksek verimli Coulter Sayacı, hücre sayımı, üç boyutlu ve düzlemdeş elektrotlar, parilen kanal yapısı

*To my parents Fakiye and Kenan LAÇIN and,
my precious sister Bilge Işık LAÇIN*

ACKNOWLEDGEMENTS

This study would not be completed without the help and support of people who were next to me throughout my master's study. First, I would like to thank my thesis supervisor Assoc. Prof. Dr. Haluk Klah for his endless support and guidance. He was always understanding to me and my future plans. Without his guidance, this work would not be completed in a short time.

I would like to thank Prof. Dr. Tayfun Akın since he founded the METU MEMS center and introduced MEMS technology to Turkey. By using this center, we are capable of fabricating state of the art devices. Many thanks to Dr. zge Zorlu for his support all the time. He was always there whenever I needed help. From fabrication steps to experimental tests he shared his invaluable knowledge with me. Without his help I could not achieve results quickly. I would also like to give my special thanks to Dr. Ebru zgr for her friendship and help throughout this study. She helped me to prepare the sample solutions and read the entire thesis. I want to thank Mr. Orhan Akar for fabricating the masks for my devices and sharing his micro fabrication knowledge with me.

I am thankful to The Scientific and Technological Research Council of Turkey (TUBITAK) for supporting this project.

I would like to thank Yağmur Demircan for her friendship and support during all the steps in this study. She shared all of her knowledge from simulation steps to test set up. I am honored to share the same working environment with BioMEMS and PowerMEMS group. I am especially so appreciated to know Hasan Uluşan, Mustafa Kangl and Salar Chamanian throughout my years in Ankara. They were much more than friends to me and never spared their help and support when needed I also would like to thank Taylan Tral for teaching me the fabrication. Many thanks to our former members Dr. Hatice Ceylan Koydemir and Levent Beker for their friendship and support. I also would like to thank Garsha Bahrieh, Grhan zkayar,

Kaveh Gherabaghi, Aziz Koyuncuođlu, Ahmet Erdal Yılmaz for creating a nice atmosphere in lab environment.

In my view friends are the family therefore I would like to give my special thanks to my closest friends, Erker Eser, Özlem Tonguç, Louma Chaddad, Sinan Tanyeri, Ersin Kılıçkap, and Ufuk Tanrıverdi for their invaluable friendship for so long. They were like a family to me. I also would like to thank my dearest relatives and cousins, Pelin Laçın, Gökmen Güven, Göksun Güven. Without them, my life in Ankara would not be bearable.

Finally, I would like to express my deepest gratitude to my parents Fakiye and Kenan Laçın and my precious sister Bilge Işık Laçın. The love I feel for them cannot be expressed with words. Without their existence, I could not achieve any of these successes I had in my entire life. They are the reason of the smile in my face.

TABLE OF CONTENTS

ABSTRACT	v
ÖZ	ix
ACKNOWLEDGEMENTS	xiv
TABLE OF CONTENTS	xvii
LIST OF TABLES	xix
LIST OF FIGURES.....	xx
CHAPTERS	
1. INTRODUCTION.....	1
1.1. Particle detection methods.....	1
1.2. Motivation	3
1.3. Implication.....	4
1.4. Goals.....	5
1.5. Overview	5
2. THEORY AND LITERATURE REVIEW	7
2.1 Resistive Pulse Method	7
2.1.1 Mathematical Model	10
2.1.2 Coincidence Theory	12
2.2 Literature Review	14
2.2.1 Optical Detection Methods	15
2.2.2 Acoustic Detection Methods	19
2.2.3 Electrical Detection Methods	19
3. ELECTRICAL MODELING AND SIGNAL PROCESSING OF COULTER COUNTERS.....	41
3.1 Device Description.....	41
3.2 Microparticle and channel resistance modeling.....	43
3.3 Signal Detection	44
4. DESIGN AND SIMULATION.....	51
4.1 Design of the Single Channel Coulter Counter	51
4.2 COMSOL Simulation Results.....	55

4.2.1	Flow profile and particle tracing simulations.....	55
4.2.2	Electric Field and Current Density Simulations.....	59
4.2.3	Resistance Change Simulations	63
5.	FABRICATION	67
5.1	Process Flow	67
5.2	Problems related to fabrication	72
6.	RESULTS AND DISCUSSION	75
6.1	Conductive medium and cell preparation.....	76
6.2	Experimental Setup	76
6.3	Signal Processing and Peak Detection	78
6.4	Results	79
6.4.1.	Counting of Polystyrene Microbeads	79
6.4.2.	Counting of K562 Cancer Cells	83
6.4.3.	Effect of Frequency change on particle counting.....	86
6.4.4.	Mixture of polystyrene and K562 cancer cell counting	87
6.4.5.	Testing Different Concentrations	87
6.4.6.	Comparing electroplated and coplanar electrodes	90
6.5	Conclusion.....	92
7.	CONCLUSION AND FUTURE WORK.....	95
	REFERENCES.....	99
	APPENDICES	
A.	FABRICATION FLOW OF THE COULTER COUNTER DEVICES.....	107
B.	MATLAB CODE FOR COUNTING THE NEGATIVE PEAKS.....	111

LIST OF TABLES

TABLES

Table 4.1: Design parameters for single channel Coulter Counter	52
Table 4.2: Design parameters for double channel Coulter Counter.....	54
Table 4.3: Design parameters for particle tracing simulations	56
Table 6.1: Cancer cell expected vs sensed count with different flow rates.	85
Table 6.2: Comparison of our device with other devices in literature	93
Table A.1: Process Flow	107

LIST OF FIGURES

FIGURES

- Figure 1.1: (a) Schematic of the original Coulter Counter patented in 1953. Two chambers are separated by an orifice. Particles suspended in the liquid pass from one chamber into another through the orifice by hydrodynamic pressure. The change in the resistance of the fluid is measured by a readout circuit. The setup includes an agitator to keep the particles suspended and a scale to measure the change in the volume [3], [4], [9]..... 2
- Figure 2.1: Schematic of the Coulter Counter..... 8
- Figure 2.2 (a) Demonstration of a change in the ionic current. (b) A particle with a negligible surface charge, reducing the number of free ions inside the microchannel; hence decreasing the ionic current. (c) A charged particle inducing the free ions inside the micro channel thus increasing the ionic current [11]..... 9
- Figure 2.3: Schematic of an aperture with length L and diameter D when a particle with a diameter d is passing through it [4]. 10
- Figure 2.4: Graphical illustration of particle coincidence. (a) Only one particle exists in the pore and voltage output just shows one valley (negative peak). (b) Two particles occupying the detection zone however voltage output still shows one valley. (c) While one of the particles is exiting the detection area the other one in behind enters it therefore the voltage output shows shoulder and indicates the existence of the second particle. Particle one has a smaller amplitude since it is exiting the detection zone [12]. 13
- Figure 2.5: (a) Picture of the commercial hemocytometer. (b) Magnified view of the grid lines placed, in the middle of the device [20], [21]. 14
- Figure 2.6: Schematic of a commercial flow cytometer device [24]. 16
- Figure 2.7: Three main parts of the Flow Cytometers: Fluidic systems to transport the particles, optical system to illuminate the particles and filters to guiding the resulting signal to detectors and electronics to process and sort the incoming signals by specialized software algorithms [22], [25]..... 16
- Figure 2.8: Experimental set up of the optical interferometer [27]..... 18
- Figure 2.9: First microfabricated Coulter Counter. Non-conducting sheath fluids confine the electrolyte inlet with the sample inlet. Particles are designed to be detected in the orifice by Au electrodes [47]. 23

Figure 2.10: Saleh and Sohn's Coulter Counter with a rectangular pore and sputtered Ti /Pt electrodes. The device can detect nanoscale latex colloids as small as 87nm [15].....	24
Figure 2.11: Design of the α -hemolysin channel to detect single RNA and DNA molecules. A U-shaped tubing connects two reservoirs, and aperture is placed inside on the right tubing. Ag-AgCl electrodes are used for sensing [53].	26
Figure 2.12: (a) The hydrodynamic focusing illustration. Horizontal control ports confine the sample stream to the center of the channel and the sheath inlet is used to direct the fluid. 2D focusing is achieved by this technique. (b) Measurement set up [55].....	27
Figure 2.13: Schematic of the Coulter Counter and 2D liquid aperture method. Top, side and 3D view of the device are presented to express 2D hydrodynamic focusing phenomenon. Drawings are not in scale [57].....	28
Figure 2.14: (a) Diagram of the three flow cytometer device. Dark gray and light gray regions indicate the thin and tall regions respectively. (b) 2D focusing of the first device. (c) 2D focusing of the second device with tall outlet channel. (c) 3D focusing of the third device by the help of the stepped outlet channel [59].	29
Figure 2.15: Top figure shows the electrical components demonstrating the channel, and double layer impedances with stray capacitance. System impedance is equal to the series combination of channel impedance, double layer impedance and the stray capacitance value. Bottom figure is the electrical equivalent model where the double layer impedance is replaced with constant phase element ZCPE [32].....	32
Figure 2.16: Diagram of microelectrodes with different geometries. (a) Sputtered electrodes on the bottom surface of the channel. (b) Side wall electrodes sputtered on silicon wet etched channel. (c) Side wall electroplated electrodes [70].	35
Figure 2.17: Coulter Counter with double sensing zones at the inlet and outlet of the device [65].....	37
Figure 2.18: Four channel Coulter Counter. Minichannels are divided by polymer microapertures and detection is performed by Ag/AgCl electrodes placed on both sides of the membrane [11].	39
Figure 2.19: Four channel Coulter Counter developed by Jagtiani. Both DC and AC signals are employed to detect the signals. Signal multiplexing technique was used to eliminate the extra need for DAQ boards [75].....	40
Figure 3.1: (a) Cross-sectional and (b) top view schematics of the single channel Coulter Counter, together with the detection circuit.....	43
Figure 3.2: Electrical cell modeling of a biological cell and conductive medium Membrane of the cell and electrolytic medium is modeled as the parallel combination of resistor and capacitor whereas cytoplasm is modeled as an impedance[78].....	45

Figure 3.3: Electrical model of a suspending medium and electrode / electrolyte interface during the passage of a particle [44] When the particle is at the sensing zone, electrical resistance is equivalent to the parallel combination of the resistance of the particle and the solution. Double layer is modeled as a capacitor in series with electrode resistance. 46

Figure 3.4: Change in the output voltage relative to the change in sensing resistor 48

Figure 3.5: Channel resistance changes during the passage of the particle and this change is recorded on the sensing resistance. 47

Figure 4.1: (a) Technical drawing of single channel Coulter Counter. (b) Closer view of the narrow channel. (c) Magnified view of the electroplated copper electrodes. (d) Magnified view of the sputtered gold electrode pair. 52

Figure 4.2. (a) Technical drawing of double channel Coulter Counter. (b) Closer view of the sub channels and cylindrical parylene obstacle. (c) Magnified view of the electroplated copper electrodes. (d) Magnified view of the sputtered gold electrode pair. 54

Figure 4.3: COMSOL boundary setting window in Incompressible Navier-Stokes module. 58

Figure 4.4: (a) Surface velocity field of the single channel Coulter Counter. (b) Magnified view of the narrower region. Velocity of the flow increases ten times when the channel width decreases from 300 μm to 40 μm 58

Figure 4.5: (a) Surface velocity field of the double channel Coulter Counter. (b) Magnified view of the narrower region. Velocity of the flow increases five times in each sub-channel when the channel width decreases from 300 μm to 40 μm 59

Figure 4.6: Dashed red box shows how to define an AC voltage in COMSOL Multiphysics 4.3b. A, w, and t represent the amplitude (V), angular frequency (rad/s) and time (s), respectively. 61

Figure 4.7: Defining the time stepping in COMSOL Multiphysics 4.3b. One period of the signal was investigated in five parts. 62

Figure 4.8: Surface electric field and current density simulations of coplanar electrodes in Coulter Counters. (a) No particle inside the detection zone. (b) Particle is at the edge of the excitation electrode. (c) Particle is on the excitation electrode. (d) Particle is at the center of the sensing zone. 63

Figure 4.9: Surface electric field and current density simulations of electroplated Cu electrodes (sidewall electrodes) in Coulter Counters. (a) No particle inside the detection zone. (b) Particle is approaching the detection zone. (c) Particle is entering the detection zone from excitation electrode side. (d) Particle is at the center of the sensing zone. 64

Figure 4.10: Electrical resistance simulations of coplanar electrodes in Coulter Counters. (a) Particle is at the edge of the excitation electrode. (b) Half of the particle is at the sensing zone. (c) Particle is at the center of the sensing zone. (d) No particle in the sensing zone.	65
Figure 4.11: Electrical resistance simulations of 3D electrodes in Coulter Counters. (a) Particle is at the edge of the excitation electrode. (b) Particle is at the center of the sensing zone. (c) Particle is at the edge of the excitation electrode. (d) No particle in the sensing zone.	66
Figure 5.1: Process flow of single and double channel Coulter Counters	68
Figure 5.2: 1st mask for generating coplanar electrodes, electrical connections, and seed layer for electroplating step. (a) Double channel (b) Single channel metal mask	69
Figure 5.3: 2nd mask for creating openings for electroplating step. Each square represents a dummy opening to provide a uniform growing.	70
Figure 5.4: Electroplated 3D copper electrodes.	71
Figure 5.5: 3rd mask-Channel mask for (a) Double Channel Coulter Counter (b) Single Channel Coulter Counter	72
Figure 5.6: 4th mask- Opening mask for (a) Double Channel Coulter Counter (b) Single Channel Coulter Counter	73
Figure 5.7: Electroplating problem due to intense current supply in a short time. Electrodes merged and blocked the channel.	74
Figure 6.1: Preparation of the cancer cells [79].	77
Figure 6.2: Test set up	78
Figure 6.3: Raw data showing the passage of 3 beads, when the flow rate is 7.5 μ l/min.	80
Figure 6.4: Low pass filtered data. The amplitude of the peaks reduced significantly.	80
Figure 6.5: Amplitude and bandwidth of Peak 3.	81
Figure 6.6: Raw data showing the passage of K562 cancer cells. Flow rate is 5 μ l/min.	84
Figure 6.7: (a) High pass filtered data. Positive peaks are followed by negative peaks showing the passage of the particles. (b) Magnified view of the negative peak occurred at the 6.2006s.	85
Figure 6.8: Resistance change during the passage of a 10 μ m polystyrene latex particle with different frequencies. (a) Response of the sensor at 20 kHz. The change in the resistance is highest with 8 mV. (b) Response of the sensor at 50 kHz.	

(c) Response of the sensor at 100 kHz. The amplitude of the negative peak decreases down to 1 – 2 mV..... 88

Figure 6.9: A graph showing the passage of microbeads and cancer cells. Microbeads creates a change of 4 to 5 mV where cancer cells reduces the base voltage up to 10 mV..... 89

Figure 6.10: (a) 9ml solution + 30ul microbeads + 2ul flow rate with with 5Vpp 50 kHz in 22sec + lowpass filtered. (b) 6ml solution + 30ul microbeads + 2ul flow rate with with 5Vpp 50 kHz in 1 min + lowpass filtered. (c) 3ml solution + 30ul microbeads + 15ul flow rate with with 5Vpp 50 kHz in 22sec + lowpass filtered 91

Figure 6.11: Comparison of the output voltages generated by 3D and coplanar electrodes respectively. 92

CHAPTER 1

INTRODUCTION

The need for inexpensive and point of care (POC) lab-on-a-chip (LOC) devices which can perform rapid and accurate analysis of biological particles is urgent. Detection and quantification of these biological particles can reveal crucial information about health status and diagnosis of a disease. Therefore, there is a significant need for portable devices, capable of performing rapid analysis of micro and nano-scale particles. The macro-scale devices, already available in the market can detect and count the desired particles such as blood cells, pollens, bacteria or microbeads. Fabricating the micro-scale version of these devices can make them available to everyone by omitting the geographic, economical and governmental obstacles. However, few problems such as processing of large sample volume, speed, and reliability etc. arise due to miniaturization of the devices. An efficient device should be capable of processing a large sample volume in a reasonable time without sacrificing reliability.

1.1. Particle detection methods

Traditional particle counting devices such as Immunoassays[1] or FACS [2]require large sample and reagents volume and take considerably long processing time. In addition, they are complex, costly and bulky. Therefore, there is an urgent need for portable and inexpensive devices which require small sample volume and suitable to work for field applications [3]. This can be achieved by the help of advanced lab-

on-a-chip devices that employ recent microfluidic techniques to detect and analyze the micro-scale particles. Resistive Pulse Sensors such as Coulter Counters[4], optical flow cytometers[5,6], optical spectroscopy devices[7], and micro PIV counters[8] are some of these LOC devices. Among these techniques, Coulter Counters are the least complex, inexpensive but one of the most reliable one, which also provides label-free detection of biological particles suspended in a medium.

Resistive pulse counter was invented in 1953 by Wallace H Coulter[4]. The principle is similar to typical impedance cytometer and states that particles passing through an orifice or a pore, separating two chambers, create a change in the channel resistance proportional to their volumes. Technical drawing of this phenomenon is shown in Figure 1. The reason of the impedance change is due to replacement of the fluid in the orifice by the particle volume. The resistance or impedance change can also be recorded in terms of voltage or current pulses by using the customized electrical circuits.

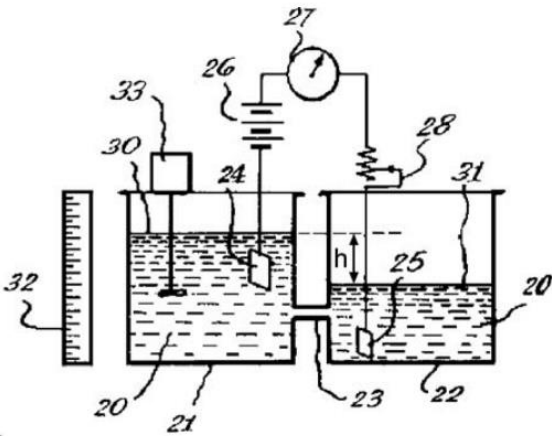


Figure 1.1: (a) Schematic of the original Coulter Counter patented in 1953. Two chambers are separated by an orifice. Particles suspended in the liquid pass from one chamber into another through the orifice by hydrodynamic pressure. The change in the resistance of the fluid is measured by a readout circuit. The setup includes an agitator to keep the particles suspended and a scale to measure the change in the volume [3], [4], [9].

1.2. Motivation

Coulter Counters' efficiency is proportional to the channel dimensions. A Coulter Counter with a large cross sectional area can analyze more samples in a given time. However, to sense the micro-scale particles, the channel dimensions should be analogous to the particle diameter. If the channel cross-section area is very large relative to the size of the particle, the microfabricated device cannot detect the particle accurately. Therefore a single channel device can only process a small volume of sample for sensing and counting the micro and nano scale particles resulting in a low throughput. This is a substantial drawback especially when detecting low concentration of bio-particles such as bacteria or sporadic cancer cells, which require porcesing of large sample volumes. Hence, there is an urgent need for a microfabricated device that is capable of performing high throughput analysis of microscale particles without complex hardware systems and software algorithms[3].

There are a few ways to improve sensing speed without sacrificing the reliability.

1. Enlarging the channel dimensions
2. Increasing the flow rate
3. Employing multiple channels

Enlarging channel dimensions is not very desirable as stated above, since it is difficult to sense the particles when the channel dimensions are relatively large compared to particle diameter. Similarly, increasing the flow rate above a critical level prevents reliable counting, since rapid passing of the particles through the orifice may not be detected by the designed sensor. Thus, increasing the channel numbers to provide multiple analyses is one of the best solution.

1.3. Implication

High throughput detection can be achieved by employing multiple channels; however, increasing the number of channels above a certain limit will simply increase the complexity of fabrication and processing of the individual signals. In addition, unbalanced distribution of the fluid resulting in clogging of the channels, crosstalk between the electrodes, and difficulty in monitoring of particle crossings are just a few adverse effects of fabricating numerous channels. To achieve multiple detections without being affected by the factors mentioned above, a novel approach is introduced in this study. The main channel is divided into two separate microscale channels by a parylene layer. This layer serves as an insulation piece and prevents the crosstalk between electrodes, placed at the bottom of the channels. 2-point measurement is used in this study to detect the change in the voltage levels when the particles pass through the orifice. Measurements were made for each microchannel then recorded by a data acquisition board. For each channel, one data acquisition input is needed. Therefore increasing the channel numbers to four or five will simply increase the cost and also complicate the signal processing steps. Apart from this, using many bench top equipment such as power supplies, oscilloscopes, function generators or data acquisition boards will make the system deviate from lab on a chip concept to a compact and expensive system. In this study, only one data acquisition board was used to collect two different signals. The measurement concept is based on the amplitude modulation and demodulation techniques completed with peak detection circuits. The concept can be fundamentally expressed as below: When a particle travels through the aperture, it changes the base resistance value of the channel with respect to its volume. Thus, the signal comes to the detection circuit as an amplitude-modulated signal. The detection circuit demodulates and amplifies it. The peak detector works as an envelope detector, which identifies the peaks when there is a change from the base voltage. The output of the peak detector is recorded and processed in a software environment.

1.4. Goals

The main goal of this research is to design a MEMS-based μ -Coulter Counter, which is capable of performing simultaneous counting without a need of extra inlets and reservoirs. The sensor was designed with similar patterns employed in the earlier designs in the literature with a few novel approaches and minor changes such as parylene microchannel structure and less complicated hardware design. Two different structures, single channel and two channels were designed, tested and compared in terms of their performances and device complexity. Single channel device was used to understand the effects of AC excitation techniques, the role of electrolyte conductivity and contact pad smoothness on channel impedance, the relationship between particle size and resistance change, and different amplitude demodulation techniques to extract the desired signal from the raw data. All these concepts were extended and improved for the novel two-channel Coulter Counter to get better results and compare them with the traditional single channel designs. Results show that the two-channel device can approximately detect two times more signals in the same time slot.

1.5. Overview

In Chapter 2, theory of the Coulter Counter was described and previously designed resistive pulse sensors and impedance flow cytometer devices were introduced and novelty of our design was compared with those designs. In Chapter 3, design, modeling and simulation of the surface velocity field, surface electric field and surface potential field were explained. Effects of the particles and cells with different conductivities on voltage and electric field change were demonstrated. Fabrication flow of the design and the problems faced during this stage were explained in detail in Chapter 4. Chapter 5 gives a detailed explanation of the test

set up, demodulation circuit, solution and particle / cell features and the problems encountered during test stages. As a final step, conclusion and future work was discussed in Chapter 6.

CHAPTER 2

THEORY AND LITERATURE REVIEW

2.1 Resistive Pulse Method

The schematic of the working principle of the resistive pulse counter (Coulter Counter) is shown in Figure 2.1. In this method, particles suspended in a conducting fluid are forced to pass through a narrow aperture (detection area), during which they replace the amount of liquid equal to their size. This volume change, together with the surface ionic properties of the particles, results in a change in the pore resistance. The change can be either positive or negative depending on the surface charge and size of the particles, and can be measured in terms of voltage or current depending on the detection circuit.

When there is no particle in the detection area, the number of ions passing through the pore (N_+) is calculated as:

$$N_+ = V\sigma \quad (2.1)$$

where, V and σ depict the volume and the ionic density of the pore respectively. If a particle with a negligible surface charge travels through the pore, Equation (2.1) takes the form of:

$$N_{++} = (V - v)\sigma \quad (2.2)$$

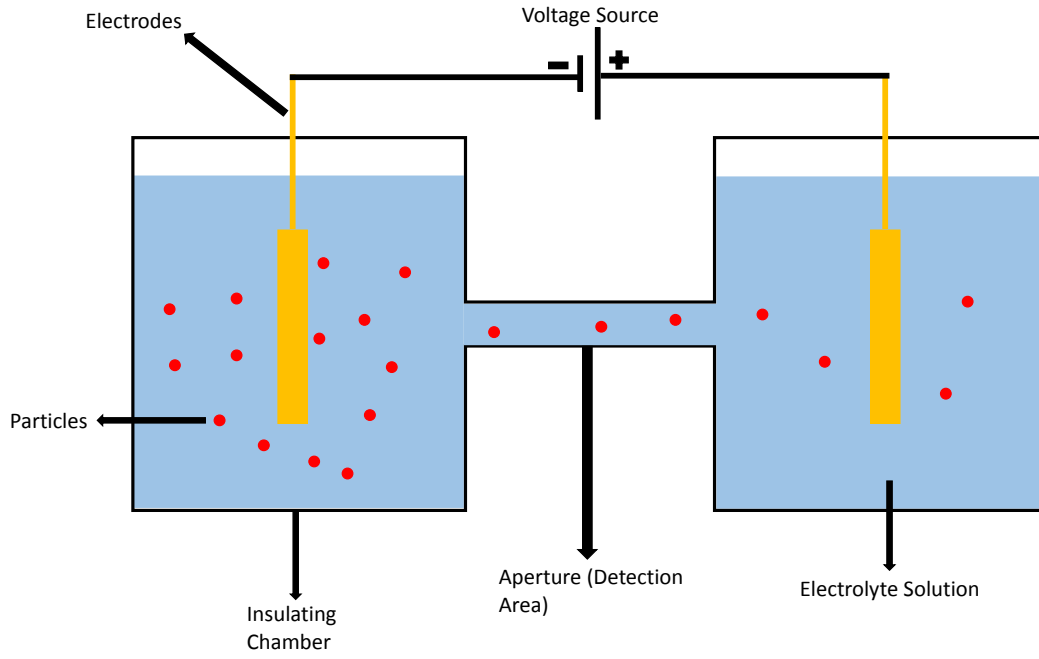


Figure 2.1: Schematic of the Coulter Counter

where, v is the volume of the particle. Since N_{++} is smaller than N_+ , the resultant current pulse is downward. However, Equation (2.2) cannot be written for a particle with a surface charge. Instead, it takes the following form of the Eq.2.3:

$$N_{++} = (V - v)\sigma + Z_{++} \quad (2.3)$$

where Z_{++} depicts the number of ions on the particle surface. A particle with a large surface charge and a solution with a low ionic concentration produces a growth in the number of ions and it consequences a positive current pulse [10]. The change in the ionic current can also be explained with the following:

$$I = \int_A \sigma \mu E dA \quad (2.4)$$

where μ and E are the mobility of the free ions and the applied electric field, respectively, and A is the cross sectional area. As stated above, a particle with a

negligible surface charge reduces the amount of free ions in the orifice, thus ion density, and ionic current ΔI_{volume} decreases.

On the other hand, a particle with a high surface charge increases the amount of free ions, hence ionic density and this leads to a rise in the ionic current ΔI_{charge} [11].

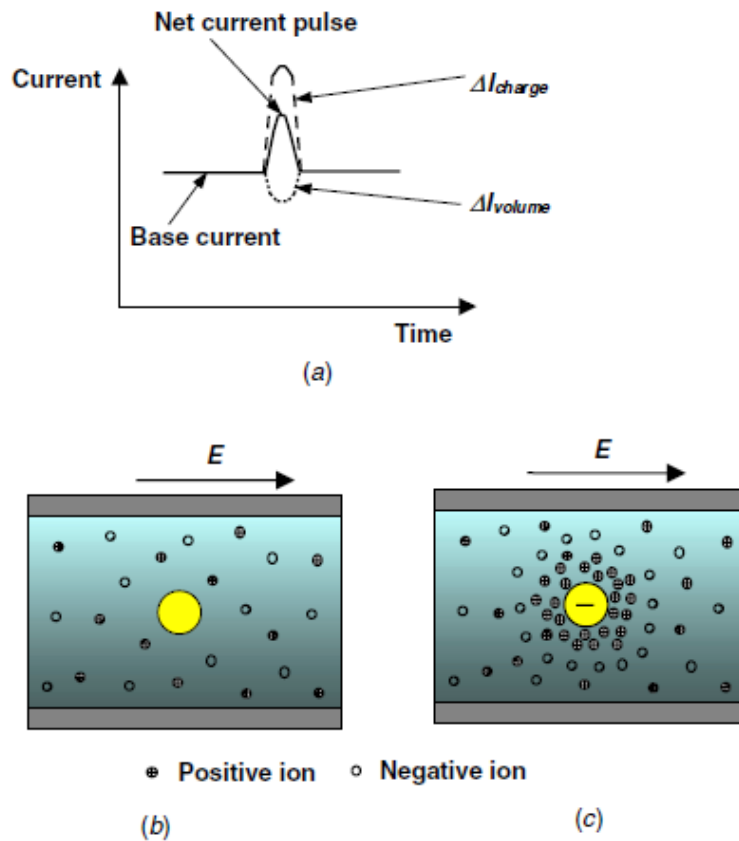


Figure 2.2 (a) Demonstration of a change in the ionic current. (b) A particle with a negligible surface charge, reducing the number of free ions inside the microchannel; hence decreasing the ionic current. (c) A charged particle inducing the free ions inside the micro channel thus increasing the ionic current [11].

The particle shape and its orientation affect the output of a signal. For example, a spherical particle does not give the same output with a biconcave disk since the passage of these particles through the detection area is not same due to their size and

orientation. A biconcave disk's traversal through the pore is longer and has a smaller amplitude than a spherical particle since its radial axis is not symmetrically aligned with the pore axis [12], [13].

2.1.1 Mathematical Model

For a spherical particle, resistance change in Coulter Counter sensors depends upon the dielectric properties of the particles, electrical conductivity of the solution and the cross-sectional area of the aperture.

$$\delta R_p = \rho \int \frac{dz}{A(z)} - R_p \quad (2.5)$$

In Equation 2.5 equation, $A(z)$ and ρ denote the cross sectional area of the aperture and resistivity of the medium and R_p is the channel resistance in the absence of any particles. This equation points that a spherical particle traveling along the z axis, creates a resistance change at the time it passes through the pore with a cross-sectional area of $A(z)$. Figure 2.3 shows the schematic of a spherical particle with a diameter of d and a cylindrical aperture with diameter D and length L [12], [14], [15].

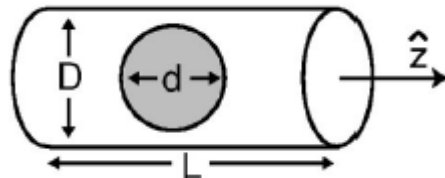


Figure 2.3: Schematic of an aperture with length L and diameter D when a particle with a diameter d is passing through it [4].

The sensitivity of a sensor is directly related to the ratio between the particle diameter and cross-sectional area of the aperture. The more they are analogous, the better the output signal is. Therefore different mathematical models were developed to calculate the change in the resistance. In the first and second model, particle diameter is assumed to be infinitely small and small compared to the size of the pore.

In this case, electric field is assumed to be uniform along the pore since the particle diameter is very small and does not distort the fringing fields. The resistance change for this situation is formulated as in Equation 2.6 - 2.8. R_p and δR_p are the base resistance and the deviation from the base resistance as stated in Equation 2.5. d is the particle diameter, D is the aperture diameter and L is the length of the aperture. $F\left(\frac{d^3}{D^3}\right)$ is a numerical factor that elucidate the protruding of the electric field lines into the pore wall [16], [17]. It is important to note that the formulations for small particles are valid when the particle is non-conducting and traveling through the central axis of the aperture.

$$\frac{\delta R_p}{R_p} = \frac{d^3}{D^2 L} \quad (2.6)$$

$$\frac{\delta R_p}{R_p} = \frac{d^3}{D^2 L} \left[\frac{D^2}{2L^2} + \frac{1}{\sqrt{1 + (D/L)^2}} \right] F\left(\frac{d^3}{D^3}\right) \quad (2.7)$$

$$F\left(\frac{d^3}{D^3}\right) = 1 + \frac{1.26d^3}{D^3} + \frac{1.1d^6}{D^6} \quad (2.8)$$

The other two models assume that particle diameter is comparable to the aperture diameter. In these cases, two different formulations were written for intermediate and large particles (Equation 2.9 and 2.10 respectively) [12], [13],[14], [15], [18].

$$\frac{\delta Rp}{Rp} = \frac{d^3}{D^2 L} \left(\frac{1}{1 - 0.8(d/D)^3} \right) \quad (2.9)$$

$$\frac{\delta Rp}{Rp} = \frac{D}{L} \left[\frac{\arcsin(d/D)}{\sqrt{1 - (d/D)^2}} - \frac{d}{D} \right] \quad (2.10)$$

2.1.2 Coincidence Theory

Coincidence occurs when more than one particle occupies the pore. It usually occurs when the channel dimensions are larger than the particle diameter. This situation is one of the most challenging problems of resistive pulse counters, since, a sensor not capable of detecting the existence of multiple particles gives inaccurate number of peaks hence distorts the reliability of the device. There are different scenarios of coincidence depending on the geometry of the device and alignment of the particles in it. These are shown in Figure 2.4 [12].

Assuming a random distribution of the particles, coincidence probability can be explained with Poisson's distribution in Equation 2.11.

$$P_k(\tau) = \frac{e^{-\lambda\tau} (\lambda\tau)^k}{k!} \quad (2.11)$$

where λ , k and τ are the bead concentration, number of coexisting beads and sensing volume, respectively [19]. One way to reduce the coincidence probability is to lower the bead concentration by diluting the solution. The other way is to change the sample volume by modifying the aperture dimensions since an increased sample volume also decreases the coincidence error.

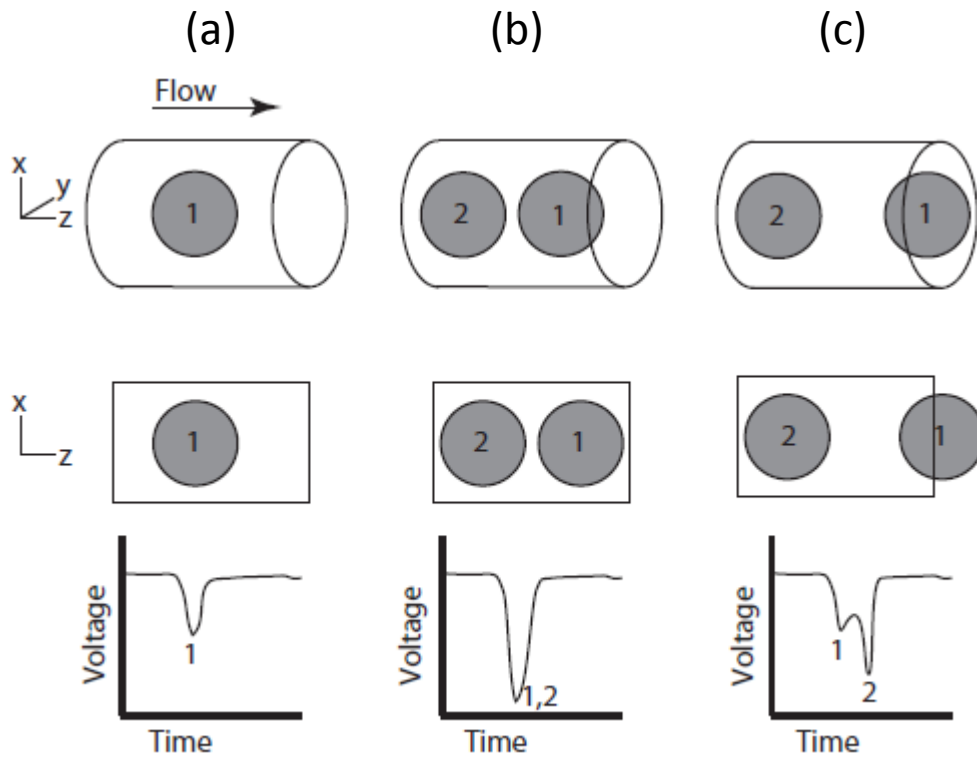


Figure 2.4: Graphical illustration of particle coincidence. (a) Only one particle exists in the pore and voltage output just shows one valley (negative peak). (b) Two particles occupying the detection zone however voltage output still shows one valley. (c) While one of the particles is exiting the detection area the other one in behind enters it therefore the voltage output shows shoulder and indicates the existence of the second particle. Particle one has a smaller amplitude since it is exiting the detection zone [12].

The following equation shows the relationship between the true count and observed count. It is also modeled by the help of the Poisson process:

$$n = \frac{V}{\Delta V} \left(1 - e^{-\frac{\Delta V N}{V}} \right) \quad (2.12)$$

where N and n depict the true count and the observed count, respectively, while V and ΔV are the sample and the aperture volumes, respectively.

2.2 Literature Review

In medical research, cell counting and sorting are of a great importance, including the indication of the patient health status, diagnosis of the illness, and the detection of the progress of a disease. One of the most widely used particle counter is hemocytometer, invented by French anatomist Louis-Charles Malassez to perform blood cell counting. The hemocytometer includes two microscope glass slides, with a grid of perpendicular lines etched in the center. A photo of hemocytometer is seen in Figure 2.5. The volume enclosed by lines is known since each grid has specific dimensions so that counting the number of particles in a specified volume is achieved accurately. By using the number of counted particles, concentration of the sample is calculated. However, all this operation takes considerably long time, since the process is performed under a microscope. In addition, the device requires a large sample volume to process counting and a trained employee to operate the device [20].

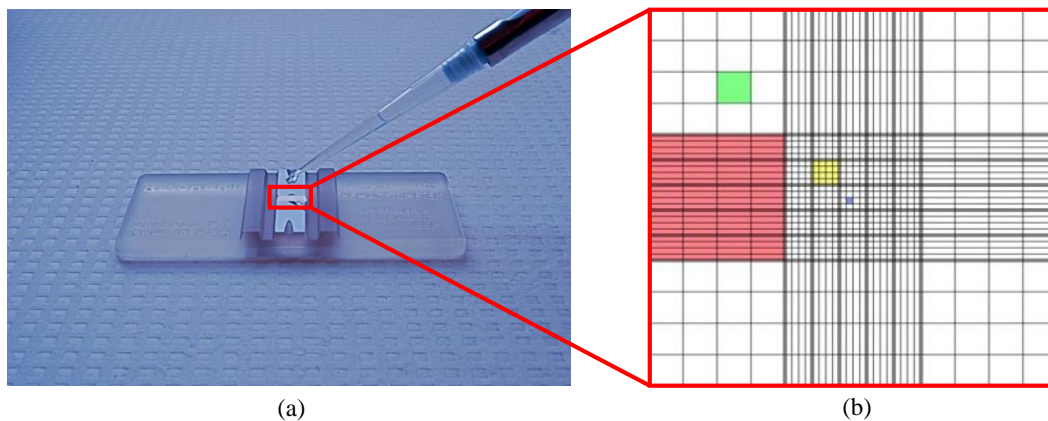


Figure 2.5: (a) Picture of the commercial hemocytometer. (b) Magnified view of the grid lines placed, in the middle of the device [20], [21].

To reduce analysis time while increasing accuracy and reliability of particle counters, automated version of these cell counters was developed. These devices

can yield variable information of the cell properties such as, diameter, shape, area by cell imaging techniques [3]. However, both manual and automated cell counters require a large number of materials and complex set up such as uniform cell suspension, Trypan Blue stain in phosphate buffered solution (PBS), micropipettes, inverted microscopes and the hemacytometer itself. Therefore, they are not very appropriate for instantaneous particle detection and analysis [20].

Microfluidic devices overcome many of these problems and perform rapid and reliable analysis. Due to their miniaturized sizes, they can also work with small amount of samples and outperform traditional particle counters. A summary of different types of particle counters is presented in the following section.

2.2.1 Optical Detection Methods

Flow cytometry is one of the most important and widely used devices used in optical detection and counting of the microparticles. The main principle of this device is based on light scattering, light blocking or emission of fluorochrome molecules to create specific multi parameter information. An optical flow cytometry device can analyze not only the size of the particles ranging from 0.2 – 150 micrometers but also give information about the internal structure of the particles such as granularity and relative fluorescence intensity [22]. Depending on how the cells or particles scatter the incoming light, they can be sorted in different groups by the help of a complex system comprised of optical, fluidic and electronic parts. [22], [23]. The schematic showing flow cytometer and its the complex set up of an optical flow cytometer is shown in Figure 2.6 and Figure 2.7, respectively.

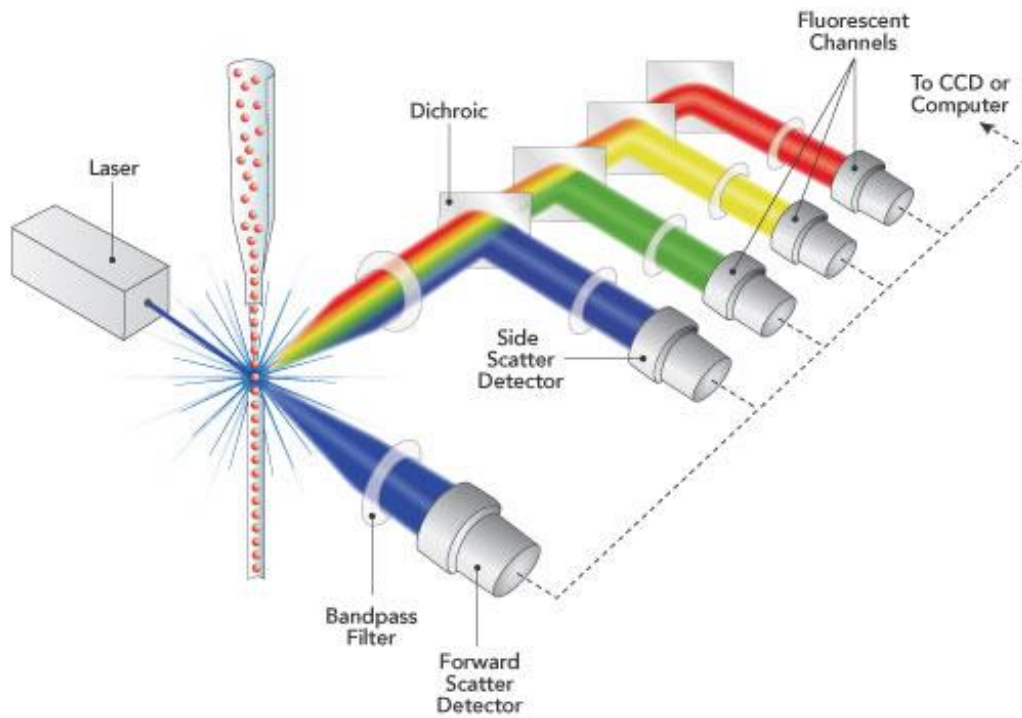


Figure 2.6: Schematic of a commercial flow cytometer device [24].

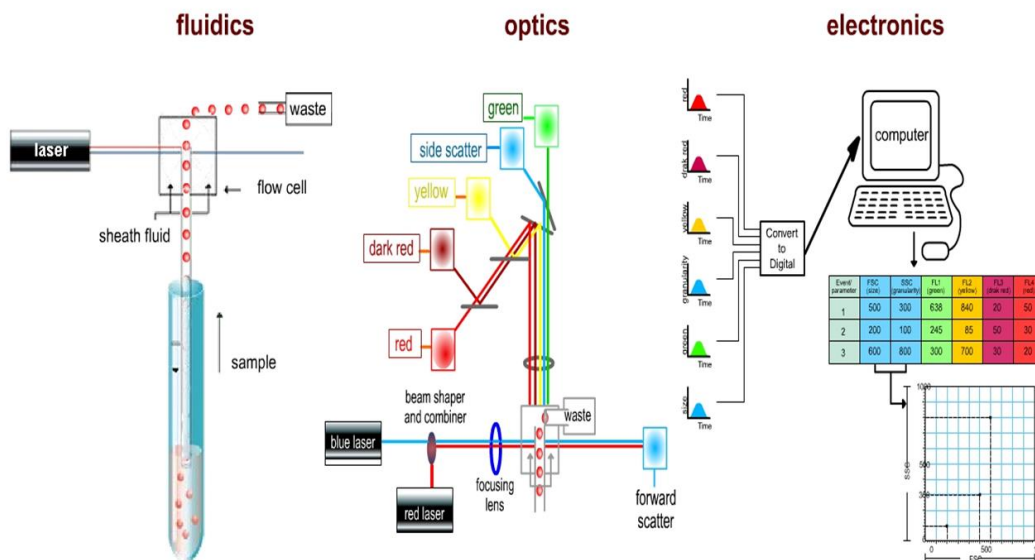


Figure 2.7: Three main parts of the Flow Cytometers: Fluidic systems to transport the particles, optical system to illuminate the particles and filters to guiding the resulting signal to detectors and electronics to process and sort the incoming signals by specialized software algorithms [22], [25].

As shown in Figure 2.7, flow cytometers have complex set up including fluidics, optics and electronics. The fluidic system is responsible of transporting the particles to the laser beam area for examination. For the most accurate analysis, particles should be hydrodynamically focused into the center of the channel by sheath fluids before entering to the detection zone. The sheath fluid is cell free environment and is just used to confine the sample stream into the center of the channel. Sample fluid width can be adjusted by playing with the flow rates of the sample and sheath fluids. The optic part is comprised of lasers and filters to illuminate the particles and direct the corresponding signal to the appropriate detectors, respectively. These detectors converts the corresponding optical signal into electrical signal and pass them to electronics part in which these electrical signals are processed by the computer for characterization and sorting [22], [23], [26]. However optical flow cytometers are bulky, expensive, and require complex hardware and software set up to analyze the signals, as seen in the figures above. In addition to that, particles need to be dyed with fluorescent stains prior to analysis.

Another non-invasive method for cell counting and characterization is the optical interferometers. In this method, the light source is divided into two separate ones by the help of a beam splitter. One of these beams is used as a reference whereas the other beam is scattered when the particle passes through the detection area. The measurements are based on the scattered field amplitude. The detection of scattered field instead of scattered power is preferred due to lower background noise. The experimental set up of the optical interferometer is shown in Figure 2.8 [27].

Working principle of the interferometers is as follows: Particles traveling along the microchannel by electro-osmotic flow are illuminated by the laser beam. Focusing objective collects the entire light scattered from each particle passing through the laser focus. The gathered signals are combined with the reference signal and are sent to photodetector. The amplitude of the scattered field is proportional to both the differential signal coming from the photodetector and the third power of the particle size [27].

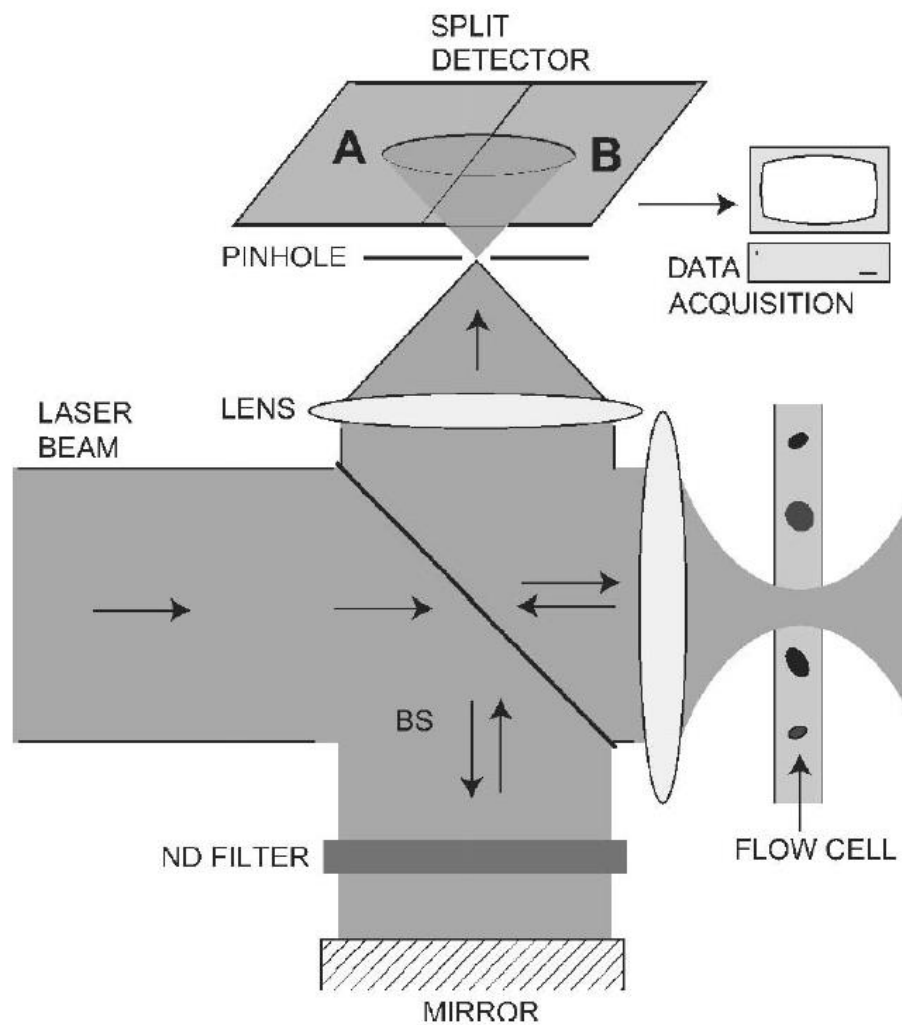


Figure 2.8: Experimental set up of the optical interferometer [27].

Even though this method is superior to optical flow cytometers for reducing the background noise, it has a similar optical set up in terms of its complexity and cost. Therefore, it is not suitable for lab-on-a-chip (LOC) devices.

2.2.2 Acoustic Detection Methods

This method mainly employs ultrasonic piezoelectric transducers to measure the amount of microparticles flowing in liquids. Acoustic detection method also reveals information about the velocity of the fluid. By adjusting the frequency range from 2MHz to 8MHz, different types of microparticles such as plastic microspheres, microemboli [28] slugs and bubbles [29] can be detected and counted in high flow rate.

2.2.3 Electrical Detection Methods

One of the most popular resistive pulse techniques is Coulter Counter. The technique utilizes a pore or an aperture, two reservoirs and two electrodes on each side of the reservoirs to count the number of particles during their passage from the sensing area. The particles suspended in a low concentration medium, are directed from one reservoir to another along a current path provided by electric field. When the particles pass through, the electrical resistance of the pore changes in proportion to the volume of the particle occupying the pore. The change in the resistance can also be recorded in terms of voltage [30] or current [10] depending on the electrical detection circuit. The measured pulse amplitude is proportional to the volume of the particle [9]. Wallace H. Coulter used this method to count the number of plankton particles, which have an adverse effect on the sonar system during World War 2 [4]. Coulter Counters are simple, rapid, and reliable, therefore, they are widely used in microfluidic and biomedical research to detect blood cells [31], [32], polystyrene latex microbeads [33]–[35] pollen [10], [36], nanoscale colloids [15]. In traditional Coulter Counter, DC voltage was employed, however, in the recent designs, AC voltage with a fixed excitation frequency is employed, since AC voltage at a high frequency reduces the double layer effect occurring on the surface

of the electrodes and provides a faster analysis. Besides from resistance change, capacitance [37], [38] or inductance [39], [40] change is used for more accurate counting and analysis. Because, these techniques not only provide a size based but also granular level detection and give information on the internal structure of the particles. Sohn et al [38] also utilized capacitive cytometry to analyze the DNA content of the eukaryotic cells and the cell-cycle kinetics of the cell populations. By taking the advantage of detecting the internal structure of the particles, they differentiated avian and mammalian red blood cells. Murali et al [37] employed real-time capacitive detection method to sense aluminum abrasive particles with a diameter size ranging from 10 μm to 25 μm , which may cause rotating and reciprocating machinery problems. When the particle passes through the detection zone, the capacitance of the aperture changes due to the various permittivity values of metal particle and the fluid. The capacitance of the aperture is not affected either by air or water bubbles and this provides an accurate counting. This technique is mainly preferred for the media with lower conductivity, where instantaneous resistance changes cannot be measured due to the very high resistance value of the microfluidic channel dominating the small peaks.

Even though Murali et al.'s technique provided an accurate counting for metal particles, it could not distinguish ferrous and non-ferrous particles in lubrication oil, hence internal structures. Therefore Du et al [40], [41] proposed an inductance based Coulter Counter which can distinguish ferrous and non-ferrous particles which have same size and volume but different internal structures. In this technique, the existence of the particle in the sensing area changes the coil inductance and the eddy currents of the particles since the magnetic permeability of the metal particle and the lubrication oil is different. This method provides valuable information about the characteristics of the particles but cannot provide a superior solution to capacitive based detection. The minimum size of the detected particles in the inductive based method is 50 μm while capacitive based method is able to detect particles down to 10 μm .

Electrical Impedance Spectroscopy (EIS) is another electrical detection method giving information about size, conductivity and dielectric properties of the biological particles by employing a frequency sweep technique ranging from Hz to MHz [42]. The working principle of EIS is very similar to Coulter Counters. EIS also senses the particles suspended in a fluid while they pass through a defined aperture except it uses a frequency sweeping technique to detect and analyze the characteristic of the particles. Different frequency range reveals variety of information about the particles. For example as at low frequencies, impedance characteristics provide information about size while at higher frequencies dielectric properties or conductivity of a biological particle can be obtained. Therefore EIS is capable of differentiating similar sized particles with different granularity such as red and white blood cells [42], [43], polystyrene latex beads [44], or bacteria [45]. Even though EIS provides valuable information about the characteristics of the particles, frequency sweeping across a wide frequency range takes considerably long time. In addition, expensive hardware such as lock-in amplifiers, rapid data acquisition boards, precision LCR meters are required to process the collected data.

2.2.3.1 Coulter Counter Devices in the Literature

Traditional Coulter Counter is comprised of two reservoirs in which microparticles are suspended in a conductive medium. The reservoirs are connected to each other by a defined aperture. These particles are forced to move from one reservoir to another along the aperture by a hydrodynamic or electrophoretic force, and they create a change in the electrical resistance during their existence in the aperture. The electrical resistance change with respect to particle diameter, and channel dimensions including the medium resistivity was formulated by DeBlois and Bean in 1970 [46]. They verified the accuracy of their formula by using polystyrene particles sizing approximately 90nm. In 1997 Larsen et al. [47] fabricated the first micro Coulter Counter (μ CPC) shown in Figure 2.9 to detect micro particle

suspended in a fluid. The device was fabricated on a silicon wafer, where the channels are located on it. A glass wafer anodically bonded on the silicon wafer includes thin film gold electrodes responsible from sensing the microparticles. The device used hydrodynamic focusing (HDF) method to focus the sample inlet to the center of the channel by the help of two non-conducting sheath fluids. In this technique, by adjusting the sheath flow rate, particles with different sizes can be confined to the center of the channel and an accurate sensing can be achieved. The trajectory of the particle, along with the size and shape, affects the sensing mechanism dramatically. Therefore, two identical particles following a different route will create different resistive pulses [13]. HDF method prevents this problem by focusing the sample to the center of the aperture. In addition, larger apertures compared to particle size can be designed and this prevents channel clogging. However, due to the reliability and corrosion factors of the gold electrodes, Larsen et al. could not publish an experimental data with this design. In 1999 Koch et al. [48] designed and fabricated a micromachined Coulter Counter with a pore having a cross section area of $5 \times 5 \mu\text{m}^2$. The resistance change of the microchannel during the particle passing was 1.8% and the device detected microparticles with $1.5 \mu\text{m}$ diameter by the help of Ti electrodes with a thickness of 100nm. Roberts [33] also designed a Coulter Counter with rectangular and a pyramidal shape aperture by Deep Reactive Ion Etching technique (DRIE) and chemical wet etching methods respectively in 1999. He used latex beads with diameters comparable to blood cells for testing two different designs. As a result of the tests, pyramidal shape aperture gave superior results than rectangular shape aperture. The signals were accurate, clear and have Gaussian shape. In the same year, Ayliffe et al.[43] used the AC excitation voltage for detection and analysis of both particles and different media for the first time. Polymorphoneuclear leukocytes (PMN) and red blood cells (RBCs) were detected using electroplated gold electrodes and it was proven that electrodes with smaller surface area provide a better spatial resolution. In addition, since AC excitation voltage was applied, impedance spectra of the different media

were investigated and shown that solution impedance starts to dominate the system with increased frequency.

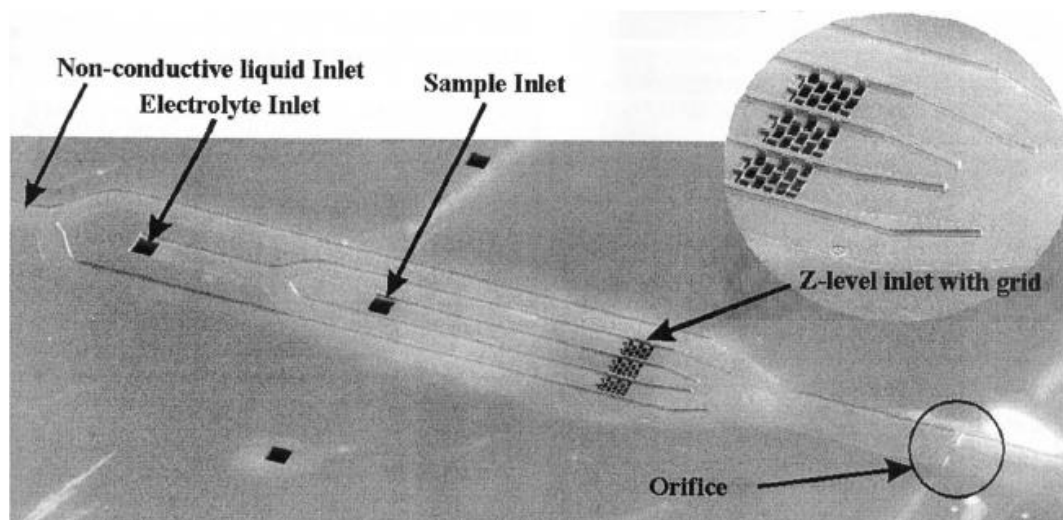


Figure 2.9: First microfabricated Coulter Counter. Non-conducting sheath fluids confine the electrolyte inlet with the sample inlet. Particles are designed to be detected in the orifice by Au electrodes [47].

following these improvements, Saleh and Sohn [15] designed a Coulter Counter in 2001. The fabricated device was able to detect latex colloids particles as small as 87nm with a pore length of 8.3 μm and a cross section area of 0.16 μm^2 by the help of Ti / Pt sputtered electrodes excited with a 0.4V DC voltage. Another aperture with a cross section area of 10.5 x 1.05 μm^2 detected nanoscale particles ranging from 190nm to 640nm. They stated that the fabricated device was capable of distinguishing nano colloids whose diameters differ by less than 10%. In 2002, Satake et al. [31] detected polystyrene latex particles (PSL) of 5.1 μm and 8 μm diameters by applying 5V DC excitation voltage to the Platinum (Pt) electrodes. Even though the DC response is considered slow compared to AC response, the device detected the PSL at a very fast flow rate of 11 $\mu\text{l/s}$. In 2003 Saleh and Sohn [49] employed resistive pulse technique to determine the antibody binding on the surface of nanoscale latex colloids.

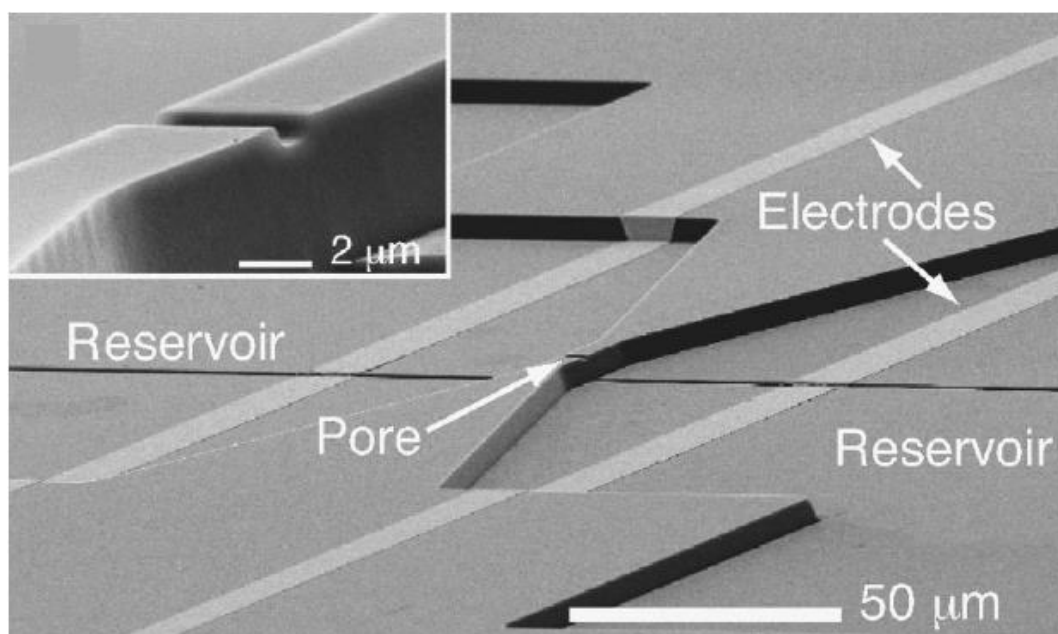


Figure 2.10: Saleh and Sohn's Coulter Counter with a rectangular pore and sputtered Ti /Pt electrodes. The device can detect nanoscale latex colloids as small as 87nm [15].

They measure the current change of latex colloids with and without bound antibody. This application of Coulter Counter allows determining any kind of thickness of the biological layer bounded to a colloid in a rapid and precise way. In 2005 Zhang et al.[10] investigated the effect of particle surface charge effect on the resistance change. They found that a particle with a negligible surface charge reduces the amount of free ions and thus the ion density in the orifice, resulting in a decrease in ionic current.

On the other hand, a particle with a high surface charge increases the amount of free ions, hence ionic density and this leads to a rise in the ionic current. They successfully distinguished same size polymethacrylate and pollen particles due to the difference in their surface charges. In addition they also observed that the medium concentration affected the polarity of the peaks. When the concentration of the KCL solution was decreased from 0.03M to 0.004M, the peak polarity was reversed. Chang et al reported a similar phenomenon for the translocation of the

DNA through a nanopore. Changing the ionic concentration resulted in a change in the polarity of the peak.

Resistive pulse technique employing nanopore sensors (NRS) attracted many scientists since 1990s, because NRS allow the detection of very small particles and single molecules such as λ - phage DNA [50]. Nanopores can be divided into two groups according to the material they are made of: Natural (mostly biological protein channel placed inside a lipid layer) and synthetic materials [9]. By using NRS method In 1996 Bezrukov et al. [51] counted the polymer molecules passing through a single nano alamethicin aperture with a length and a diameter of 5nm and 2nm, respectively. In the same year Kasianowicz et al. [52] designed a nanopore with a diameter of 2.6 nm, which is capable of detecting the single-stranded RNA and DNA in a membrane made of lipid bilayer. In 1999 Akeson et al. [53] detected the same molecules by applying an electric field in an α -hemolysin channel. The schematic of the channel is depicted in Figure 2.11.

One of the most important techniques developed for the Coulter Counter devices is the hydrodynamic focusing (HDF). This technique was first introduced by Larsen et al in 1996 [47]. HDF allows the detection of different sized particles by keeping a fixed size aperture. The flow rate and width can be controlled by adjusting the flow rate of sample and sheath fluids, with different conductivities. The width of the sample fluid determines the size of the particle that can be confined into the sample stream. The larger the sample fluid width, the bigger the particle is. Therefore, without changing the aperture dimension, both smaller and larger particles can be detected. Also, by directing the particles along the center of the channel, uniform, reliable and accurate pulses can be obtained from the device, since the particle trajectory and its axis position will affect the resistance change [13] [54]. In addition, HDF allows the use of larger channels hence prevents the clogging problem. Another advantage of this method is that, it prevents particle clogging due to focused particle trajectory.

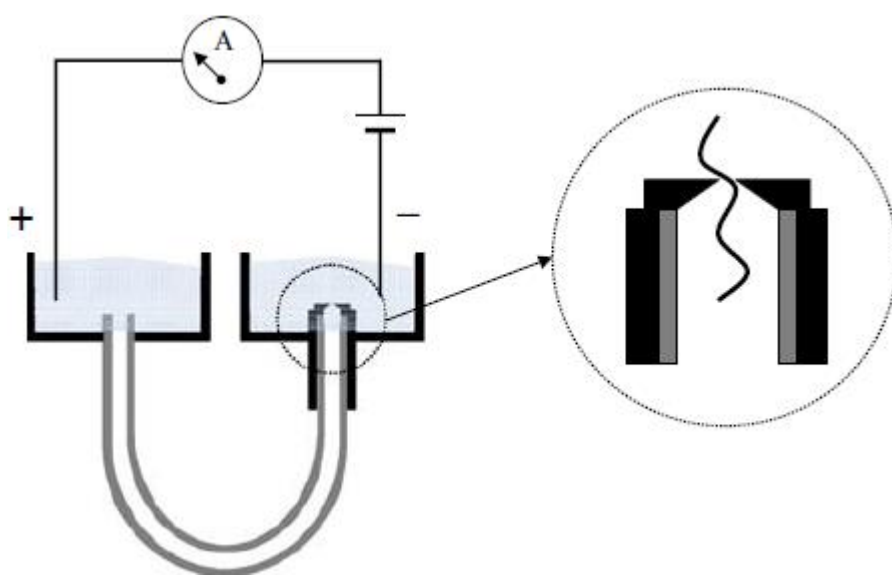
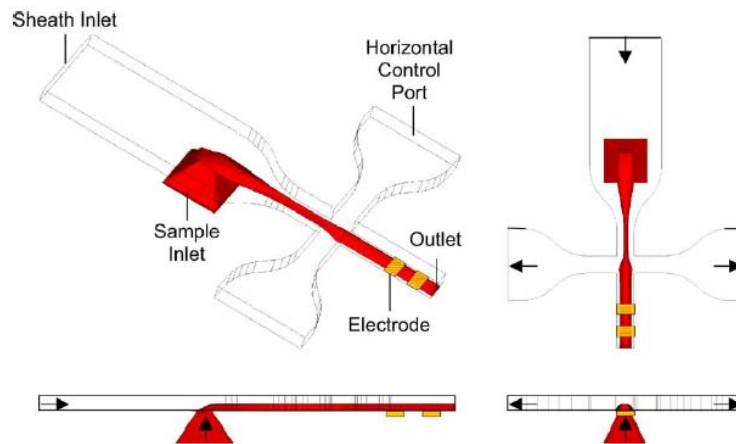
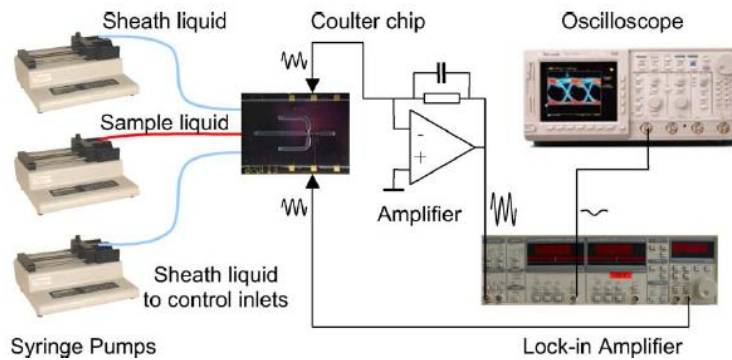


Figure 2.11: Design of the α -hemolysin channel to detect single RNA and DNA molecules. A U-shaped tubing connects two reservoirs, and aperture is placed inside on the right tubing. Ag-AgCl electrodes are used for sensing [53].

After Larsen et al., Nieuwenhuis et al. [55] worked on adaptable aperture method and did the first successful measurements by using HDF technique in 2003 (Figure 2.12). The fabricated pore with a cross section area of $30 \times 35 \mu\text{m}^2$ detected $5 \mu\text{m}$ and $10 \mu\text{m}$ polystyrene beads in a flow rate of $0.5 - 10 \mu\text{l/s}$. Planar gold electrodes having a surface area of $100 \times 150 \mu\text{m}^2$ placed on the glass wafer were used to detect the changes in the resistance. Even though the system was rapid and reliable, complex and expensive hardware such as lock-in amplifiers were required to get the desired signal. Rodriguez et al. [56] also used the liquid aperture method to detect $20 \mu\text{m}$ latex microbeads in 2006. Device was fabricated on glass wafer covered with PDMS layer, and eight pairs of interdigitated electrodes placed on the bottom of the glass layer were used for sensing.



(a)



(b)

Figure 2.12: (a) The hydrodynamic focusing illustration. Horizontal control ports confine the sample stream to the center of the channel and the sheath inlet is used to direct the fluid. 2D focusing is achieved by this technique. (b) Measurement set up [55].

In 2008, Rodriguez et al. [57] improved the design which is capable of performing 2D focusing for high speed analysis shown in Figure 2.13. The novelty of this design was the extra vertical inlet, controlling the vertical size of the sample inlet and bringing the microparticles closer to the electrode surfaces. Width and height of the sample fluid can be calculated by Equation 2.12 and 2.13 [58]. This technique overcomes the problem of the non-uniformity in the electric field.

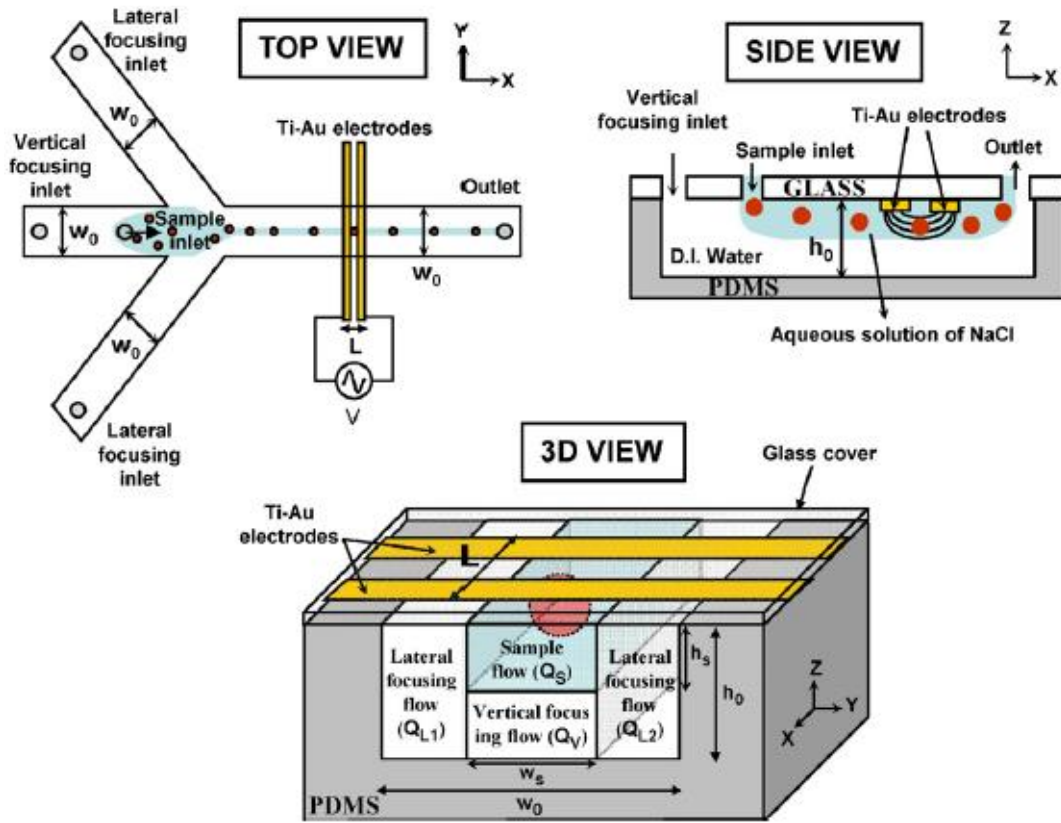


Figure 2.13: Schematic of the Coulter Counter and 2D liquid aperture method. Top, side and 3D view of the device are presented to express 2D hydrodynamic focusing phenomenon. Drawings are not in scale [57].

$$h_s = h_0 \frac{Q_s}{Q_s + Q_v} \quad (2.12)$$

$$w_s = w_0 \frac{Q_s + Q_v}{Q_s + Q_v + Q_L} \quad (2.13)$$

By applying an AC excitation voltage with 0.25V at 1MHz, Rodriguez et al. was able to detect the 20 μm latex beads and 5 μm yeast cells with a cross section area of 180 $\mu\text{m} \times 65 \mu\text{m}$ and 100 $\mu\text{m} \times 43 \mu\text{m}$ respectively. The detection rate of the device was 1000 sample/s, which is superior to the detection rate of Nieuwenhuis 20 sample/s.

Same year, Scott et al. [59] developed a Coulter Counter capable of performing 3D hydrodynamic focusing. The geometry of the device was similar to one developed by Rodriguez et al. [57] with a minor change as depicted in Figure 2.14.

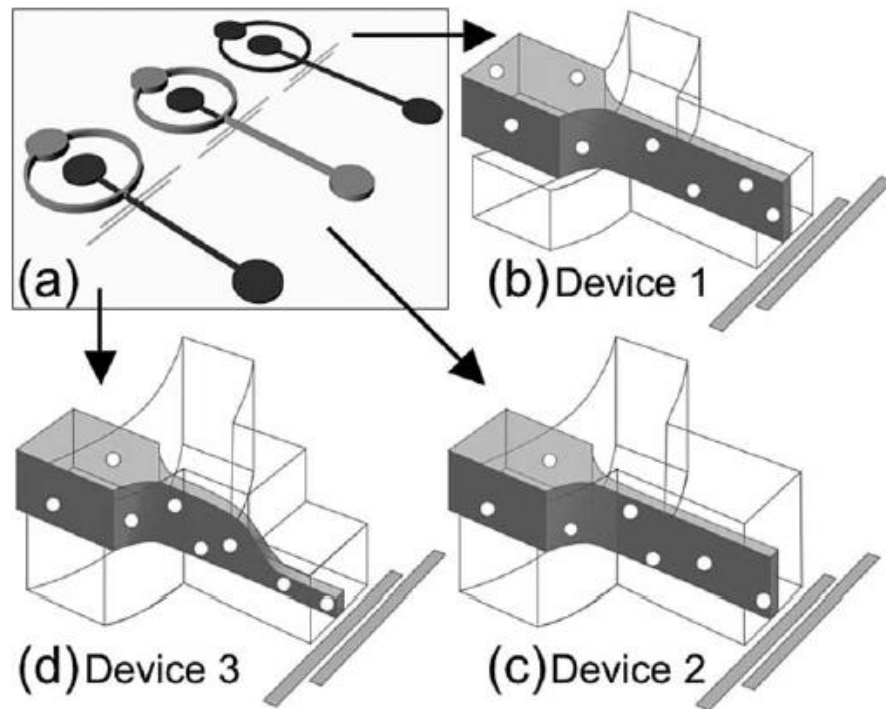


Figure 2.14: (a) Diagram of the three flow cytometer device. Dark gray and light gray regions indicate the thin and tall regions respectively. (b) 2D focusing of the first device. (c) 2D focusing of the second device with tall outlet channel. (d) 3D focusing of the third device by the help of the stepped outlet channel [59].

By employing a stepped outlet channel, focusing in the third dimension is achieved. Developed device was capable of detecting 20 μm and 6 μm yellow and green polystyrene fluorescent particles with a microchannel whose diameters are five to fifteen times bigger than the particle size. Hydrodynamic focusing provided many advantages to the fabricated Coulter Counter devices such as adaptable liquid aperture and anti-clogging. However the extra inlets occupy a large area on the chip and the device size increases greatly. In addition, for each inlet there is also a need for a syringe pump and it increases the cost and complexity of the device. All those

fabricated devices [47], [55]–[57], [59] performed single channel analysis but occupied a larger space. For a multiple analyses, which requires a few channels, number of the inlets will be a lot and the device complexity will increase greatly. Therefore hydrodynamic focusing does not seem to be the best solution for multiple parallel analyses.

2.2.3.2 Electrode Polarization Effect

Immersing a metal electrode into a conductive solution, biological tissue or a cellular suspension, creates a DC-borderline between the surface of the electrode and the fluid. This layer is known as an electrical double layer (EDL). Electrode polarization creates errors in the measurement of biological impedance and distorts the reliability of the system. It is seen in AC excitation with low-frequencies or in DC excitation based systems [60]. However, in traditional Coulter Counters mainly DC voltage [6], [28], [4] was applied due to the ease of signal detection. DC voltage causes double layer and creates bubbles in the microchannel; therefore, the recent designs preferred to employ AC excitation voltage with an intermediate frequency, since it diminishes the EDL significantly. The relationship and the modeling of EDL is formulated by Zheng et al. and depicted in the Figure 2.15 [32]. Z_{dl} represent the double layer impedance between the electrodes and the fluid, whereas C_{st} denotes the parasitic capacitance between the electrodes. It is not dominant in the low frequency region. Z_{ch} comprises the impedance of both the particle and the conductive path between the two electrodes [32]. The double layer impedance is replaced with constant phase element (CPE) in the circuit diagram due to the infinite resistance value of the leakage resistance crossing the double layer [62], [63]. Therefore CPE is comprised of double layer capacitance, charge transfer occurring on the surface of the electrodes, electrochemical traversal active components and the inhomogeneous reaction rates. Surface roughness, electrode porosity, various

coating composition, heterogeneity and the non-uniform current are some of the factors affecting the CPE [64].

The overall impedance is the series combination of the channel impedance and the constant phase element in parallel with the coupling capacitance. Calculation of the CPE impedance and the overall system impedance is given in the equations below.

$$Z_{CPE} = \frac{1}{Q(j\omega)^\alpha} \quad (2.14)$$

$$Z_{SYS} = \frac{1}{j\omega C_{st} + \frac{1}{Z_{ch} + \frac{1}{Q(j\omega)^\alpha}}} \quad (2.15)$$

Q is the double layer constant and proportional to active area, $j = \sqrt{-1}$, ω is the angular frequency, and α is the exponential constant between zero and one [62]. Aperture impedance should dominate the system when the particle exists in it, satisfying the below equation:

$$\left| \frac{1}{Q(j\omega)^\alpha} \right| \leq |Z_{ch}| \leq \left| \frac{1}{j\omega C_{st}} \right| \quad (2.16)$$

Taking out Z_{ch} from Equation 2.17 we get,

$$|Z_{ch}| \geq \left(\frac{C_{st}}{Q} \right)^{\frac{1}{1-\alpha}} \quad (2.17)$$

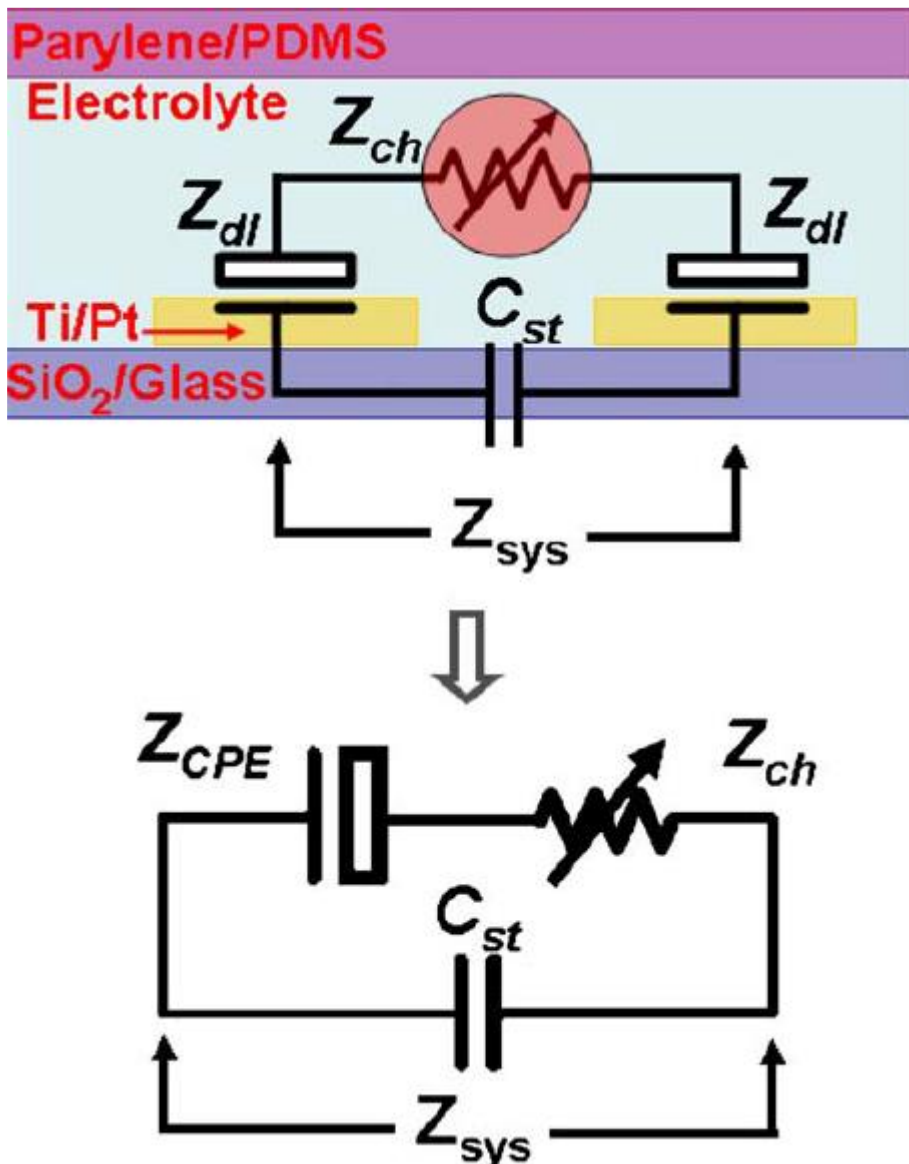


Figure 2.15: Top figure shows the electrical components demonstrating the channel, and double layer impedances with stray capacitance. System impedance is equal to the series combination of channel impedance, double layer impedance and the stray capacitance value. Bottom figure is the electrical equivalent model where the double layer impedance is replaced with constant phase element Z_{CPE} [32].

For a better particle sensing, it is required to have a lower stray capacitance or an increased double layer capacitance Q . At the conditions where the channel impedance satisfies Equation 2.17, system shows asymptotical behaviors. At very low frequencies, the circuit model will take the form of a series connection of the

channel impedance and the CPE and at very high frequencies (> 10 MHz) the system will be the parallel combination of the channel impedance and the stray capacitance and channel impedance will be dominated by C_{st} .

To reduce the double layer impedance, electrodes with large surface area should be employed. However, increasing the surface area of the electrodes, have both positive and negative effects on the measurement system. Big electrodes will generate a larger detection area and this will increase the probability of coincidence and result in unreliable measuring. However, this problem can be solved by creating a relatively small aperture in proportion to the particle diameter, and placing the electrodes on both sides of the aperture. By this method, coincidence error can be fixed. The advantage of employing large thin film electrodes, on the other hand, is that they decrease double layer impedance [31][65]. Another way to reduce double layer impedance is to increase excitation frequency. However, at high frequencies, stray capacitance between sensing electrodes will dominate the system and disallow measurements. Therefore, the excitation frequency should be chosen at an intermediate range that neither double layer impedance nor stray capacitance will dominate the system [42]. In the next section, electrode geometry effect on microfluidic applications and on different electrode structures to reduce double layer impedance will be investigated.

2.2.3.3 Electrode Geometry Effect on Measurement System and Electrode Structures used in Coulter Counters

Microelectrodes are used in different applications such as dielectrophoresis [66], electrorotation [67], electrofusion [68], and electrical impedance [44], [57], [61], [69], capacitance [37] or inductance [39] sensing. There are mainly four types of electrode structures that can be employed inside a microchannel: sputtered planar electrodes, electroplated vertical side wall electrodes, sputtered electrodes on the side walls of the anisotropically etched trapezoidal channels, symmetrically placed

surface electrodes on top and bottom layers of the channel as a result of anodically bonded wafers [70] [42]. In Figure 2.16 surface and side wall electrodes including E-field distributions along the depth of the channel are shown. In Figure 2.16 (a) surface electrodes generates the highest electric field on the bottom part of the channel and the intensity of it decreases along with the height. This type of electrode structure is not very suitable for electrical sensing if the channel height is not comparable with the particle diameter. Because, the resistance change of the microchannel will be very small or even negligible if the particle passes from a point close to the top surface of the channel. In Figure 2.16 (b) surface electrodes placed on the side wall of the anisotropically etched silicon wafer are shown. The intensity of the E-field is highest on the bottom edges of the electrodes and gradually decreases along the z direction. However this decrease is not as much as the coplanar electrodes; therefore, they are more suitable for particle sensing. The electroplated electrodes shown in Figure 2.16 (c) provide a uniform E-field along the channel and are the best for particle sensing however electroplating is the most troublesome method among all, in terms of fabrication, therefore not preferable. Considering all these effects, different kinds of electrode structures were designed to prevent electrode polarization and provide a good spatial resolution. In 2001 Gawad et al. [44] designed Ti/Pt sputtered electrodes on the bottom of the channel and performed differential measurements. Even though their results were satisfying for the 10 μm polystyrene particles, due to the non-uniformity of the E-field, they could not get the same satisfying results with the 5 μm and 8 μm particles. Gawad et al [44] also investigated the difference in electrode alignments and compare the analytical results with the Finite Element Method (FEM) results. They concluded that the analytical results of the up- and downstream electrodes match with the FEM results by only 80% and this is due to the inhomogeneity of the current density nearby the cell. Even though the coplanar electrodes generated a lower impedance change, they are favored due to ease of fabrication. In 2003, Oh et al. [71] fabricated nano-gap electrodes to overlap double layers and reduce its effect on impedance measurements.

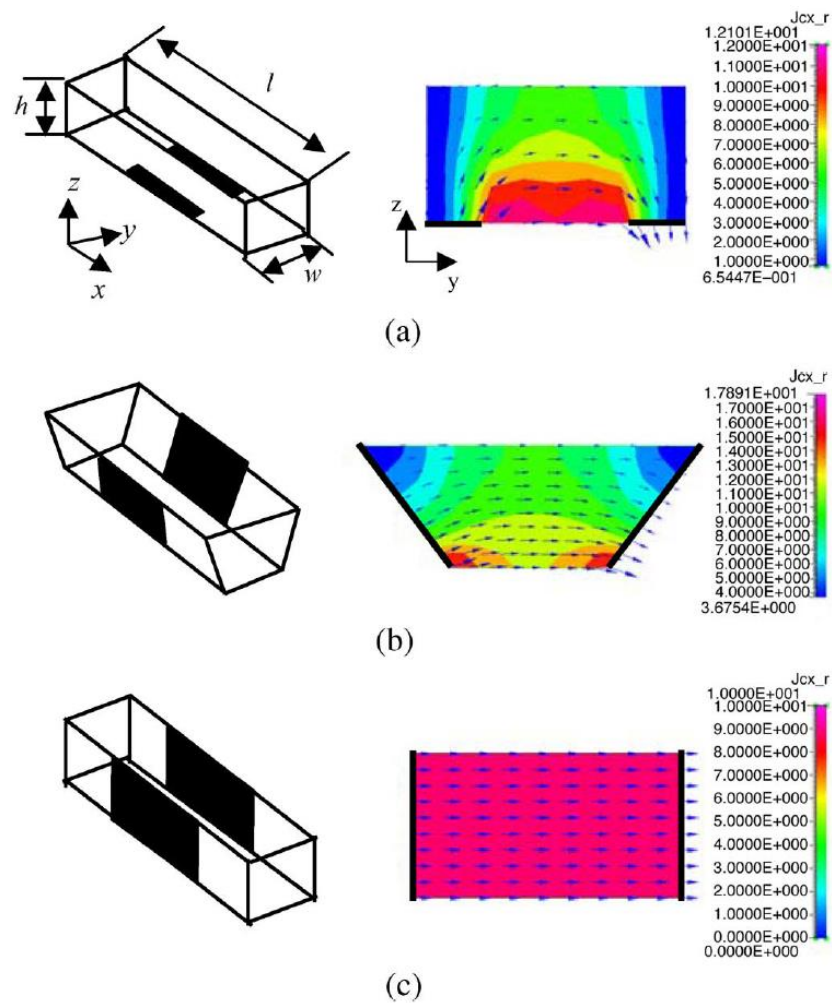


Figure 2.16: Diagram of microelectrodes with different geometries. (a) Sputtered electrodes on the bottom surface of the channel. (b) Side wall electrodes sputtered on silicon wet etched channel. (c) Side wall electroplated electrodes [70].

They stated that, in the microscale channels, the EDL occurs on the surface of the electrodes and the equivalent circuit is modeled as a series connection of double layer impedance and the sample impedance. However, for nanogap channels ($<100\text{nm}$) the EDL occupies the whole region between the electrodes thus, the electrical model turns into a parallel combination of the double layer impedance and sample impedance. By this method, they detected the DNA hybridization without

labeling. Jagtiani and Zhang et al. [10], [11] demonstrated the Ag/AgCl non-polarizable electrodes for DC detection systems but the fabrication of these electrodes was cumbersome and they have short-winded operation time. Another method to reduce electrode polarization effect is the electroplating technique. Zheng et al. [32] used electroplated platinum black electrodes to sense 5 μm and 10 μm polystyrene beads together with leukocytes and erythrocytes. Due to the porous surface of these electrodes, a large surface area is achieved and electrode polarization is reduced effectively. Measurements were performed successfully under 10 kHz. However electroplating is cumbersome and non-uniformities regarding the size of the electrodes are expected. In addition, platinum black electrodes require conditioning in the electrolyte for a long time before they are ready to use. Wu et al. [72] also used electroplated gold electrodes with DC excitation voltage to sense the latex microparticles having 5, 10, and 15 μm diameters and fibroblast cells with 19 μm diameter. Gold is a preferred material since it does not require conditioning like platinum black electrodes. In recent years, alternative electrode materials such as liquid or gel were used to investigate the electrode polarization. In 2012, Richard et al. [73] used liquid metal electrodes filled with Eutectic Gallium-Indium (EGaIn) to detect 20 μm and 60 μm polymer resin microspheres. The fabrication of the device requires just one mask and can work at low frequencies. Even though the double layer impedance could not be totally neglected with this design, successful measurements were performed. Mei et al. (2012) [34] developed an off-the-shelf gold pins to count microparticles with diameter size ranging from 7.6 μm to 14.7 μm . Since the electrodes do not touch the fluid, electrode polarization problem was solved. In 2013 Choi et al. [74] designed a novel T-shape channel structure. Sample fluid flows through the vertical channel and lateral channel is filled with polyelectric gels for detection. When a DC excitation voltage is applied to the detection channel, a current density occurs on the central region of the channel and existence of the particles creating a resistance change directly affects this current density.

2.2.3.4 High Throughput Coulter Counter Designs

Single channel Coulter Counters in literature provided reliable and accurate results so far; however, the analysis time is considerably long and they cannot process a large volume of sample in a short period of time. Therefore, high throughput particle counter devices were designed. In 2005 Lee et al. [66] designed a microchannel with double electrical sensing zones placed at the inlet and outlet of the device shown in Figure 2.17. Concentration of the solution was determined by counting the cells from both sensing zones and taking the difference. The results obtained with RBC, were compared with the commercial hemocytometer and it is shown that double electrical sensing zone provides better results for determining the sample concentration with an error rate of 16.1%.

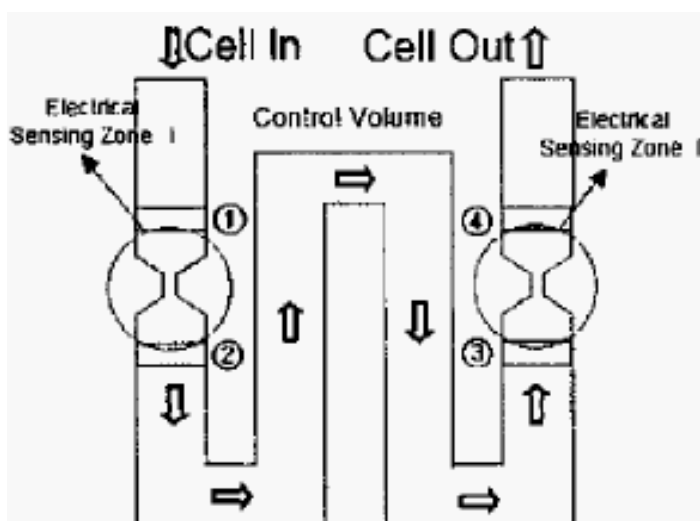


Figure 2.17: Coulter Counter with double sensing zones at the inlet and outlet of the device [65].

Employing multiple channels and achieving a high throughput by using large amount of sample and decreasing processing time were introduced by Jagtiani et al. [3], [11], [75]. In 2006 Jagtiani and his colleagues [36] developed a four channel

Coulter Counter to detect and differentiate polymethacrylate and pollen particles. The device consists of one main reservoir connected to four peripheral reservoirs by mini channels (Figure 2.18). Each mini channel works as a separate Coulter Counter and includes a polymer micro aperture in it for sensing. Ag/AgCl electrodes were preferred since they reduced the electrode polarization greatly. 300% efficiency compared to single channel coulter counters was achieved and the device also distinguished same size polymethacrylate and pollen particle from different surface charge properties. Even though the device was able to detect different particles in a shorter time, four reservoirs occupied a large area and expectedly enlarged the size of the design. In addition, four separate detection circuits with data acquisition cards are needed to run this system, increasing the complexity and the cost of the device. In 2010, Jagtiani et al. [75] developed another design to perform multiplexed counting. By using amplitude modulation technique, individual signals from each channel were multiplexed and combined. To detect the combined response, only one detection circuit was required. The device schematic and the electrical detection circuit are given in Figure 2.19. Main channel is divided into four separate channels by soft lithography techniques without adding extra inlets. One side of major electrode is excited by DC voltage whereas the other side is connected to the negative terminal of the OPAMP. Each central electrode is excited with an AC signals with a fixed frequency. All individual currents are directed into the inverting summing amplifier and the combined response is obtained. By demodulating the signal and employing peak detection algorithms, individual peaks corresponding to the passage of the particles were obtained. By this method, Jagtiani et al. detected and counted 30 μ m latex particles with an efficiency of 300% compared to traditional single channel Coulter Counters.

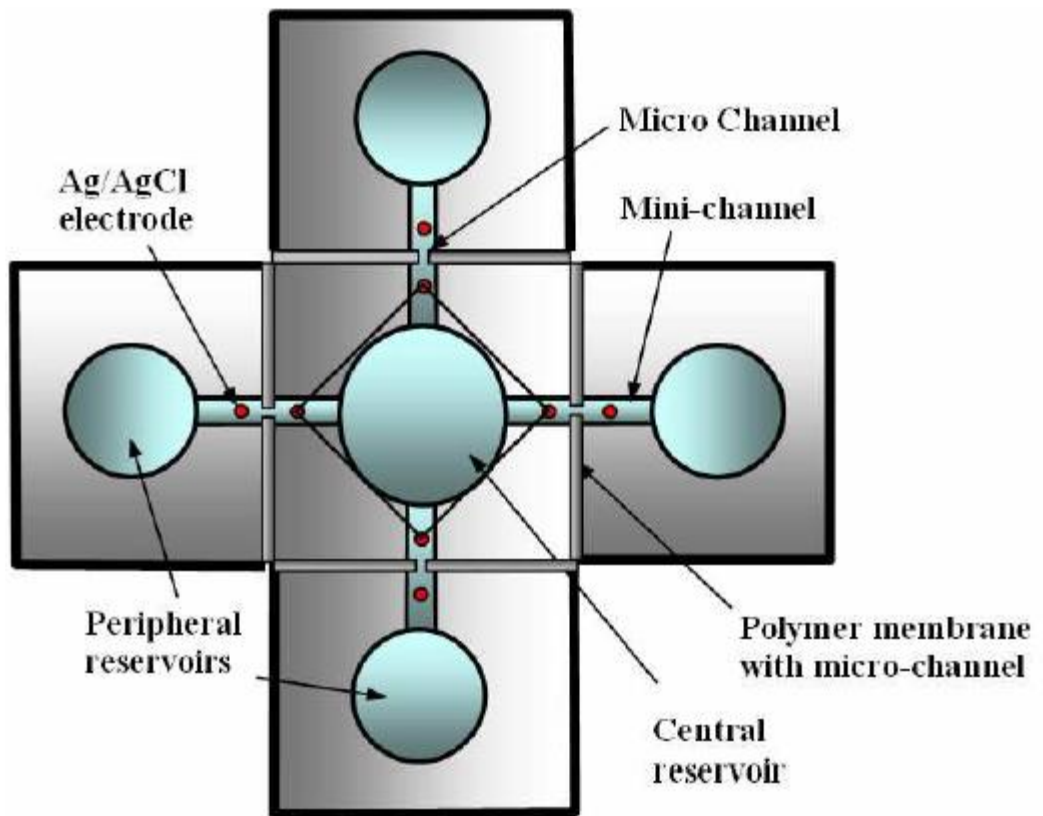
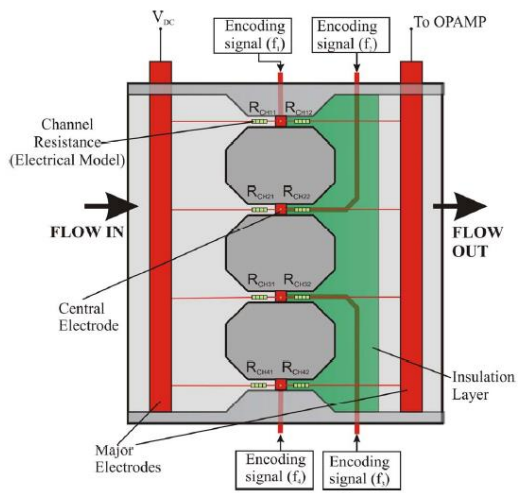
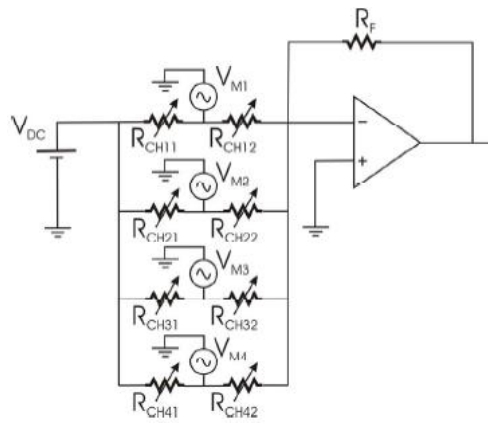


Figure 2.18: Four channel Coulter Counter. Minichannels are divided by polymer microapertures and detection is performed by Ag/AgCl electrodes placed on both sides of the membrane [11].



(a)



(b)

Figure 2.19: Four channel Coulter Counter developed by Jagtiani. Both DC and AC signals are employed to detect the signals. Signal multiplexing technique was used to eliminate the extra need for DAQ boards [75].

CHAPTER 3

ELECTRICAL MODELING AND SIGNAL PROCESSING OF COULTER COUNTERS

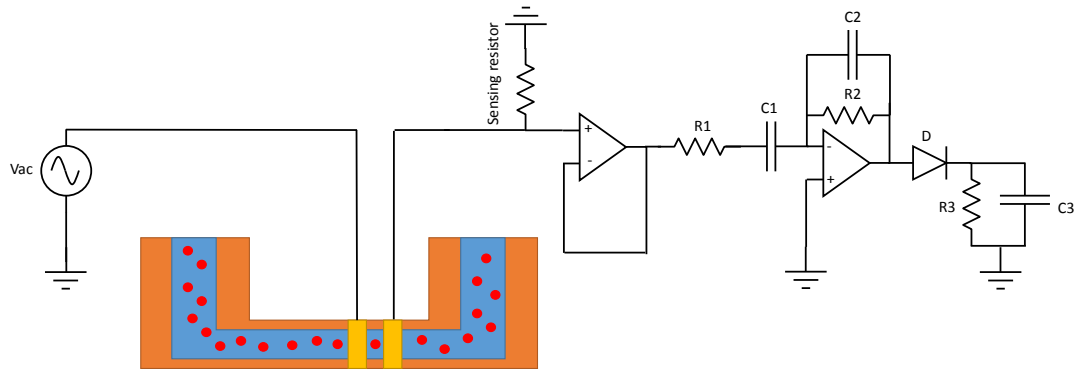
This chapter explains the cell detection method in a conductive medium and amplitude demodulation technique to obtain the desired signal. Single channel Coulter Counter is utilized to explain the phenomena. Then, two-sided microaperture technique is introduced to show the novelty of the design. A medium with a conductivity of 2.28 mS/cm was used. As explained in the previous chapters, a particle passing through the sensing area increases the resistance. This change results from the replacement of the fluid in proportion to the particle volume occupying the aperture. When AC excitation voltage is used for experiments, the traversal of the particle will change the value of the base voltage, in other words modulate the amplitude of the signal. Therefore by employing demodulation methods, desired signal can be obtained. The schematic of the single channel Coulter Counter together with the cell and particle modeling and the corresponding electrical detection circuit are demonstrated in Chapter 3.1 and 3.3 to explain the amplitude demodulation technique

3.1 Device Description

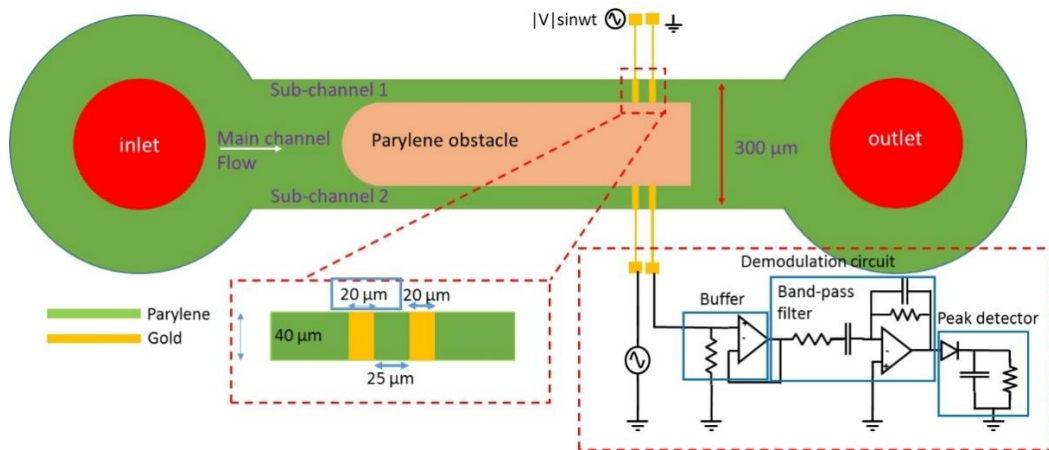
Two different designs were developed in this study. Both designs have almost the same structures but one of them has a single channel whereas the other design has

two channels for multiple analyses. The fluid coming from the inlet port is flowing into the main channel, which has 300 μm length and 30 μm height. The width of the main channel is narrowed down to 30 μm for sensing. In the detection area, a smaller channel whose size is comparable to micro particles is preferred since it provides a sharper peak during the passage of the particle. On the other hand larger channels allow faster flow rates and prevent clogging; therefore, a medium sized channel large enough to prevent clogging and small enough to sense particles accurately is designed. K562 cancer cells used in the experiments have diameter between 12 μm – 20 μm hence, a microchannel with a 30 μm x 30 μm cross section area is ideal for analysis. In addition, a narrowing the main channel removes the necessity of extra inlets required for hydrodynamic focusing and reduces the overall size of the device. Figure 3.1 shows the cross sectional and top view schematics of the design together with the electrical detection circuit for amplitude demodulation. The channels were formed by parylene, a bio-compatible material having excellent properties of the chemical resistance for biological analysis and longer shelf life[32]. Second design has a similar structure except that the main channel is divided into two microchannels, allowing parallel analyses. When the fluid enters the main channel, it is directed into two narrower channels by the help of a parylene obstacle placed in the middle part of the wider channel. Cylindrical shape of the obstacle separates the flow into two equal flows and prevents clogging of particles due to its curved structure. Since parylene is an insulation material, it also blocks the cross talk between the sensing electrodes. Each of the channels works as a separate counter; hence, provides a high throughput counting. Creating a channel inside a wider channel is the novelty of the second design that eliminates the extra inlets and reduces the size of the device. In both designs, planner gold electrodes at the bottom surface of the microchannel provide sensing. In literature, coplanar electrodes were criticized for not providing a uniform electric field along the height of the channels; however for our case, the channel dimensions are comparable with the particle diameters, and thus, the electric field intensity even at the upper part of the channel is enough to sense particles. Measurements are recorded over a sensing resistor,

placed in series with the channel resistance. This relatively small resistor creates a voltage division and provides an easier sensing.



(a)



(b)

Figure 3.1: (a) Cross-sectional and (b) top view schematics of the single channel Coulter Counter, together with the detection circuit.

3.2 Microparticle and channel resistance modeling

The biological cells possess complex structures such as cytoplasm and membrane; therefore, electrical equivalent models are developed to study them. Cell membrane protects the cell from external damages and also works as an insulation layer. By

its semi-permeable structure, it allows specific molecules to penetrate inside the cells while blocking others. Thickness of the membrane ranges between 5nm to 10nm [76]. The cell membrane can be modeled as a parallel combination of a capacitor and a resistor. Two very low conductive phospholipid layers in which a dielectric structure exists form the basis of this electric model. On the other hand, cell cytoplasm includes cytosol and organelles and it is high conductive due to the dissolved organic materials in it. Electric model of the cytoplasm can be represented as a resistor or a series combination of resistor and capacitor. Therefore, Foster and Schwan [77] developed the cell suspension impedance as the series combination of cell membrane and cytoplasm impedance in parallel with the conductive medium. The schematic showing this relationship is given in Figure 3.2. To be able to comprehend the fundamentals of particle passing from the detection area, complete electrical circuit including electrode solution and particle impedances is required. Gawad et al. [44] developed a model including double layer effects, stray capacitance, membrane capacitance, cytoplasm resistance, and cell size (Figure 3.3). As mentioned in Chapter 2.2.3.2 double layer impedance is dominant in low frequencies < 20 kHz and parasitic capacitance occurring between the electrodes is dominant for frequencies above >100 MHz. Therefore while designing a Coulter Counter, it is important to choose an intermediate frequency range which increases double layer capacitance and decreases stray capacitance, hence, make the channel impedance dominant in overall. To achieve this aim, electrodes with larger surface area is preferred. Keeping the spacing between the electrodes large and designing long microchannels are other factors that can eliminate undesired effects.

3.3 Signal Detection

Passage of the particles was detected by sputtered gold electrodes on the bottom of the channels and measured by the sensing resistor connected in series with the channel resistance. When a particle is in the detection area, it increases the

resistance. According to Ohm's Law, $V = I * R$ voltage also increases in proportion to the resistance increase.

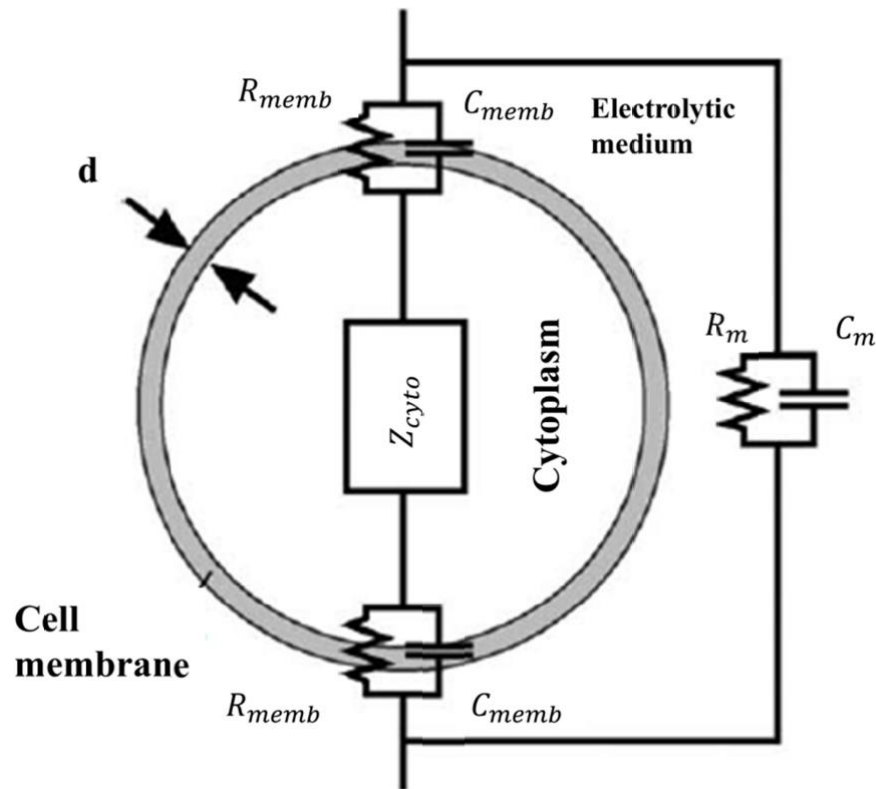


Figure 3.2: Electrical cell modeling of a biological cell and conductive medium Membrane of the cell and electrolytic medium is modeled as the parallel combination of resistor and capacitor whereas cytoplasm is modeled as an impedance [78].

However, the divided voltage on the sensing resistor decreases. This situation is simulated with MATLAB and shown in Figure 3.4. As it is seen, increasing the channel resistance value decreased the output voltage of the sensing resistor. In the bottom figure, channel resistance is the lowest therefore output value has the

highest. Output signal includes the noise coming from the nature of the device and environmental facts therefore it needs to be filtered

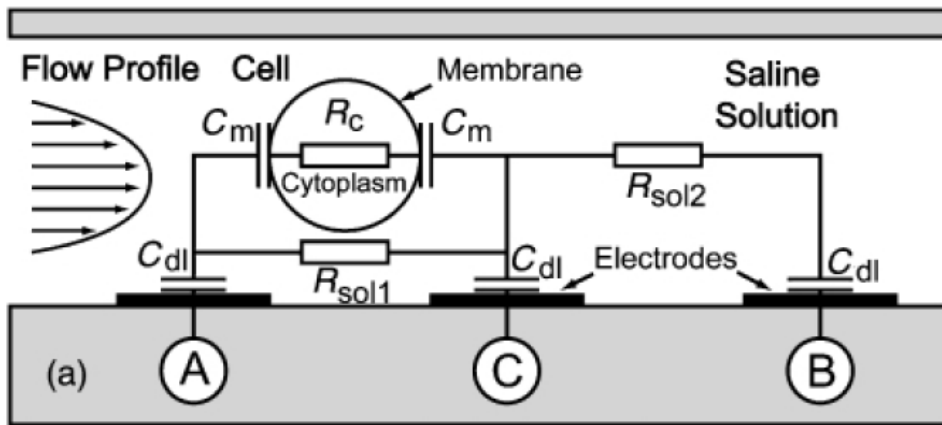


Figure 3.3: Electrical model of a suspending medium and electrode / electrolyte interface during the passage of a particle. When the particle is at the sensing zone, electrical resistance is equivalent to the parallel combination of the resistance of the particle and the solution. Double layer is modeled as a capacitor in series with electrode resistance [44].

A bandpass filter is used to filter out all frequencies other than the ones centered on the excitation signal. The filtered signal is then passed through the envelope detection circuit to get the instantaneous peaks occurring on the base signals. Here it is worthwhile to note that, particle passage creates a negative peak called as valley or troughs. Electrical equivalent circuit showing the channel resistance and the sensing resistance is shown in Figure 3.5.

R_{ch} indicates the channel resistance when the channel is filled with only liquid and there is no particle present in the sensing region. The value changes when the particle enters the detection zone. Depending on the surface charge, resistance may increase or decrease. For cylindrical channels, resistance value of the detection area is calculated as follows:

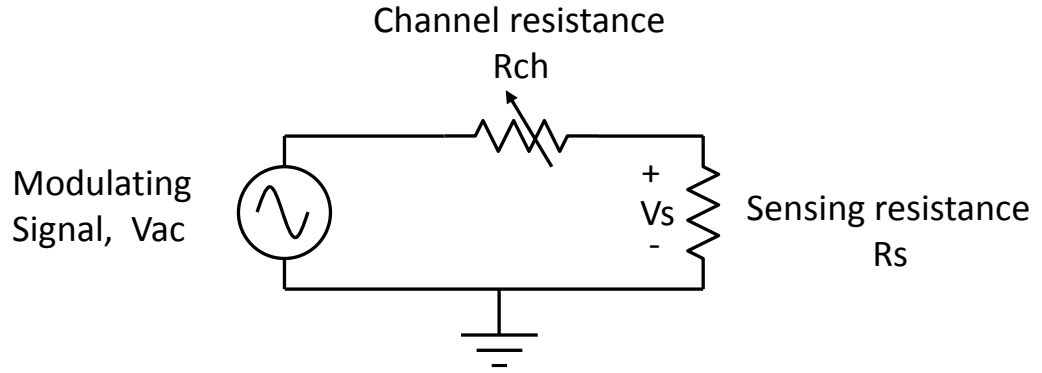


Figure 3.4: Channel resistance changes during the passage of the particle and this change is recorded on the sensing resistance.

$$R = \rho \frac{l}{A} \quad (3.1)$$

where, l is the length and A is the cross section area of the channel and ρ is the medium resistivity ($\Omega.m$). The increase in the channel resistance decreases the output voltage on the sensing resistance due to voltage division rule. The output voltage V_s is calculated as:

$$V_s = V_m \frac{R_s}{R_s + R_{CH}} \quad (3.2)$$

where, V_m is the modulating AC voltage excited with a fixed frequency. Change in the channel resistance is the critical value in this equation. If it is very small compared to the base resistance value, it cannot be detected.

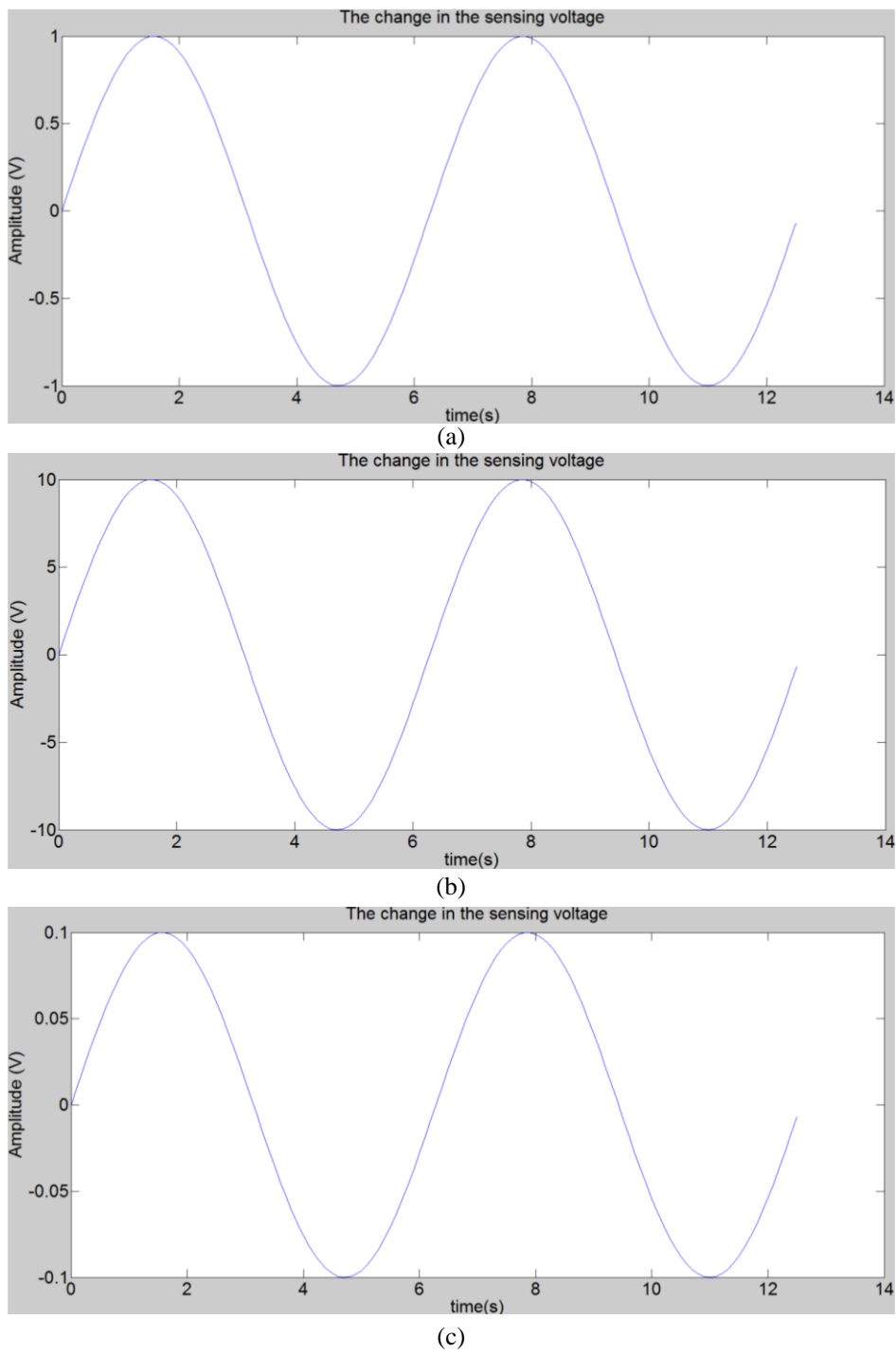


Figure 3.5: Change in the output voltage relative to the change in sensing resistor

The change in the resistance for the particles whose diameters are comparable to the channel dimensions is expressed as:

$$\frac{\Delta R}{R} = \frac{d^3}{LD^2} \left(\frac{D^2}{2L^2} + \frac{1}{\sqrt{1 + \left(\frac{D}{L}\right)^2}} \right) \quad (3.3)$$

where ΔR represents the deviation from the base resistance value R . d is the particle diameter, D is the aperture diameter, and L is the length of the aperture [15]. For the microchannels fabricated by soft lithography techniques, there is a need for a diameter conversion to the rectangular dimensions since the channel is not cylindrical. The corrected diameter formula is given as:

$$D = \sqrt{\frac{4wh}{\pi}} \quad (3.4)$$

where w and h represent the width and height of the microchannel respectively. For a particle with 20 μm diameter suspended in a medium with resistivity 4.48 $\Omega\text{-m}$, passing through a microchannel with 25 μm (length), 30 μm (height), and 40 μm (width) the resistance change ΔR is calculated as 3.15×10^4 , where the base channel resistance value was 87 k Ω . The ratio of the maximum resistance change relative to channel resistance, $\frac{\Delta R}{R}$, is calculated as 0.3620.

Equation 3.5 calculates the ratio between the detected current pulse, ΔI , and the base current value I . The formula is valid when the channel length is comparable to channel diameter [18].

$$\frac{\Delta I}{I} = \frac{d^3}{D^2(L + 0.8D)} \quad (3.5)$$

CHAPTER 4

DESIGN AND SIMULATION

This chapter explains the design and simulation of micro Coulter Counters developed by our team. Cadence Design Tool Layout Editor® was used for drawing masks, and COMSOL Multiphysics® simulation tool version 3.4 was employed for performing Surface Velocity, Electric Field, and Electrical Resistance simulations. Schematic of the designs are shown in 3D view to enlighten the reader visually and provide a better explanation.

4.1 Design of the Single Channel Coulter Counter

While designing a Coulter Counter, there are important factors that should be taken into consideration. Mainly, these factors are aperture dimension, electrode type and material, excitation voltage, and wafer type. Single Channel Coulter Counter device was designed as a proof of concept and used to understand, experience, and explain the cell counting phenomenon in such devices. Therefore, we tried to stay with the designs in the literature. However, fabricating the channels by parylene technology, and employing 3D and planar electrodes still put this design apart from the traditional designs and adds novelty. 3D schematic of the single channel coulter counter device is shown in Figure 4.1. The conductive medium is introduced into the channel by pressure driven flow and forced to flow through the sensing area. Sputtered coplanar gold electrodes excited with a fixed frequency AC voltage sense the passage of the particles and the raw signal is sent to electrical detection circuit

to analyze and record the desired signal. Rectangular shape electrodes were chosen for ease of lithography and fabrication. The technical drawings of single and double channel Coulter Counters formed in CADENCE are shown in Figure 4.2 and Figure 4.3 respectively. For single channel Coulter Counter, the main channel, carrying the fluid coming out of the inlet port is narrowed down to achieve better sensing. Both electroplated copper and sputtered gold electrodes placed inside the narrower channel are used for sensing. Design parameters, including channel, aperture, and electrode dimensions are provided in Table 4.1

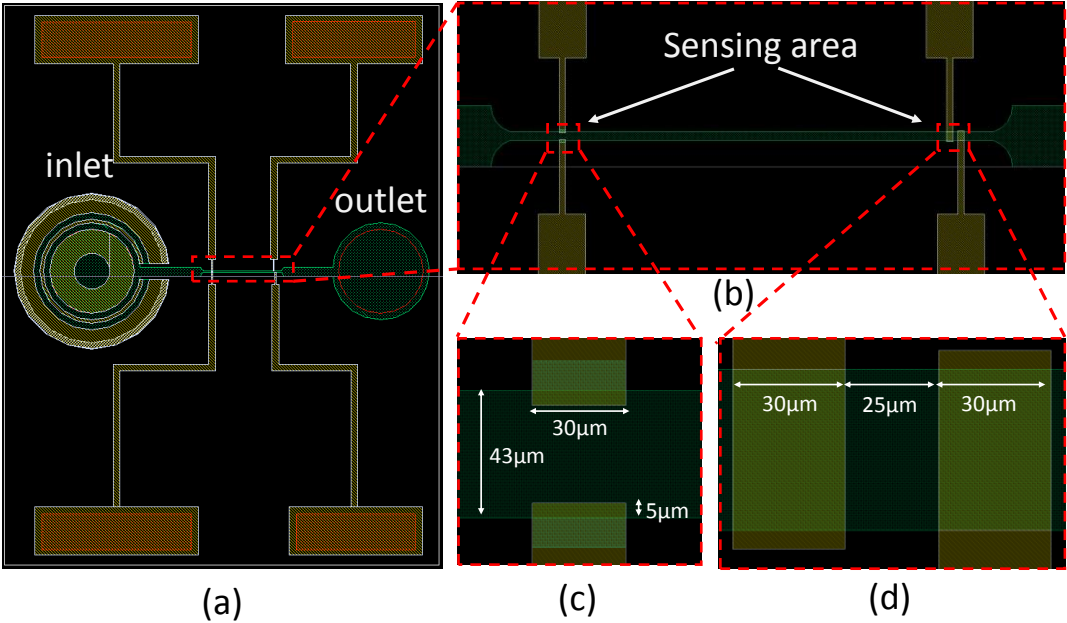


Figure 4.1: (a) Technical drawing of single channel Coulter Counter. (b) Closer view of the narrow channel. (c) Magnified view of the electroplated copper electrodes. (d) Magnified view of the sputtered gold electrode pair.

Table 4.1: Design parameters for single channel Coulter Counter

Parameters	Value
Main channel width	300 µm
Main channel height	30 µm

Table 4.1 (continued)

Narrow channel width	43 μm
Narrow channel height	30 μm
Electroplated copper electrode length	30 μm
Electroplated copper electrode height	30 μm
Electroplated copper electrode width	5 μm
Distance between copper electrodes	33 μm
Sputtered gold electrodes' length	30 μm
Sputtered gold electrodes' height	500 nm
Sputtered gold electrodes' width	43 μm
Spacing between the gold electrodes	25 μm

For double channel Coulter Counter design, the flow, coming out of the inlet port is distributed evenly between two sub-channels. These channels are formed by the help of a cylindrical parylene obstacle, fabricated by soft lithography techniques. The obstacle also works as an insulating layer due to the nature of the parylene and prevents the cross talk between the electrodes. The dimensions of the sub-channels are exactly same to stabilize the flow. Therefore, only one sub-channel design parameters are introduced in Table 4.2 together with the other features in the design.

The device schematics drawn in CADENCE can be transported into COMSOL as a .gds file. This allows the user to do simulations without defining all the features from the scratch. Since an exact copy of the features, which will be printed on the mask, is transported into the COMSOL, the results will be more reliable and provide the most realistic test scenarios.

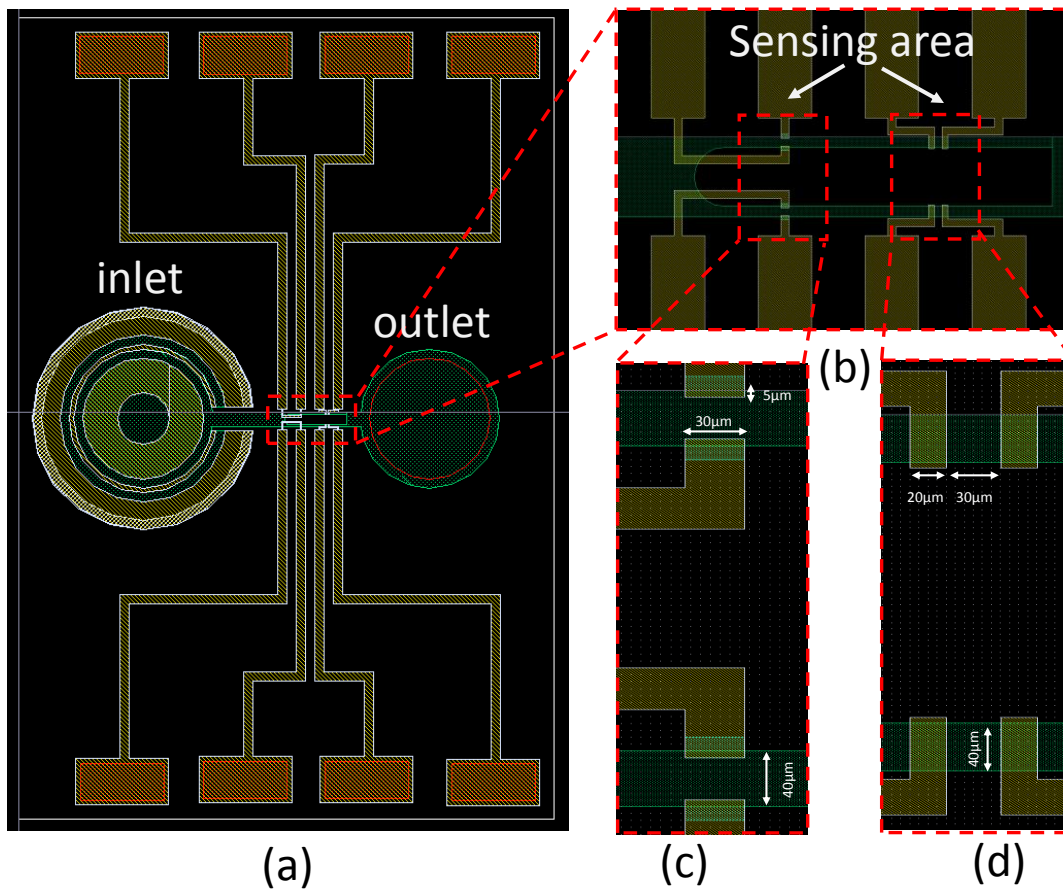


Figure 4.2. (a) Technical drawing of double channel Coulter Counter. (b) Closer view of the sub channels and cylindrical parylene obstacle. (c) Magnified view of the electroplated copper electrodes. (d) Magnified view of the sputtered gold electrode pair.

Table 4.2: Design parameters for double channel Coulter Counter

Parameters	Value
Main channel width	300 μm
Main channel thickness	30 μm
Narrow channel width	40 μm
Narrow channel thickness	30 μm
Parylene obstacle length	1.3 mm
Parylene obstacle width	220 μm

Table 4.2 (continued)

Parylene obstacle thickness	30 μm
Electroplated copper electrode length	30 μm
Electroplated copper electrode height	30 μm
Electroplated copper electrode width	5 μm
Distance between copper electrodes	30 μm
Sputtered gold electrodes' length	20 μm
Sputtered gold electrodes' height	500 nm
Sputtered gold electrodes' width	40 μm
Spacing between the gold electrodes	25 μm

4.2 COMSOL Simulation Results

There are three important scenarios that should be considered for Coulter Counters before fabricating any of these designs.

1. Flow profile and particle tracing simulations,
2. Electric field and surface current density simulations, and,
3. Resistance change simulations during the passage of the particle from the aperture.

4.2.1 Flow profile and particle tracing simulations

Flow profile simulations form the basis of microfluidic devices. Since Coulter Counters' working principle employs microfluidics, designing an effective channel will yield reliable and accurate results. Simulations help the designer to foresee the possible problems and allow to fix those before fabricating the device. One of the most important problems of microchannels is the clogging. It occurs when the channel dimensions are very close or even same with the particles flowing inside

the inside a microchannel. When this is the case, particles lose their velocity either in the sharp edges of the channel or in the narrow regions. Accumulation of these particles in those regions clogs the channel and block the flow. This is an irreversible problem and makes the device useless and irreproducible. Another problem is the unstable flow, which creates turbulences and air bubbles. Reynolds number calculation (Equation 4.1) is used to see the characteristics of the flow.

$$Re = \frac{QD_H}{vA} = \frac{VD\rho}{\eta} \quad (4.1)$$

In this equation, Q is the volumetric flow rate (m^3/s), D_H is the hydraulic diameter of the microchannel or pipe (m), v is the kinematic viscosity (μ/ρ) and A is the cross sectional area of the microchannel or pipe. V denotes the velocity of the flow (m/s), D is the diameter of the pipe (m), ρ is the density of the fluid (kg/m^3) and η is the dynamic viscosity ($\text{kg}/\text{m}\cdot\text{s}$). If the Reynolds number is bigger than 4000, turbulent flow occurs. Reynolds number was calculated as 0.8 for the parameters used in our experiments given in Table 4.3.

Table 4.3: Design parameters for particle tracing simulations

Parameters	Values
Velocity of the flow (m/s)	0.018
Diameter of the microchannel (μm)	40
Density of the medium (kg/m^3)	1000
Dynamic viscosity of the medium ($\text{kg}/\text{m}\cdot\text{s}$)	8.92×10^{-4}

Considering all these facts, 2D simulations, demonstrating surface velocity field for single and double channel Coulter Counters, were performed. Incompressible Navier Stokes equation already defined in COMSOL environment was used to determine particle velocity and trajectory.

$$L_{entr} \nabla_t \cdot [pI - \eta(\nabla_t u + (\nabla_t u)^T)] = -\eta p_{entr}, \nabla_t u = 0 \quad (4.2)$$

where u is the average velocity, $P_{o, entry}$ is the entrance pressure and L_{entr} is the entrance length. The boundary conditions are defined as follows: Channel walls are defined as no slip, inlet port is defined as an average velocity and the outlet is defined as pressure with no viscous stress.

COMSOL allows the user to define boundaries, such as inlets, outlets, and walls, along with the average velocities or entrance pressures. Figure 4.3 shows a COMSOL window to input all the required values for inlets. It is important to note here that the medium passes through the tubing before reaching the inlet port hence losing its initial velocity. Laminar flow is a suitable boundary condition to simulate this phenomenon. When modeling the device, it is also important to note that entrance length (L_{entr}) should be comparable to the length of the tubing to take the velocity loss into account. Figure 4.4 and 4.5 shows the surface velocity field distribution of single and double channel Coulter Counter devices. Streamline surface distribution is chosen to demonstrate the particle tracing and investigating particle trajectories to see the possible clogging or turbulence inside the channel. As it is seen from both of the graphs, the velocity of the flow is slower in the wider region and increase towards the narrower region by ten times in single channel and five times in each sub-channels in the double channel Coulter Counter devices. In addition, no particle clogging or unstable flow is observed along the channel. Therefore, we can state that the fabricated channel is not supposed to create any problems and provide accurate results.

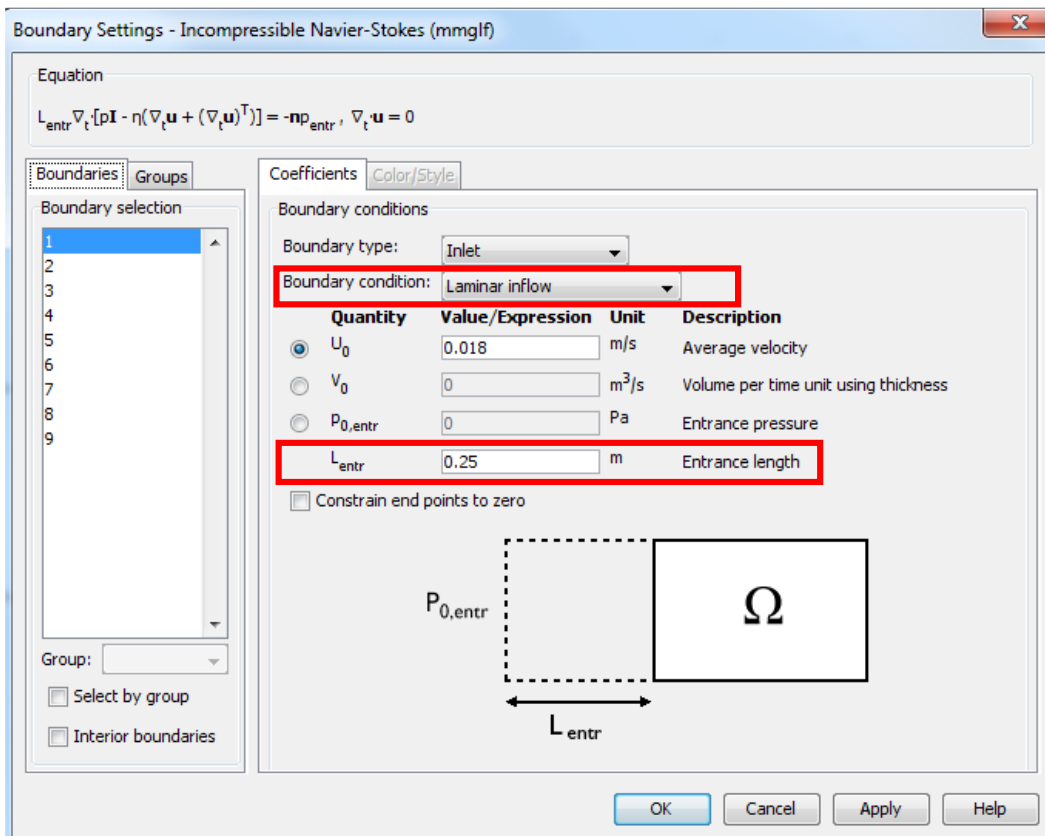


Figure 4.3: COMSOL boundary setting window in Incompressible Navier-Stokes module.

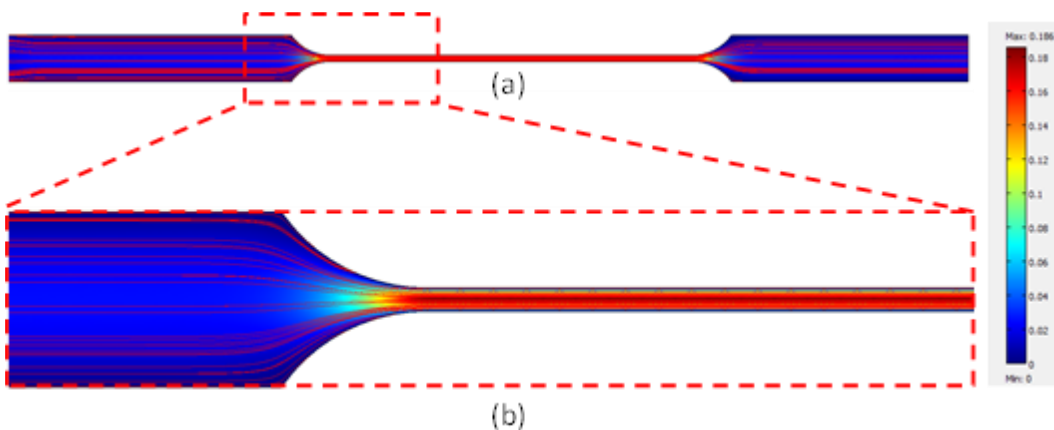


Figure 4.4: (a) Surface velocity field of the single channel Coulter Counter. (b) Magnified view of the narrower region. Velocity of the flow increases ten times when the channel width decreases from 300 μm to 40 μm .

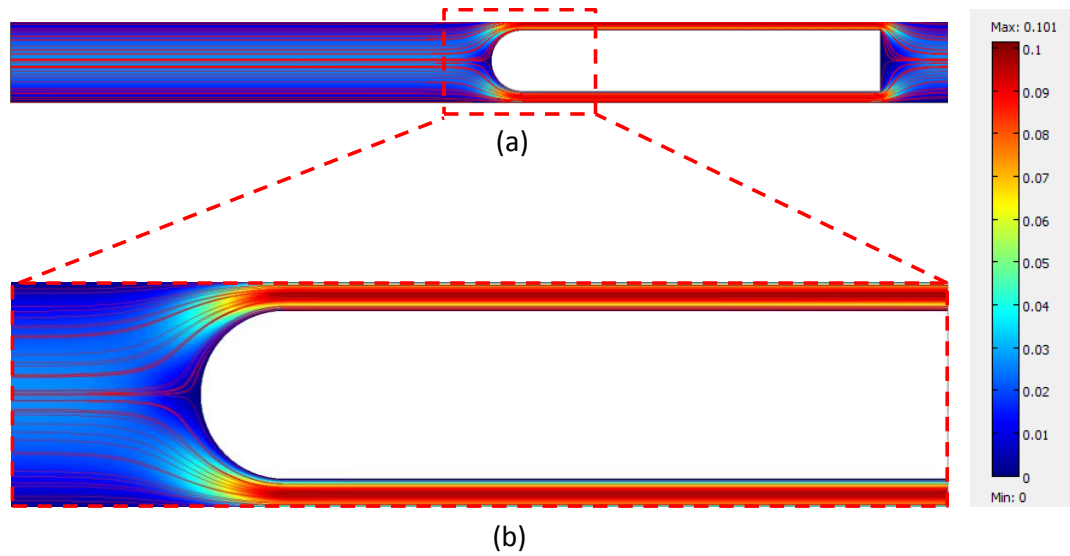


Figure 4.5: (a) Surface velocity field of the double channel Coulter Counter. (b) Magnified view of the narrower region. Velocity of the flow increases five times in each sub-channel when the channel width decreases from 300 μm to 40 μm .

4.2.2 Electric Field and Current Density Simulations

As stated in the Chapter 2, sidewall electrodes generate uniform electric field (E-field) and provide better sensing whereas coplanar electrodes are easier to fabricate but generate a non-uniform electric field. If the channel dimensions are relatively larger than the particle dimensions, sensing may not be achieved with coplanar electrodes. Because, the electric field intensity is highest at the edges of the electrodes and it follows a trajectory from the excited electrode to grounded electrode. The E-field intensity diminishes gradually along the height of the channel and disappears eventually. However; in both designs, channel diameter is comparable with the particle diameter, therefore the passage of the particle falls into the stronger region of the electric field and an accurate sensing is achieved. For 3D electrode structures, E-field intensity is constant along the height of the channel; therefore, these electrodes provide better sensing. Simulations regarding surface

electric field and current density were performed in COMSOL 4.3b Multiphysics under Electric Current (EC) module. To be able to perform these simulations, both coplanar and 3D electrodes should be excited with either AC or DC voltage. In our case, we used AC voltage with a fixed frequency. Using terminal and ground options under EC module, one of the electrodes is excited with an AC voltage whereas the other is grounded. Figure 4.6 shows how to define an AC voltage in COMSOL. A represents the amplitude of the signal (V), ω is the angular frequency (rad/s), and t represents the time (sec). Upon defining these variables, time stepping should be adjusted to simulate the signal for the desired timing interval. Figure 4.7 shows how to define time stepping under solver parameters option in COMSOL. In red-dashed box, total simulation time with the specified timing interval is defined. For our case, 50 kHz AC voltage was employed and one period of this signal is investigated. Signal is divided into four parts in which three zero-crossing parts, one positive and one negative peak are included. While plotting the results, the local maxima point is shown. After defining all these variables and adjusting time stepping, current density and electric field norm vectors were investigated for both electroplated and sputtered electrodes. Arrow surface option is included in all simulations to demonstrate the fringing fields. Figure 4.8 shows the change in the current density and electric field vectors during the passage of the particles for single and double channel Coulter Counters. As it is seen, during the passage of a particle, current density is distorted and uniformity is lost. The arrows, travel around the particle instead of passing through it due to the employed frequency range. In lower frequencies (<100 kHz) cell counting is based on just the size of the particles. Therefore, internal structures of the cells do not affect the measurement results. The electric field, on the other hand, follows a stable change. When the particle is away from the detection area, E-field has the highest value, as the particle approaches the detection zone, this value diminishes and reaches its minimum when the particle is at the center of the electrodes. Electrical field equation already defined in COMSOL is solved by the help of Laplace equation and is given as follows:

$$\nabla^2 \phi = \frac{\partial^2 \phi}{\partial \mu^2} + \frac{\partial^2 \phi}{\partial v^2} = 0 \quad (4.3)$$

where ϕ phasor of the AC potential μ , v represents the vertical and horizontal axes. Boundary conditions in the electric field simulations were defined as follows: Channel walls are defined as electric insulation, excitation electrodes are defined as electric potential whereas grounded electrode is ground.

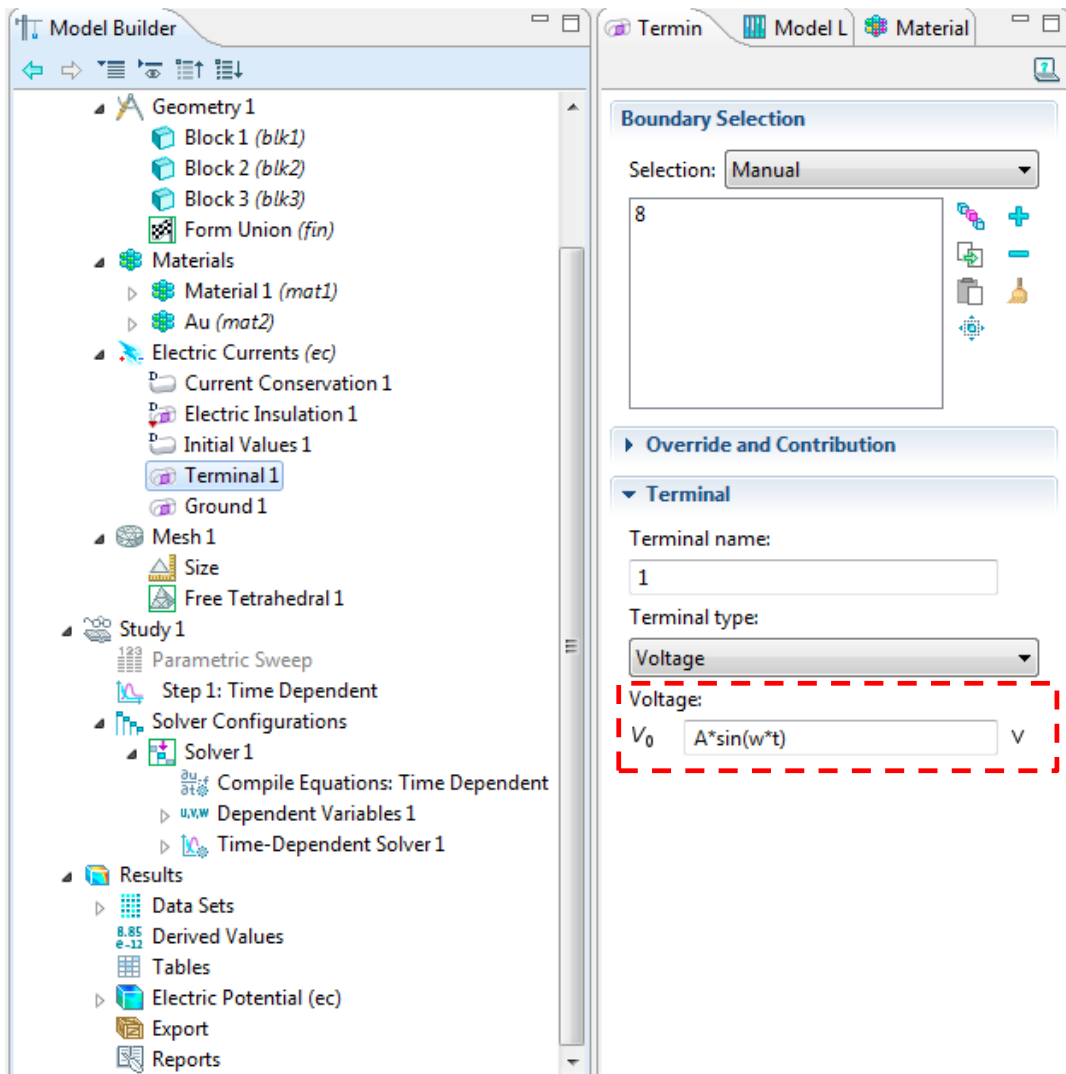


Figure 4.6: Dashed red box shows how to define an AC voltage in COMSOL Multiphysics 4.3b. A , w , and t represent the amplitude (V), angular frequency (rad/s) and time (s), respectively.

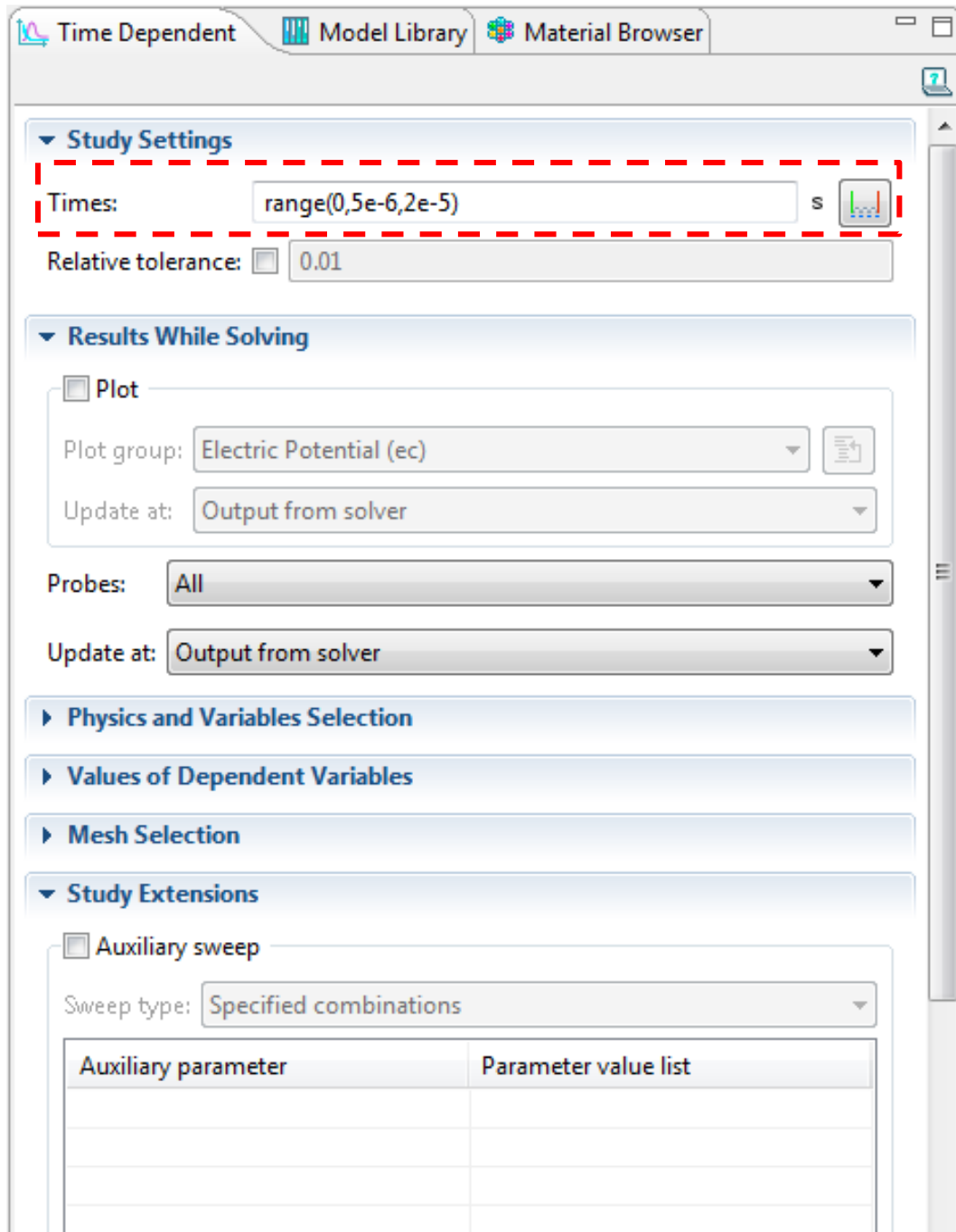


Figure 4.7: Defining the time stepping in COMSOL Multiphysics 4.3b. One period of the signal was investigated in five parts.

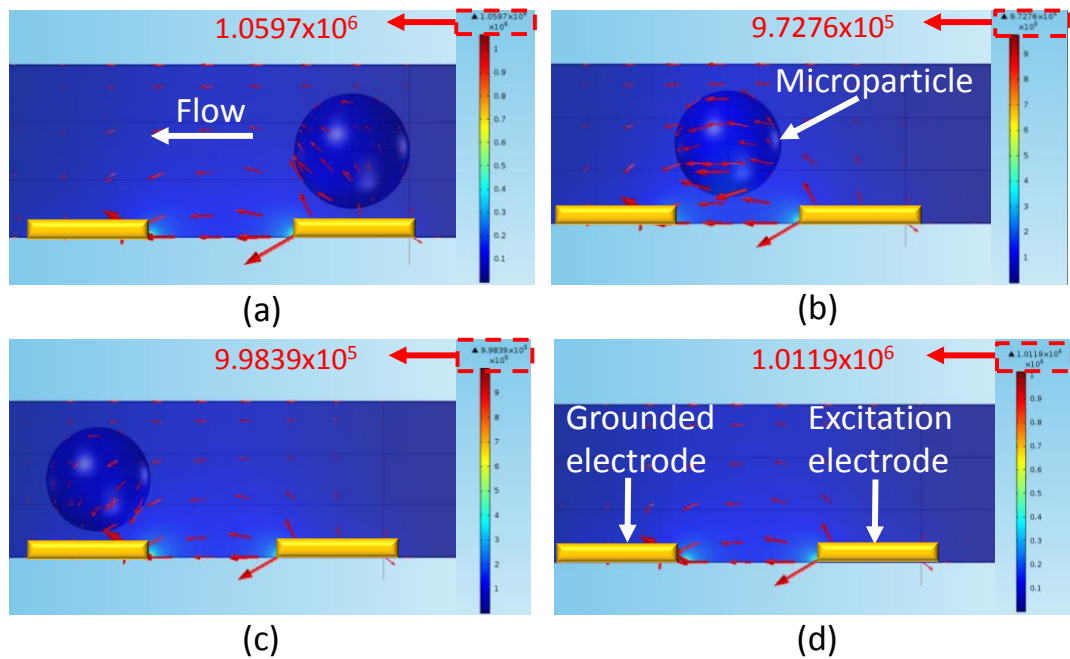


Figure 4.8: Surface electric field and current density simulations of coplanar electrodes in Coulter Counters. (a) No particle inside the detection zone. (b) Particle is at the edge of the excitation electrode. (c) Particle is on the excitation electrode. (d) Particle is at the center of the sensing zone.

4.2.3 Resistance Change Simulations

Resistive pulse sensors' -Coulter Counters- working principle is based on the change of the resistance of the aperture. As the name implies, passage of the particle from the aperture, creates a sharp peak indicating the increase of the channel resistance for a short period of time. The main reason of this increase is the reduction in the area of the aperture (Equation 3.1). Particle inside the pore replaces the same amount of volume in proportion to its size therefore the area of the aperture reduces resulting in an increased resistance.

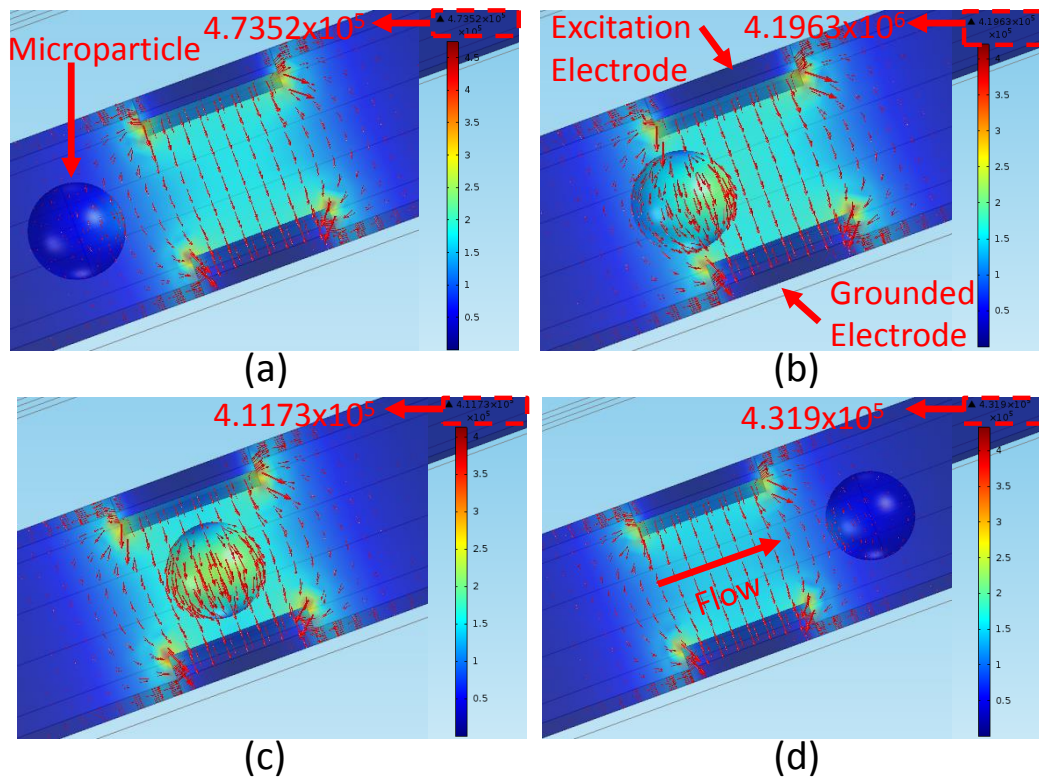


Figure 4.9: Surface electric field and current density simulations of electroplated Cu electrodes (sidewall electrodes) in Coulter Counters. (a) No particle inside the detection zone. (b) Particle is approaching the detection zone. (c) Particle is entering the detection zone from excitation electrode side. (d) Particle is at the center of the sensing zone.

Simulations for resistance change are very similar to the ones for electric field and current density. However, in this case, a current source is applied to one of the electrodes whereas the other is grounded. Similar to hand held multimeters, voltage is read as an output while the current is supplied to the electrodes. By changing the type of the plot from the post processing tools, measured resistance is plotted. Figure 4.8 and 4.9 demonstrate the change in the resistance of the aperture for coplanar and electroplated electrodes, respectively, when particle is present at different locations. As expected, the resistance of the aperture increases for both types of electrodes, when the particle approaches the detection area and reaches the maximum level when the particle is at the center of the pore.

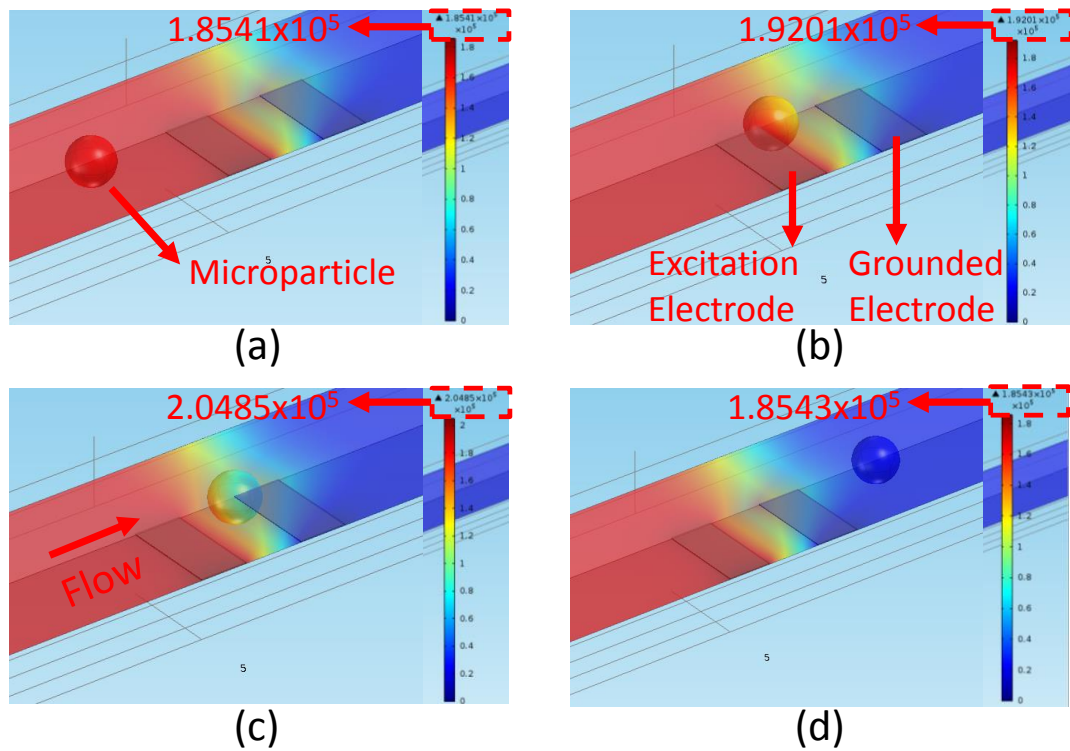


Figure 4.10: Electrical resistance simulations of coplanar electrodes in Coulter Counters. (a) Particle is at the edge of the excitation electrode. (b) Half of the particle is at the sensing zone. (c) Particle is at the center of the sensing zone. (d) No particle in the sensing zone.

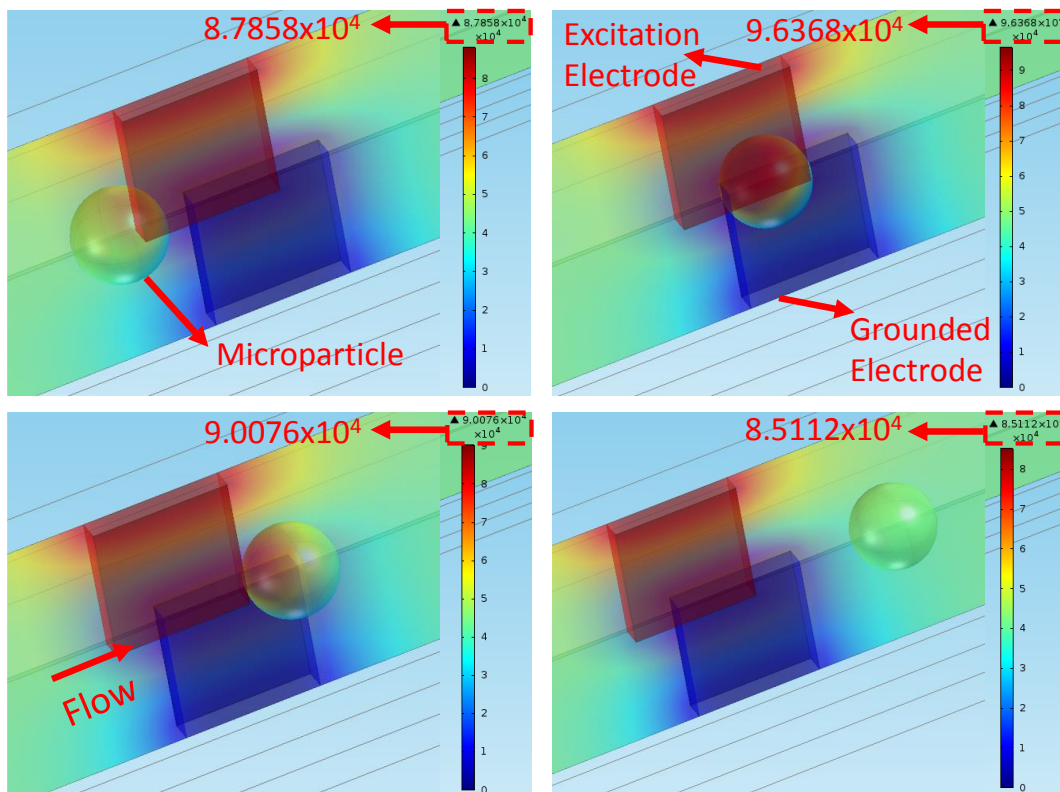


Figure 4.11: Electrical resistance simulations of 3D electrodes in Coulter Counters. (a) Particle is at the edge of the excitation electrode. (b) Particle is at the center of the sensing zone. (c) Particle is at the edge of the excitation electrode. (d) No particle in the sensing zone.

CHAPTER 5

FABRICATION

This chapter explains the fabrication of single and double channel Coulter Counters. Since both designs were fabricated on the same wafer, there is one type of process flow. Surface micromachining, thin film metal coating, and electroplating were utilized during the fabrication. All the details of the process flow together with the necessary pictures are presented in this chapter.

5.1 Process Flow

Fabrication of the single and double channel Coulter Counters requires four masks. First mask is used to create the electrical connections and coplanar electrodes, whereas the second mask is employed to create openings to provide seed layer prior to electroplating step. Microchannel is fabricated with the third mask. The fourth mask is utilized to create openings for obtaining electrical connections to perform measurements. Figure 5.1 shows the process flow diagram. 4" Quartz wafers were utilized for this fabrication due to electrical insulation and transparent surface features of glass.

Fabrication of this process started with piranha cleaning of glass wafers, which creates a rough surface suitable for material coating. Piranha is also responsible of removing the organic contaminants. After piranha etch, glass wafers were immersed into the buffered hydrofluoric acid (BHF) for one minute. BHF is

generally used for etching polysilicate glass or thin film oxide. The first two steps were performed to provide a clean environment before coating steps start. Then, 2 μm parylene coating with silane treatment was performed. According to the optimizations developed for the parylene device in our clean room, it is enough to add grams of parylene that is two times the desired thickness of parylene layer. For example, to coat 2 μm parylene layer, 4g of parylene dimer should be used. Silane is an inorganic material and provides adhesion of parylene to bare glass/silica surfaces. However, when coating parylene on a photoresist surface, no silane treatment is required as it damages the quality of the photoresist.

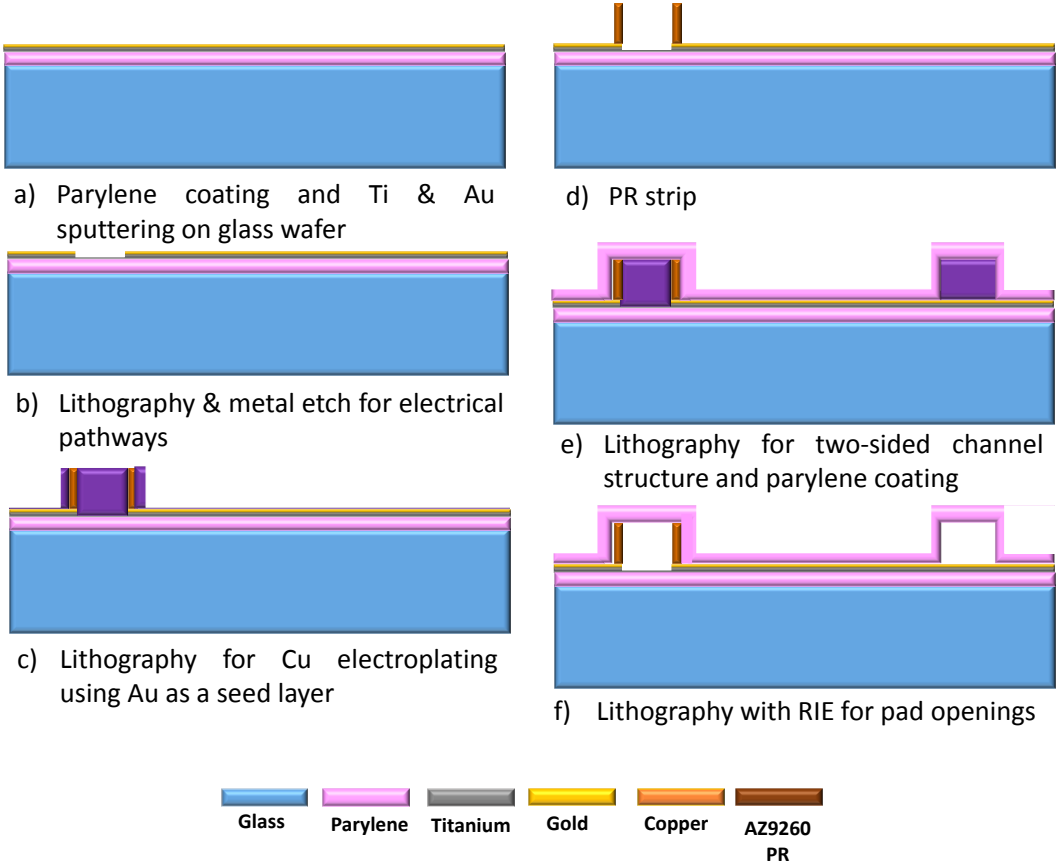


Figure 5.1: Process flow of single and double channel Coulter Counters

After parylene coating, which takes approximately four to five hours, Ti & Au sputtering were performed and a thin layer photoresist S1813 was coated, exposed,

and developed to create coplanar electrodes, electrical connections, and the seed layer prior to electroplating steps. Figure 5.2 shows the 1st mask for a single die to create these features. To pattern the sputtered metals, commercial Au etchant together with custom-made Ti etchant were used. The ratio for preparing a Ti etchant is given as 10 ml HF + 10 ml H₂O₂ + 80ml DI water. Since this etchant is very strong and difficult to control, just ten ml of this mixture is combined with 800 ml of DI water and used to etch the Ti in a controlled way.

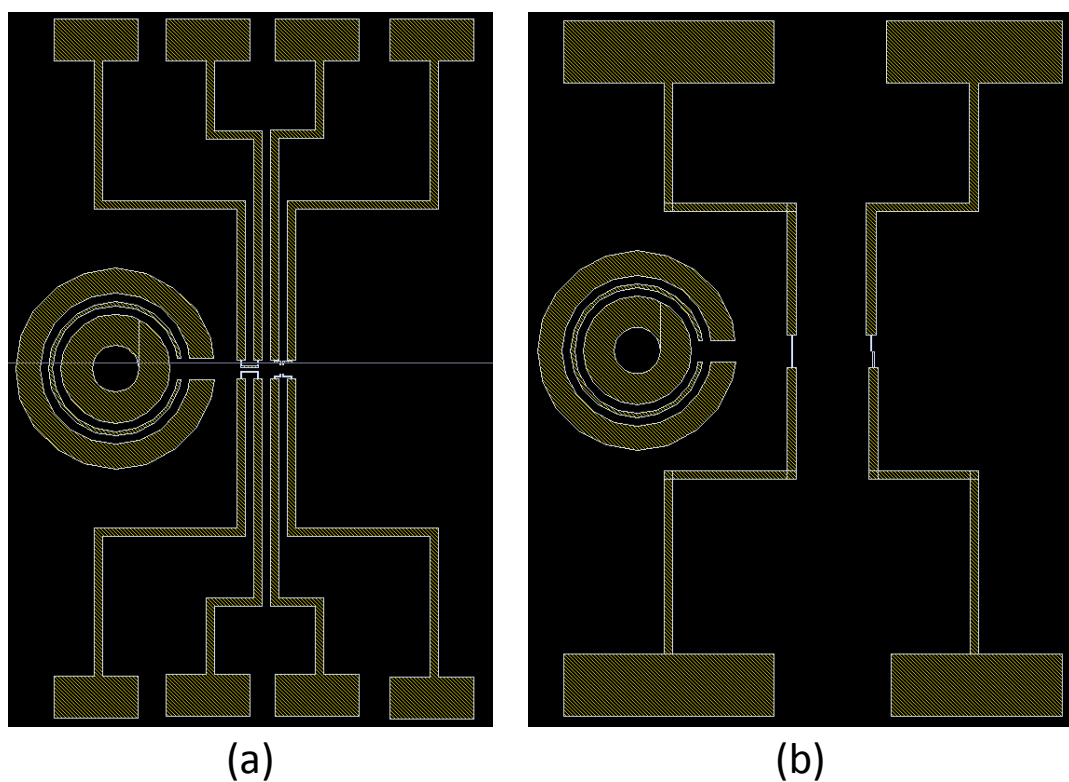


Figure 5.2: 1st mask for generating coplanar electrodes, electrical connections, and seed layer for electroplating step. (a) Double channel (b) Single channel metal mask

Then the wafers were immersed into acetone to get rid of all the etchant on the surface. Then, a thick layer of photoresist (AZ9260) was coated and patterned with double spin and double expose by 2nd mask to create openings for electroplating step

(Figure 5.3). Here it is important to note that, many dummy pads were placed on the 2nd mask for a uniform growing of copper. In general, 8 – 12 cm² of electroplating area provides a controlled and reliable growing. In our case electroplating area was approximately 11 cm². Copper electroplating was performed at 100mA for 65 minutes and as a result, 25-29µm of copper thickness was measured. The height and width of the 3D electrodes were sufficient for sensing and counting both the microbeads and the cells. Figure 5.4 shows the 3D electrodes. As it is seen there is no faulty during electroplating.

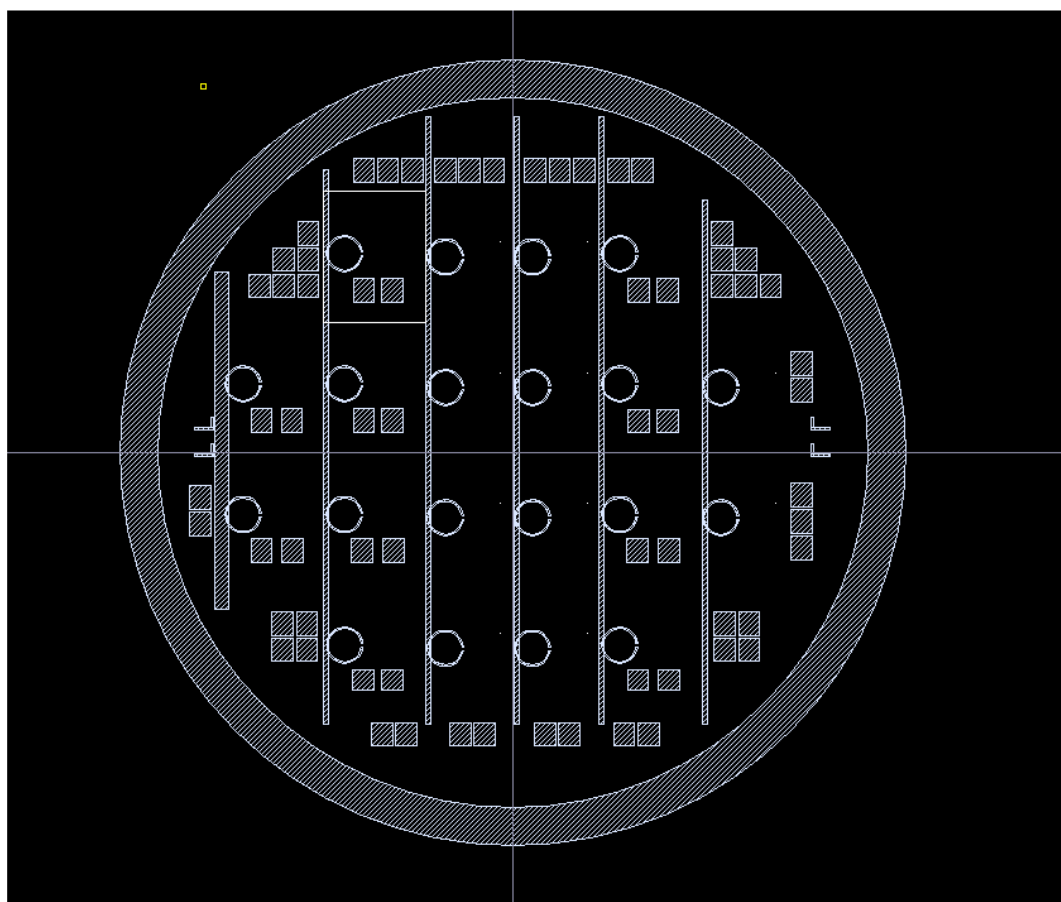


Figure 5.3: 2nd mask for creating openings for electroplating step. Each square represents a dummy opening to provide a uniform growing.

After forming 3D copper electrodes, channel is formed by using the 3rd mask. For single channel Coulter Counter, the main (wider) channel is narrowed down to a smaller channel where the sensing is accomplished. For the double channel Coulter Counter, a cylindrical obstacle divides the main channel into 2 narrower channels where counting is performed. Channel height should be bigger than the cell diameter to prevent particle clogging; hence, we designed a channel with a 30 μ m height. To achieve this thickness, AZ9260 photoresist was coated with double spin and double expose by 3rd mask (Figure 5.5). To cover the top surface of the channel and form the sidewalls, 20 μ m thick parylene was coated.

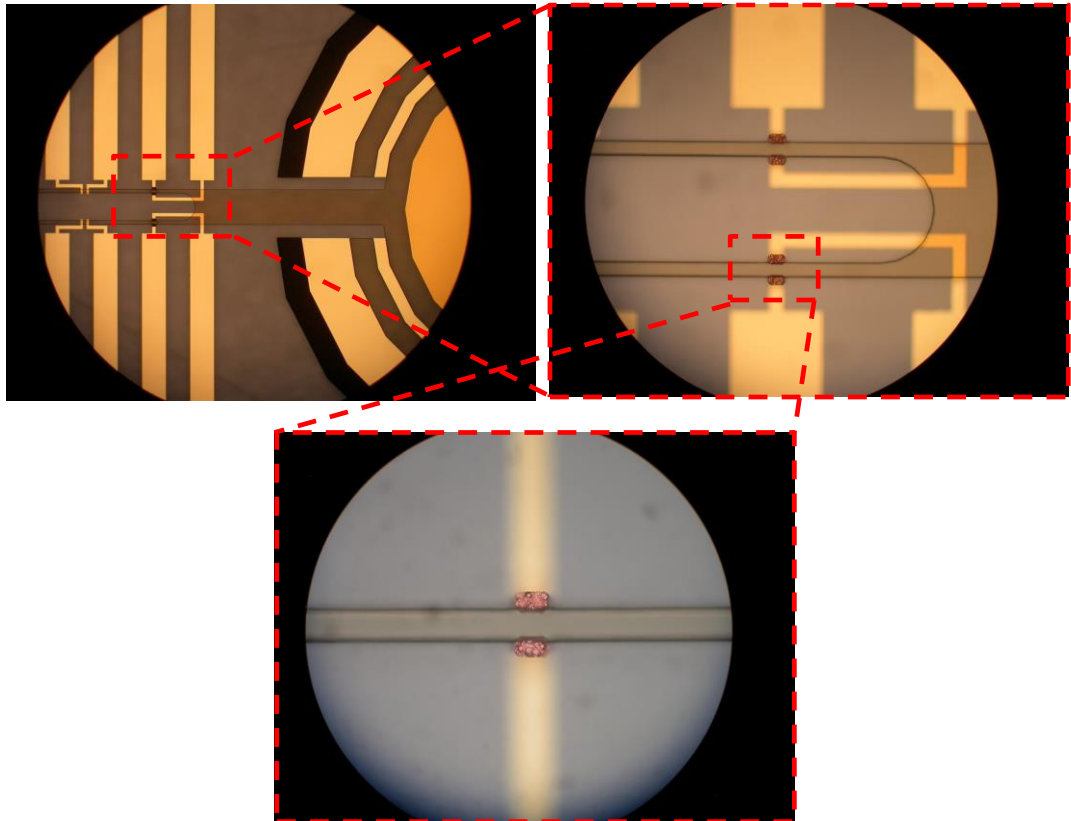


Figure 5.4: Electroplated 3D copper electrodes.

The last mask (4th mask) was utilized to create openings to get electrical connections and release the photoresist confined between parylene layers (Figure 5.6). As a last

step in clean room, wafers were sent to dicing and 20 devices were obtained for each wafer. After getting the individual devices from dicing, the ones that will be used during experiments were immersed into acetone for 2 days to get rid of AZ9260 photoresist. Upon taking the devices out of acetone, alcohol (isopropanol) treatment for 5 minutes was done to clean all the possible residues on device surfaces. Finally, nanoports were placed on inlet ports and glued with white and yellow epoxy, and air-dried for one day. It is important to note here that inlet and outlet ports must have a copper layer to carry the nanoport, otherwise, the parylene layer will collapse downward to block the flow of the fluid. Fabricated devices with nanoparts attached are shown in Figure 5.7.

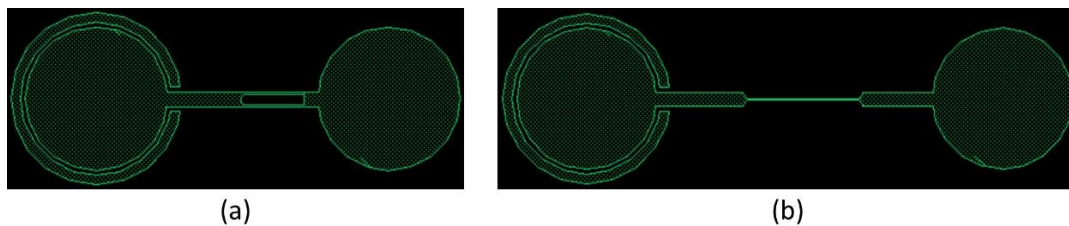


Figure 5.5: 3rd mask-Channel mask for (a) Double Channel Coulter Counter (b) Single Channel Coulter Counter

5.2 Problems related to fabrication

There are some problems faced during the fabrication process that affect the measurements. One of them is the peeling of the gold from the surface of the glass. Even though the silanization was performed before coating parylene to the glass surface, gold was peeled off very easily and it was affecting all the measurements negatively. Even the tips of probe station could remove the gold, damaging the electrode contact area. The distortion occurring on the contact area gives unstable result for channel impedance and creates a big problem during tests. Other than

gold peeling, we also faced a problem during electroplating step; however, this problem was related to excessive current supply to the electroplating device.

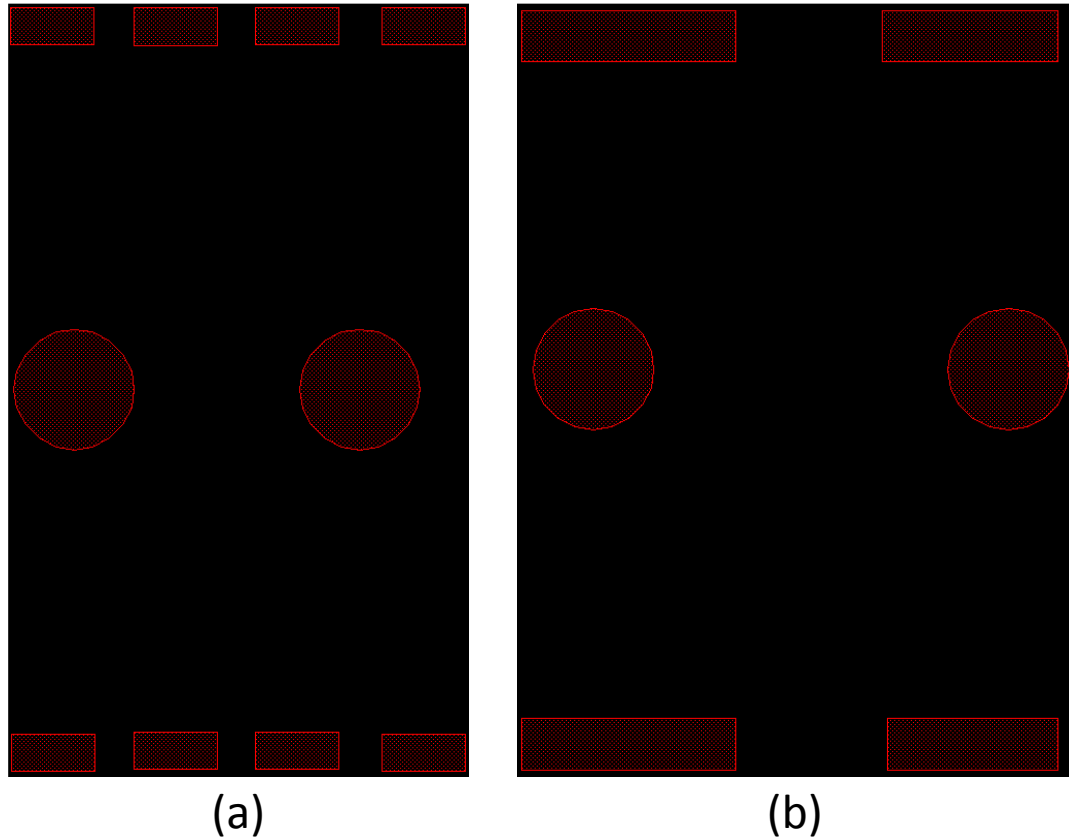


Figure 5.6: 4th mask- Opening mask for (a) Double Channel Coulter Counter (b) Single Channel Coulter Counter

To be able to shorten the process time, we tried to increase the supplied current value but we could not control the growing and electrodes merged as a result of this process. Figure 5.9 depicts the problem. As it is seen, electrodes merge in the middle of the channel and block the channel.

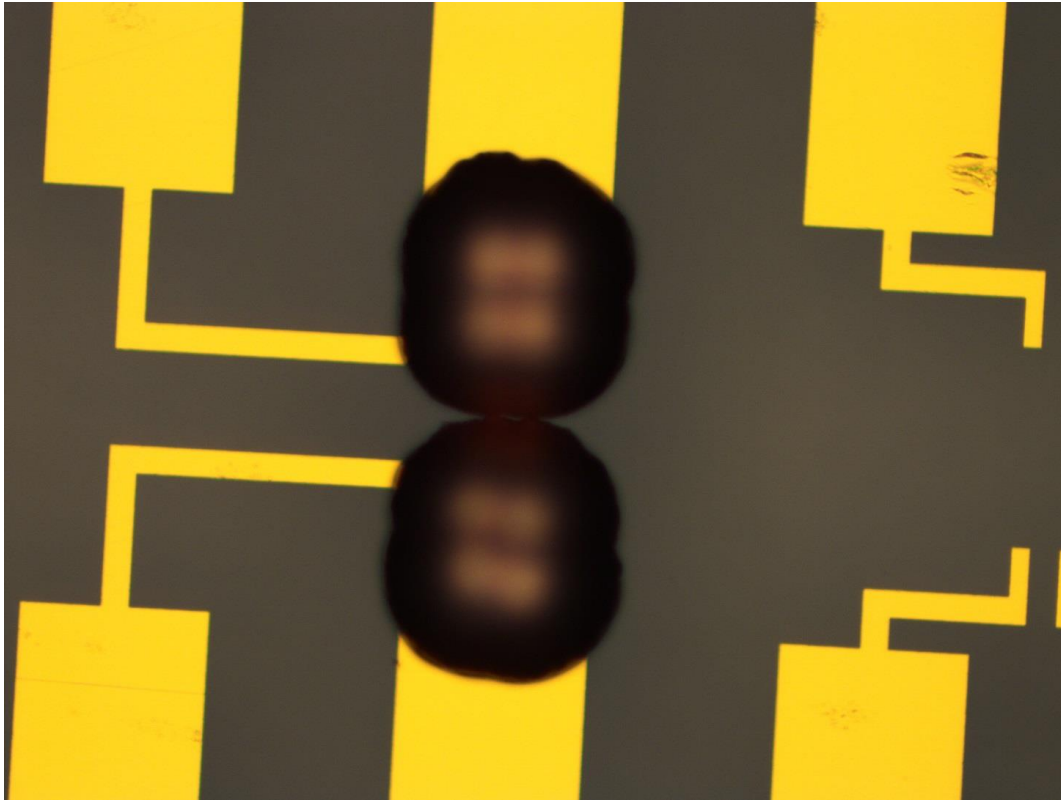


Figure 5.7: Electroplating problem due to intense current supply in a short time. Electrodes merged and blocked the channel.

The last problem was not directly related to fabrication but the design of the whole chip. During the adhesion operation of nanoports to inlets, yellow epoxy covered the electroplated copper electrodes area and did not allow us to get results since we could not see the passage of the particles. The distance between inlet ports and the 3D electrodes were not adequate. So, for the future designs, it should be noted that the distance between the closest feature and the inlets should be minimum 2.5 mm if the nanoports will be glued with white / yellow epoxy.

CHAPTER 6

RESULTS AND DISCUSSION

In chapter 6, results obtained from both single and double channel Coulter Counters are represented. It is proved that, double channel Coulter Counter was capable of processing 1.8 times more samples than the single channel Coulter Counter device in the same time interval. First, the preparation of the conductive medium and the dielectric properties cancer cell are presented. Next, devices and how they are used in these experiments are introduced. Then the electrical circuit and signal processing steps for the recovery the desired signal are explained in detail. As a last step, particle detection with different scenarios listed below is demonstrated.

1. Polystyrene microbeads counting
2. K562 cancer cells counting
3. Testing different frequencies
4. Mixture of polystyrene and K562 cancer cell counting
5. Testing different concentrations
6. Comparing electroplated electrodes with coplanar electrodes

Initial measurements were recorded with single channel Coulter Counter to prove the concept of resistive pulse theory. Voltage values obtained from experiments were used to find the diameter range of the microbeads and compared with the actual size. Then double channel Coulter Counters were employed and the results were

compared with the single channel Coulter Counters to see the increase in the speed of detection.

6.1 Conductive medium and cell preparation

Conductive medium where the cells are suspended contained 8.5% (w/v) sucrose and 0.3% (w/v) dextrose dissolved in DI water. Conductivity of this solution is adjusted by adding 10X phosphate buffered saline (PBS) to the prepared medium. For our case the conductivity is adjusted to 0.23 mS/cm. Culturing of the cancer cells were performed at METU Biology Department in a special medium RPMI 1640, containing gentamicin (0.2% w/v), and fetal bovine serum (FBS) (10% w/v) in a humidified incubator containing 5% CO₂ at 37° C. The cells were washed with the prepared medium (0.23 mS/cm) before each test. The process is shown in Figure 6.1.

6.2 Experimental Setup

To detect the particles flowing inside the microchannel, various hardware and software are required. The most important thing in this design is to provide a stable flow profile to the microchannels to obtain accurate results. Introducing fluid in microliters is provided by Longer Dual Channel Syringe Pump (China), capable of providing fluid flow rates between 2.779 µl/min and 72.24 ml/min. To excite the electrodes and OPAMPs used in the electrical detection circuit, Agilent 33220A Function / Arbitrary Waveform Generator, 20 MHz (USA) and Power Supply (Hewlett Packard E3631A, USA) are needed. To transmit the generated AC signal to both the microchip and the electrical signals, probe station (Mituyoto) is employed.

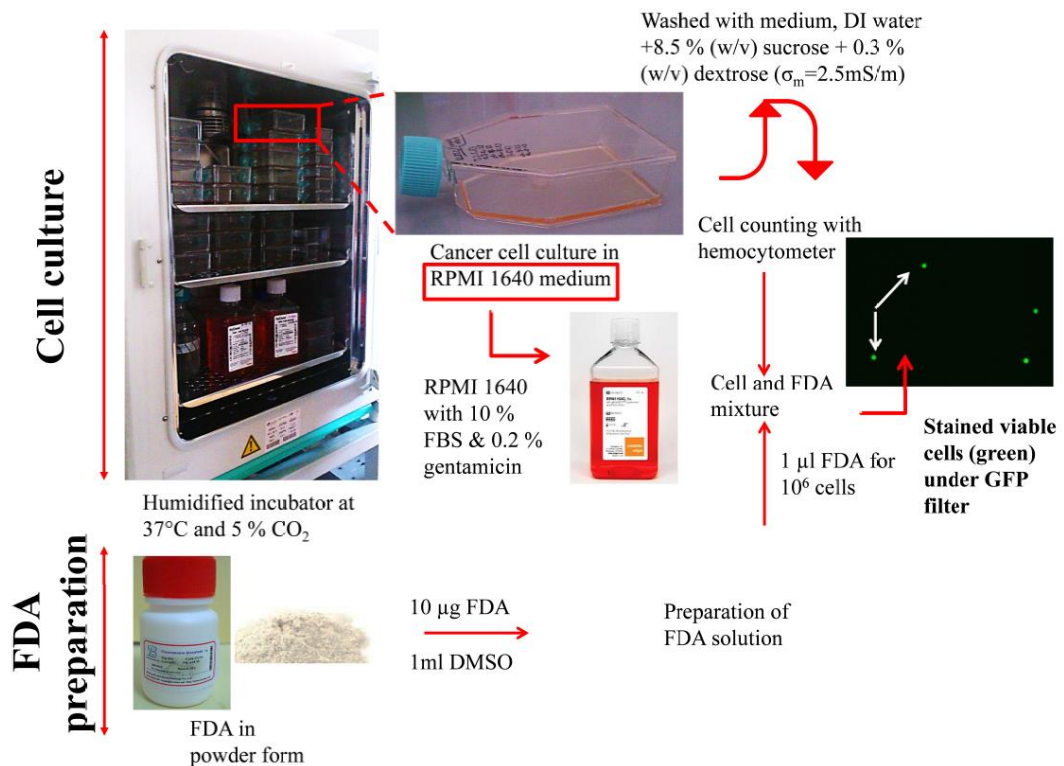


Figure 6.1: Preparation of the cancer cells [79].

By the help of the embedded microscope on it, it is also possible to monitor the particles, air bubbles or any other problems occurring inside the microchannels, inlet, and the outlet of the device. This microscope is connected to a TV screen and TV screen is connected to a computer to record the images or motion inside the channel. Agilent precision LRC meter is used to measure the channel resistance and capacitance at a given frequency. Before starting the measurements, it is important to measure the channel resistance since a high resistance value will not allow the instant peaks. Recording of the voltage in a specified sampling rate is accomplished by National Instruments Data Acquisition Board (NI 6337) and continuous monitoring of the voltage level is performed by LabVIEW Signal Express 2.5. The measured signal can be processed in LabVIEW without a need for hardware. In our experiments, we filtered the raw signal with a low pass filter before recording it.

Finally MATLAB R2013a is used to detect negative peaks and count the total number of them in a given interval.

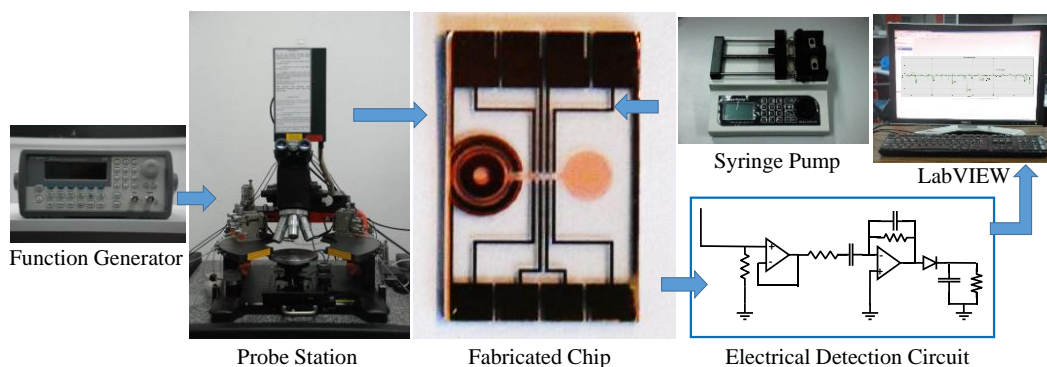


Figure 6.2: Test set up

6.3 Signal Processing and Peak Detection

Schematics of the peak detection circuit is given in Figure 6.3. The electrodes are excited with an AC signal ($5V_{p-p}$) at a fixed frequency (55 kHz). This source is supplied directly to the electrodes by probe station tips. The output of the channel resistance is connected in series to sensing resistor and the positive terminal of the unity gain buffer. This buffer allows the voltage transfer from a circuit having high output impedance to another circuit with low impedance value. In addition, it precludes the loading of the second circuit. Output of the buffer amplifier is connected to a band pass circuit, filtering out all the frequencies other than the ones centered around the excitation frequency (50 kHz) with a bandwidth of ± 5 kHz. The output of the rectangular band pass filter is connected to a peak detector circuit including a diode and a low pass filter. This part of the circuit detects the envelope and the variations occurring on it. Therefore, when there is a significant drop on the voltage, peak detector senses this change and shows it as a negative peak. Finally,

peak counting algorithm was developed on MATLAB R2013a (Appendix B) to count the number of peaks in a given time interval.

6.4 Results

In this section, different scenarios listed in the beginning of Chapter 6 will be investigated. Before starting the measurements, it is important to observe the particle trajectories inside the microchannel. Because, in some of the experiments it is observed that, particles clog at the nanopore and do not reach the detection area. After verifying the existence of the particles at the detection zone, channel resistance should be measured. If the measured channel resistance value is in the range of tens of $M\Omega$, it makes the sensing of small changes in resistance or voltage value very difficult.

6.4.1. Counting of Polystyrene Microbeads

10 μm dark red polystyrene latex beads (61946, Sigma Aldrich, Germany,), with 5% solid concentration were used during this experiment. These particles were injected into a medium having conductivity and relative permittivity of 0.23 mS/cm and 78, respectively. 5Vp-p AC excitation voltage with a fixed frequency of 50 kHz was applied to the coplanar electrodes. Sampling rate was determined as 200 kHz. For frequencies below 100 kHz, the sensing is based on just the size of the particles travelling through the aperture. Therefore two same sized particles having different granularity will generate the same peaks. Figure 6.3 and 6.4 show the raw data and lowpass filtered data, respectively, when the flow rate is 10 $\mu\text{l}/\text{min}$. As it is seen from Figure 6.3, it is hard to see the valleys, occurring on the base voltage value of approximately 0.51V. The velocity of the particles is around 1.5 ms when they are passing through the sensing area. This corresponds to 588 Hz. A low pass filter with a cut off frequency of 1 kHz was designed both in LabVIEW and MATLAB

to get the instant valleys and eliminate the noise. The measurement was recorded for 5 seconds.

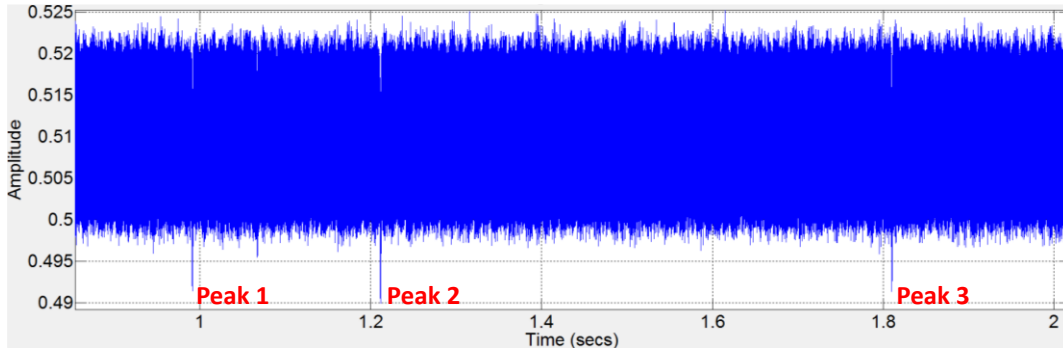


Figure 6.3: Raw data showing the passage of 3 beads, when the flow rate is 7.5 μ l/min.

As it is seen from Figure 6.3, a particle creates an approximately 20mV of change during its passing from the sensing area. Filtering the raw data by eliminating the background noise shows the peaks much more clearly; however, the amplitude of the peaks decreases by almost two times. Figure 6.4 shows this phenomenon. A particle passing through the pore decreased the base voltage by 8 – 10mV.

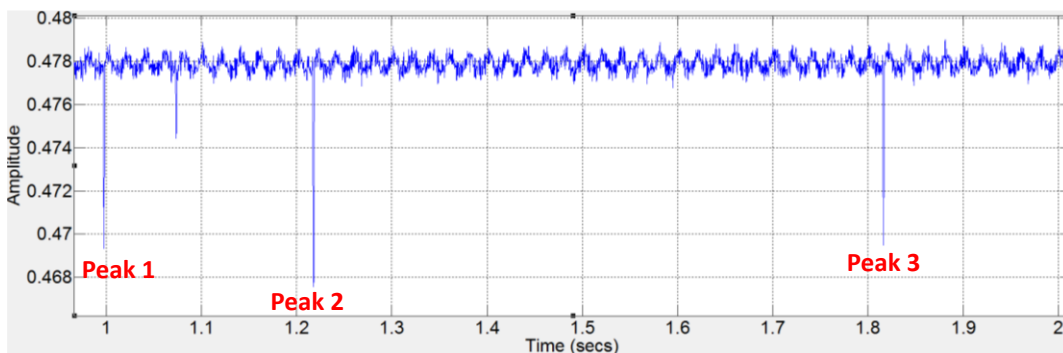


Figure 6.4: Low pass filtered data. The amplitude of the peaks reduced significantly.

Figure 6.5 shows the bandwidth and the amplitude of peak or valley 3. It is clear that the amplitude is 8 mV and the bandwidth showing the traversal time is 1.75ms.

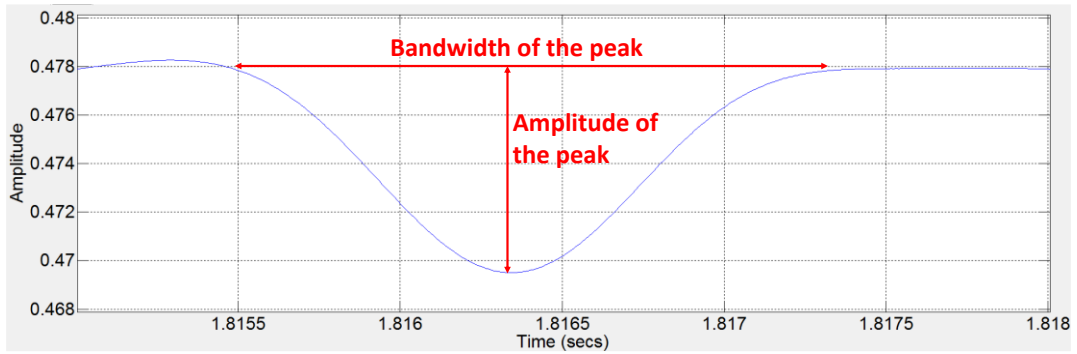


Figure 6.5: Amplitude and bandwidth of Peak 3.

Equation 6.1 gives the conversion of the flow velocity from l/min to m/s. According to this equation, theoretical value of the transit time of the particle shows very similar results with the measured one.

$$v (m/s) = \frac{\text{liter}}{\text{min}} * \frac{\text{min}}{\text{s}} * \frac{m^3}{1000lt} * \frac{1}{A_c} \quad (6.1)$$

A_c stands for the cross sectional area of the channel. For our case, the flow rate introduced to the channel is 1 $\mu\text{l}/\text{min}$. The wider part of the channel has a cross section area of $300 \times 30 \mu\text{m}^2$ and the narrower part where the sensing happens has a cross section area of $40 \times 30 \mu\text{m}^2$. Therefore the flow rate increases 7.5 times and reaches 7.5 $\mu\text{l}/\text{min}$. The diameter of the particle can be calculated by using the relative change of the voltage value. Equation 6.2, actually derived from Equation 2.3, shows this relationship.

$$d = \left(\frac{\left| \frac{\Delta R_{CH}}{R_{CH}} \right| LD^2}{\left[\frac{D^2}{2L^2} + \frac{1}{\sqrt{1 + \left(\frac{D}{L}\right)^2}} \right] \cdot F\left(\frac{d^3}{D^3}\right)} \right)^{\frac{1}{3}} \quad (6.2)$$

As stated earlier in Chapter 2, d , D and L represent the particle diameter, channel diameter and channel length respectively. $F\left(\frac{d^3}{D^3}\right)$ is the correction factor developed by DeBlois and Bean [18]. The relative change in resistance $\frac{\Delta R_{CH}}{R_{CH}}$ can be correlated with the change in the voltage value. For our case, since voltage is measured, this change should be converted to resistance change. Equation 6.3 shows the conversion formula.

$$\left| \frac{\Delta Z}{Z} \right| = \left| \frac{\Delta R_{CH}}{R_{CH}} \right| = \frac{\Delta V_s}{V_s + \Delta V_s} \quad (6.3)$$

Correction factor, on the other hand, is calculated by Equation 6.4.

$$F\left(\frac{d^3}{D^3}\right) = 1 + 1.26 \frac{d^3}{D^3} + 1.1 \frac{d^6}{D^6} \quad (6.4)$$

For our case, ΔV_s equals to 8 mV whereas V_s is 478 mV. $\left| \frac{\Delta R_{CH}}{R_{CH}} \right|$ is calculated as 0.016. Correction factors for 10 μm polystyrene microbeads and K562 cancer cells are 1.01 and 1.102, respectively. Placing all these values into equation 6.2 gives a diameter of approximately 7.6 μm . This value is smaller than the expected value. The reason of this may be the non-uniformity of the E-field distribution and when

the particle is traveling closer to the top surface of the channel, it may not be sensed very efficiently.

6.4.2. Counting of K562 Cancer Cells

K562 cancer cells are larger than the polystyrene latex beads with an average diameter of 17 μm . Therefore, the drop from the base voltage is expected to be larger. As explained in the earlier chapters, the cell is modeled as a cytoplasm covered by an insulating membrane with a very low conductivity. However, for the frequency value we adjusted for this experiment, the sensing is just based on the size of the particle instead of its granular level. An AC voltage with $5V_{\text{p-p}}$ at 55 kHz was applied to the coplanar electrodes. The base voltage was measured as 0.3V. Medium was introduced to the double channel Coulter Counter with a flow rate of 5 $\mu\text{l}/\text{min}$. This velocity of the flow increased approximately 25 $\mu\text{l}/\text{min}$ in every sub channel since they are approximately five times smaller than the wider channel. During the passage of the particles, the voltage decreased by 18 – 42 mV. Figure 6.6 shows the raw data for the cancer cells detected in the aperture. The data contains a white noise with a frequency of 50 Hz. To remove it, high pass filter with a cut off frequency of 300 Hz was employed. Even though the filter smoothed the signal and removed the DC offset and indicated the valleys sharply, it reduced the amplitude of some of the peaks a few mV. Therefore, for a more reliable particle diameter estimation, the variation in the raw voltage should be calculated. Figure 6.7 (a) shows the high pass filtered data. As it is seen, noise is reduced greatly and peaks are more observable. It is important to note here that due to the nature of the high pass filter, a negative peak follows positive peaks, during the passage of the particles. This makes the detection of cancer cells easier.

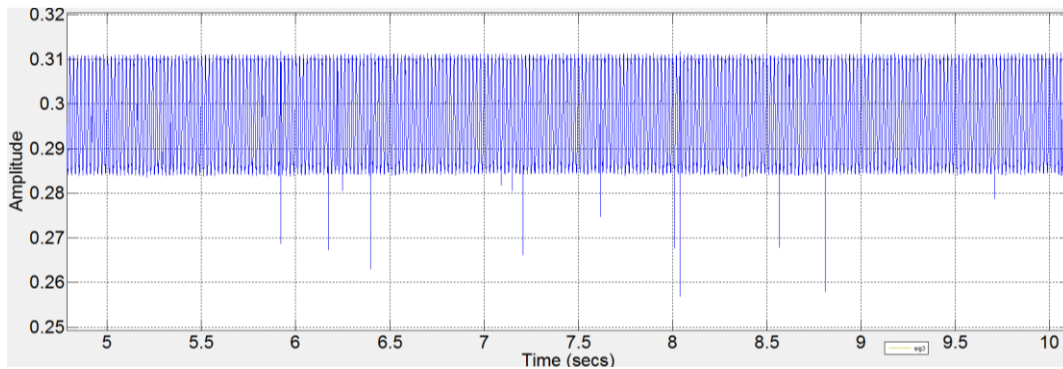
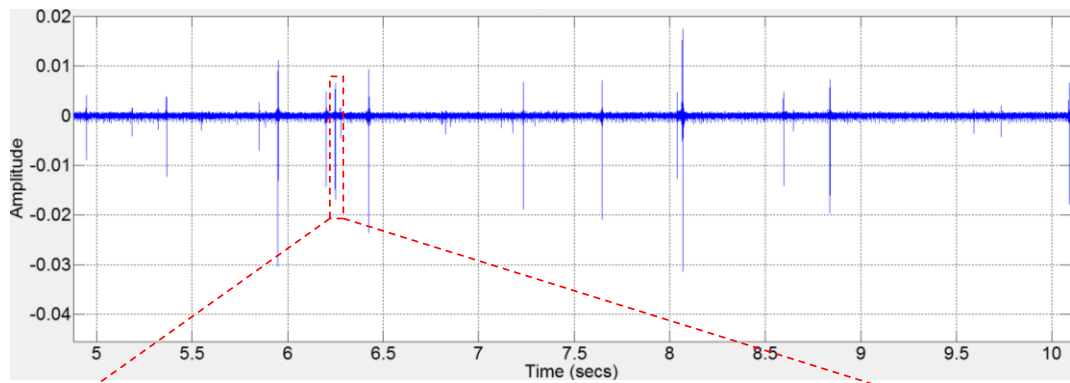


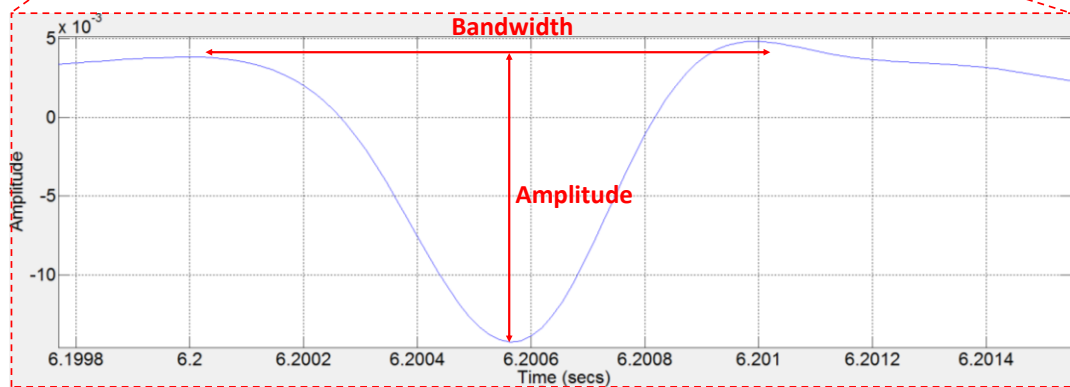
Figure 6.6: Raw data showing the passage of K562 cancer cells. Flow rate is 5 $\mu\text{l}/\text{min}$.

Figure 6.7 (b) shows the amplitude and the bandwidth of a valley started at 6.2s and continued till 6.201s corresponding to 1ms of transit time. In ideal case, a particle traveling with 0.045m/s (25 $\mu\text{l}/\text{min}$) is supposed to pass the 30 μm long aperture in 0.6ms. The experimental results do not match perfectly with the theoretical value. The reason of this may result from the flow profile of the particle. Due to the air bubbles created inside the channel, the velocity of the flow sometimes slows down then accelerate suddenly and thus, affects the flow stability. Therefore, it is expected to have these variations in flow velocity.

Concentration of the K562 leukemia cancer cells used in these tests is not provided exactly. However according to the information supplied by the biology department the approximate concentration of the solution is 300,000 cells / ml. By taking this number as a reference, we created a table and compare the counted peaks with the expected peaks. Table 6.1 shows this comparison. As it is seen, the sensed particles are very close to the expected values. The difference between the expected and the sensed resulted from the adhesion of cancer cells to the channel walls, nanoports or the tubing.



(a)



(b)

Figure 6.7: (a) High pass filtered data. Positive peaks are followed by negative peaks showing the passage of the particles. (b) Magnified view of the negative peak occurred at the 6.2006s.

Table 6.1: Cancer cell expected vs sensed count with different flow rates.

Flow rate ($\mu\text{l}/\text{min}$)	Approximate concentration (cells / ml)	Time (s)	Expected	Counted
1	300,000	30	150	120
5	300,000	30	750	696
10	300,000	40	2000	1713

6.4.3. Effect of Frequency change on particle counting

As stated in Chapter 2, frequency range in Coulter Counters affects the results dramatically. Electrical double layer (EDL), occurring on the surface of the electrodes exposed to the fluid, affects the sensing negatively. Equations 2.11 to 2.14 show the relationship between frequency and the double layer impedance. At low frequencies, the EDL impedance will dominate the overall impedance of the device and the relative change in the resistance of the channel will be very difficult to observe. On the other hand, at high frequencies, the signal will follow a path along the substrate instead of channel. Therefore a medium frequency range (20 kHz to 100 kHz) should be employed for accurate sensing. We tested the double channel Coulter Counter devices with three different frequencies (20 kHz, 50 kHz and 100 kHz) to see if the particles will be sensed and how the signal to noise ratio (SNR) will change. 20 kHz of excitation frequency is used to see if double layer impedance will dominate the overall impedance and affect the results negatively. It is shown that the device sensed the passage of the particles successfully and gave reliable results. The amplitude of the noise is highest with 4 mV at 20 kHz. The noise is due to the ionic particles gathered on the surface of the electrodes. Increasing the frequency from 20 kHz up to 100 kHz decreased the amplitude of both the noise in the base voltages since EDL effect decreased gradually. The amplitude of the valleys also decreased because of the gain of the OPAMPs. (Texas Instruments LF 353) employed in the experiments. The gain of the OPAMPs decreases with an increased frequency. Figure 6.8 shows the base voltage and relative voltage change with respect to different frequencies. As it is seen, base voltage has the highest value at 20 kHz with 0.643V including highest noise in it and 100 kHz has the lowest base voltage and peak amplitude. Therefore, 50 kHz is the optimal frequency to work with ,in terms of signal to noise ratio.

6.4.4. Mixture of polystyrene and K562 cancer cell counting

For this experiment, K562 cancer cells were injected into the suspension medium containing 10 μm polystyrene microbeads. The aim of this test was to investigate if the device capable of differentiating polystyrene microbeads from K562 cancer cells. Coplanar electrodes in single channel design was excited with 3V_{p-p}, 55 kHz AC signal and the measurements are recorded by Data Acquisition Board with 200 kHz sampling rate. The experiment was conducted for 9 s and the result is shown in Figure 6.9. The threshold indicates the passage of any particles. Changes occurring below this value may result from the environmental noise. Microbeads possess a uniform size and shape whereas this cannot be stated for cancer cells. K562 cancer cells have a diameter ranging from 12 to 23 μm . Therefore some of the cancer cells may also be recorded as a polystyrene microbeads. On the other hand, the amplitude of the valleys resulting from the passage of the microbeads gave 4 – 5mV decrease and verified by eye witnessing whereas cancer cells reduced the base voltage between 5 – 10mV.

6.4.5. Testing Different Concentrations

The concentration of the microbeads and cancer cells is not known exactly for our case. Therefore it is not possible to compare the introduced amount with the sensed amount. Both microbeads and the K562 cancer cells adhere to the nanoports, tubing or the channel itself during the tests. This prevents the counting negatively. Therefore we decided to prepare a test scenario including conductive mediums with different concentrations and compare these solutions with each other. Three different concentrations were prepared.

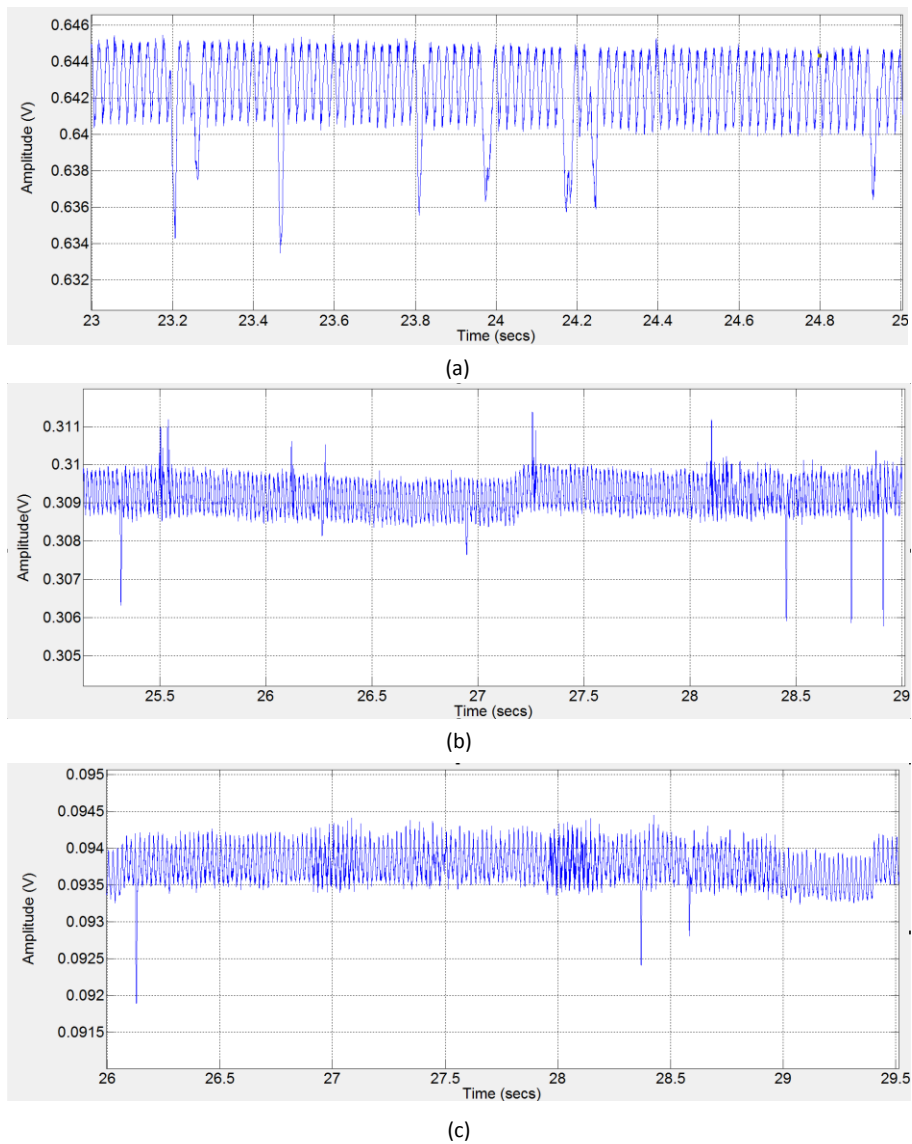


Figure 6.8: Resistance change during the passage of a 10 μm polystyrene latex particle with different frequencies. (a) Response of the sensor at 20 kHz. The change in the resistance is highest with 8 mV. (b) Response of the sensor at 50 kHz. (c) Response of the sensor at 100 kHz. The amplitude of the negative peak decreases down to 1 – 2 mV.

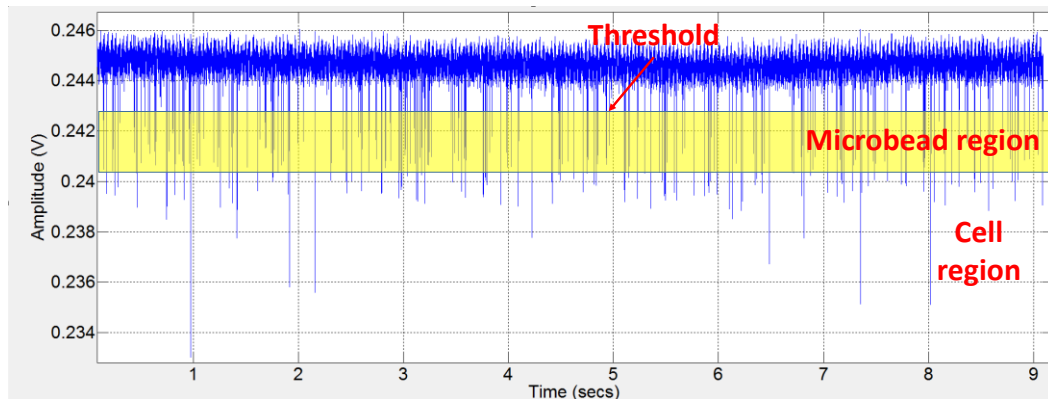


Figure 6.9: A graph showing the passage of microbeads and cancer cells. Microbeads creates a change of 4 to 5 mV where cancer cells reduces the base voltage up to 10 mV.

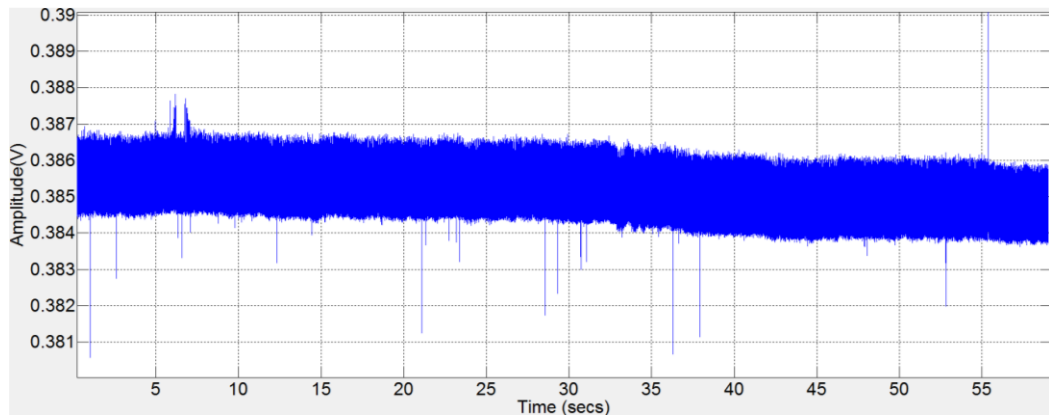
1. 3 ml solution ($\sigma = 0.23 \text{ S/m}$) + 30 μl microbeads
2. 6 ml solution ($\sigma = 0.23 \text{ S/m}$) + 30 μl microbeads
3. 9 ml solution ($\sigma = 0.23 \text{ S/m}$) + 30 μl microbeads

All these solutions were introduced into the devices with a flow rate of 2 $\mu\text{l}/\text{min}$. 5V_{pp} AC voltage with 50 kHz fixed frequency applied to the coplanar electrodes and results were recorded by the help of NI 6337 DAQ and LabVIEW Signal Express 2.5a software with a sampling rate of 100 kHz. All the tests were recorded for 1 min. Figure 6.10 shows the results, obtained from the scenarios listed above. As it is noticed, the concentraion in the 9ml solution is the lowest therefore shows the least number of peaks whereas the 3ml solution comprises approximately 3 times of beads than 9ml solution and hence has much more negative peaks. However it can easily be observed that the number of peaks were more than expected. The reason of this is the unstable flow resulted due to the air bubbles occured inside the channel. The existence of a bubble first blocks the flow. When this bubble escapes from the sensing zone, the flow, confined behind the bubble accelerates greatly and carries a lot of bubbles than the ideal flow of the fluid. During our tests, we faced with bubble

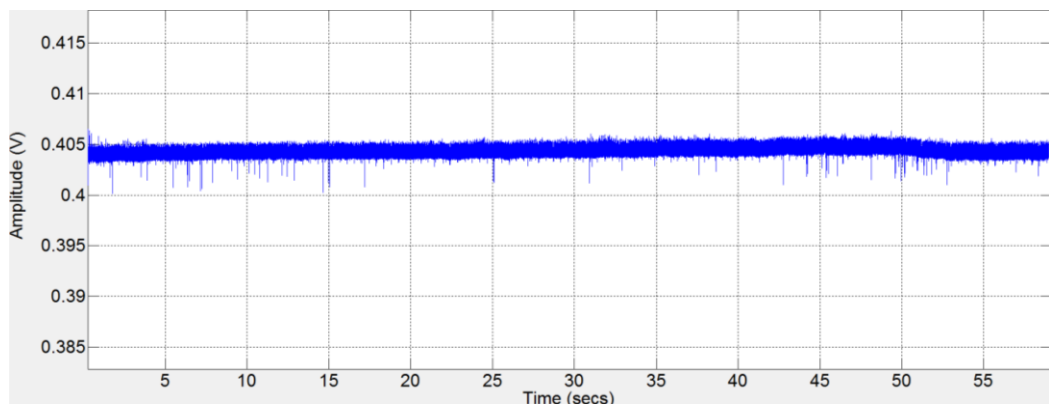
problem in 3ml concentration therefore the number of beads were more than expected. However it was noticed that 9ml solution has the lowest number of peaks and 3ml of solution has the highest number of peaks indicating the bulk amount of beads in the solution. The counted number of peaks are 13, 20 and 60 for 9ml, 6ml and 3ml solutions respectively.

6.4.6. Comparing electroplated and coplanar electrodes

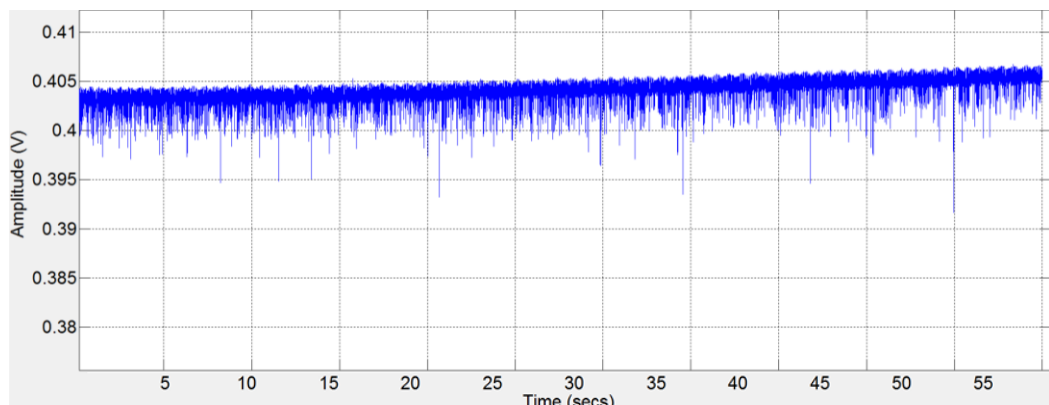
As discussed in Chapter 2, side wall electrodes provide better sensing since they generate a uniform electric field along the height of channel. Therefore, the position of the particle passing does not create a dramatic change in the output voltage. In comparison, coplanar electrodes provide a non-uniform electric field. The intensity of the electric field is highest at the surface of the electrodes (bottom of the channel) and lowest close to the top surface of the channel. Therefore a particle or a cell passing at different positions does not generate the same output voltage. A microparticle passing close to the stronger section of the electric field generates the highest voltage whereas a particle passing from the upper section of the electric field generates a weak output signal. Therefore it is expected that the output voltage produced by the coplanar electrodes has smaller value than the 3D electrodes. Figure 6.11 shows this phenomenon. In the top figure, the output voltage value belongs to the electroplated electrodes and is between 11 – 17 mV. The lower figure belongs to the coplanar electrodes and is between 8 – 10 mV.



(a)

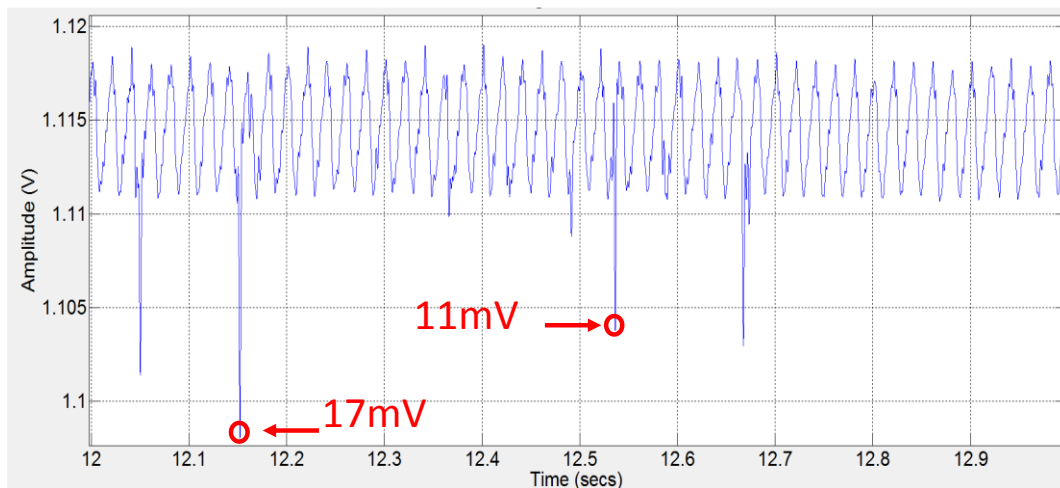


(b)

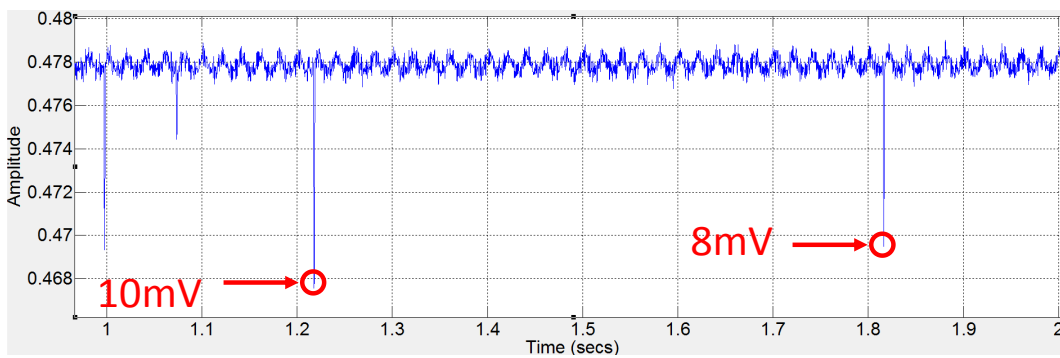


(c)

Figure 6.10: (a) 9ml solution + 30ul microbeads + 2ul flow rate with with 5Vpp 50 kHz in 22sec + lowpass filtered. (b) 6ml solution + 30ul microbeads + 2ul flow rate with with 5Vpp 50 kHz in 1 min + lowpass filtered. (c) 3ml solution + 30ul microbeads + 15ul flow rate with with 5Vpp 50 kHz in 22sec + lowpass filtered



(a)



(b)

Figure 6.11: Comparison of the output voltages generated by 3D and coplanar electrodes respectively.

6.5 Conclusion

In this chapter fabricated devices were tested under different scenarios. The aim was to prove that both of the designs are capable of detecting different particles (latex microbeads and cancer cells) in different concentrations, different frequencies and different flow rates. Apart from this, electrical double layer was also investigated and found that the fabricated devices can work around 20 kHz and is not dramatically affected by double layer. As a last step, 3D electroplated electrodes were compared with coplanar electrodes and it was proved that due to the uniformity

of the electric field produced by 3D electrodes, the observed voltage was higher and particle diameter calculations were more accurate obtained from 3D electrodes.

A comparison table showing the flow rates, detected particle diameters and type of electrode placement is shown in Table 6.2. Even though it is difficult to compare the other MEMS – based devices in the literature with our design, this table provides valuable information and shows where our design is. As it is seen, the fabricated double channel Coulter Counter device by our group can detect different sized particles with a very high flow rate (75 $\mu\text{l} / \text{min}$) and employs different electrode structure in one channel.

Table 6.2: Comparison of our device with other devices in literature

Author	Particle Diameter	Flow rate or detected samples	Channel width	Electrode placement
1) Saleh et al.(2001)	87 nm	3 colloids/s	1 μm	Planar electrodes
2) Nieuwenhuis et al. (2003)	25 μm	10 $\mu\text{l/s}$	620 μm	Coplanar
3) Jagtiani et al. (2006)	20 - 40 μm	8 $\mu\text{l/s}$	10 mm	Coplanar
4) Mei (2012) et al.	7.66 μm , 10.5 μm and 14.7 μm	2000 particles /s	30 μm	Gold – pin
5) Benson et al. (2012)	5 μm , 10 μm , and 15 μm .	0.4 $\mu\text{l/m}$	100 μm	Side wall
6) Choi et al. (2013)	16 μm	13 $\mu\text{l/m}$	NA	Polyelectric gels
7) Laçın (2014)	10 -20 μm	75 $\mu\text{l/m}$	40 μm	Side wall+coplanar

CHAPTER 7

CONCLUSION AND FUTURE WORK

In this work, counting of particles suspended in a conductive medium was studied by employing resistive pulse method (Coulter principle). High throughput microchannels, made of Parylene C, were formed to provide parallel sensing and counting. Electroplated 3D copper electrodes and sputtered coplanar Ti/Au electrodes placed inside the channels were employed for sensing the passage of the particles traveling along a defined aperture. Cell is modeled with electrical components to explain how the existence of a cell affects the channel resistance. In addition, other factors such as electrical double layer impedance and stray capacitance are included in the electrical model for accurate analysis of two μ -Coulter Counter designs. One of them has a single channel in which the main channel is narrowed down to a smaller one to perform sensing and the other one has a novel double channel structure to provide parallel analysis and higher efficiency. The proof of concept was successfully demonstrated with simulations and experimental results. Theoretical values were compared with the measured ones to verify that developed devices provide accurate and reliable output. Below is the list of the achievements throughout this study:

- 1) Design of the single and double channel Coulter Counters, and modeling of the channel and cells.
- 2) Finite Element Method (FEM) simulations, showing the surface velocity field (flow profile), surface electrical field, current density field, and electrical resistance changes during the passage of the particles by COMSOL 4.3b Multiphysics.

- 3) Parylene microchannel and 3D and coplanar electrode fabrications on a glass wafer. Particle focusing was achieved in these microchannels without a need for extra inlets since dimensions of the channels were adjusted to be comparable to the particle diameter.
- 4) Single and double channel Coulter Counters were fabricated successfully. Single channel design was mainly employed for the proof of concept and double channel design was introduced to demonstrate the possibility of sensing micro particle without enlarging the chip size and eliminating the need for complex hardware and software.
- 5) Different scenarios were inspected to show the capability and working range of both devices. 10 μm polystyrene latex beads and K562 leukemia cancer cells with diameters ranging from 12-23 μm were used in the experiments to prove that device is capable of detecting different particles.
- 6) The factors such as Electrical Double Layer (EDL) and Stray Capacitance affecting the sensing negatively were investigated and shown that both of the developed designs were not affected from these factors.
- 7) In conclusion, it is proved that both of the developed designs are capable of detecting microparticles larger than 10 μm in a rapid and reliable way.

Future Work:

Resistive pulse counters are responsible for sensing and counting the cells based on their size and sort them with respect to their diameters. Both of our designs are capable of performing this task. On the other hand, a cell counter capable also of detecting the internal structures of the microparticles with similar sizes would be preferable to get more information about the cell granularity. Faster peak detection algorithms and better filtering methods can be developed to get rid of environmental and white noise occurred in the experiments and to provide more reliable and rapid results. The number of the hardware employed can be reduced and all the filtering

and peak detection algorithms can be handled with software programs such as MATLAB, LabVIEW etc. These leads to faster and better results and also reduce the size of the set up while providing a lab on a chip device. Few problems, faced in fabrication, can be overcome by changing the design parameters. For example, test results could not be obtained from 3D electrodes since they were very close to the inlet port. While epoxying the ports, 3D electrodes were covered with especially yellow epoxy and they could not be seen under microscope. Since eye verification of the passage of the particles could not be performed, we preferred to take the measurements with coplanar electrodes. To deal with this problem, it is important to place any of the important features away from the area that will be epoxyed.

One of the important features of the Coulter Counters is the ability of processing the sample in a reasonable time. To achieve this aim, flow ratio can be increased or channel size can be enlarged. However, increasing any of these features gives rise to sensing problems and harm the counting efficiency. Therefore researchers came up with the multiple channel designs to perform parallel counting. In our design, instead of increasing the number of channels, we decided to divide a wide channel into smaller channels. The problem we faced with this design was the air bubbling issue. Because, T-junctions were formed inside the channel and it affected the flow profile negatively. The problem we faced with this design was the air bubbling issue. To overcome this issue, Y junctions can be employed in the future generation of these devices.

REFERENCES

- [1] L. E. Schaeffer, J. W. Dyke, F. D. Meglio, P. R. Murray, W. Crafts, and A. C. Niles, "Evaluation of microparticle enzyme immunoassays for immunoglobulins G and M to rubella virus and *Toxoplasma gondii* on the Abbott IMx automated analyzer," *J. Clin. Microbiol.*, vol. 27, no. 11, pp. 2410–2413.
- [2] D. Li, M. He, and S. C. Jiang, "Detection of infectious adenoviruses in environmental waters by fluorescence-activated cell sorting assay.," *Appl. Environ. Microbiol.*, vol. 76, no. 5, pp. 1442–8, Mar. 2010.
- [3] A. V. Jagtiani, "Novel multiplexed Coulter counters for high throughput parallel analysis of microparticles," 2011.
- [4] W. H. Coulter, "Means for counting particles suspended in a fluid," 1953.
- [5] G.-B. Lee, C.-H. Lin, and G.-L. Chang, "Micro flow cytometers with buried SU-8/SOG optical waveguides," *Sensors Actuators A Phys.*, vol. 103, no. 1–2, pp. 165–170, Jan. 2003.
- [6] S.-Y. Yang, S.-K. Hsiung, Y.-C. Hung, C.-M. Chang, T.-L. Liao, and G.-B. Lee, "A cell counting/sorting system incorporated with a microfabricated flow cytometer chip," *Meas. Sci. Technol.*, vol. 17, no. 7, pp. 2001–2009, Jul. 2006.
- [7] Y. Zhang, J. T. Bahns, Q. Jin, R. Divan, and L. Chen, "Toward the detection of single virus particle in serum.," *Anal. Biochem.*, vol. 356, no. 2, pp. 161–70, Sep. 2006.
- [8] J.-T. Yang, Y.-H. Lai, W.-F. Fang, and M.-H. Hsu, "Simultaneous measurement of concentrations and velocities of submicron species using multicolor imaging and microparticle image velocimetry.," *Biomicrofluidics*, vol. 4, no. 1, p. 14109, Jan. 2010.
- [9] H. Zhang, C. H. Chon, X. Pan, and D. Li, "Methods for counting particles in microfluidic applications," *Microfluid. Nanofluidics*, vol. 7, no. 6, pp. 739–749, Aug. 2009.

- [10] Z. Zhang, J. Zhe, S. Chandra, and J. Hu, “An electronic pollen detection method using Coulter counting principle,” *Atmos. Environ.*, vol. 39, no. 30, pp. 5446–5453, Sep. 2005.
- [11] A. V Jagtiani, R. Sawant, and J. Zhe, “A label-free high throughput resistive-pulse sensor for simultaneous differentiation and measurement of multiple particle-laden analytes,” *J. Micromechanics Microengineering*, vol. 16, no. 8, pp. 1530–1539, Aug. 2006.
- [12] A. L. McPherson, “A Passive Pumping Microfluidic Coulter Counter,” 2009.
- [13] Z. Qin, J. Zhe, and G.-X. Wang, “Effects of particle’s off-axis position, shape, orientation and entry position on resistance changes of micro Coulter counting devices,” *Meas. Sci. Technol.*, vol. 22, no. 4, p. 045804, Apr. 2011.
- [14] E. C. Gregg and K. D. Steidley, “Electrical counting and sizing of mammalian cells in suspension,” *Phys. Med. Biol.*, vol. 12, no. 1, pp. 79–92, 1968.
- [15] O. A. Saleh and L. L. Sohn, “Quantitative sensing of nanoscale colloids using a microchip Coulter counter,” *Rev. Sci. Instrum.*, vol. 72, no. 12, p. 4449, 2001.
- [16] M. J.C, *A Treatise on Electricity and Magnetism*, vol. 72, no. 12. 1904.
- [17] Lord Rayleigh, “On the influence of obstacles arranged in rectangular order upon the properties of a medium,” *Philos. Mag.*, vol. 34, pp. 481–502, 1892.
- [18] R. W. DeBlois and C. P. Bean, “Counting and sizing of submicron particles by the resistive pulse technique,” *Rev. Sci. Instrum.*, vol. 41, no. 7, pp. 909–916, 1970.
- [19] D. K. Wood, M. V Requa, and a N. Cleland, “Microfabricated high-throughput electronic particle detector,” *Rev. Sci. Instrum.*, vol. 78, no. 10, p. 104301, Oct. 2007.
- [20] [Http://amrita.vlab.co.in/?sub=3&brch=188&sim=336&cnt=1](http://amrita.vlab.co.in/?sub=3&brch=188&sim=336&cnt=1), “Hemocytometer, Counting of cells” (31.07.2014)
- [21] [Http://en.wikipedia.org/wiki/Hemocytometer](http://en.wikipedia.org/wiki/Hemocytometer), “Hemocytometer” (31.07.2014)
- [22] D. and C. Becton, “Introduction to Flow Cytometry: A Learning Guide,” 2000.

- [23] [Http://crl.berkeley.edu/flow_cytometry_basic.html](http://crl.berkeley.edu/flow_cytometry_basic.html), “Flow Cytometry Basics.” (31.07.2014)
- [24] “<http://www.semrock.com/flow-cytometry.aspx>.” (31.07.2014)
- [25] [Http://www.bu.edu/flow-cytometry/files/2010/09/Picture11.png](http://www.bu.edu/flow-cytometry/files/2010/09/Picture11.png), (31.07.2014)
- [26] M. Korampally, “A MEMS based Coulter counter for cell sizing,” 2007.
- [27] F. V. Ignatovich, D. Topham, and L. Novotny, “Optical Detection of Single Nanoparticles and Viruses,” *IEEE J. Sel. Top. Quantum Electron.*, vol. 12, no. 6, pp. 1292–1300, Nov. 2006.
- [28] T. J. B. Patterson, R.H., Jr, Kessler K., Brennan R. W., “Ultrasonic Detection of Microemboli from Artificial Surfaces: Evidence of Microembolic Tissue Damage,” *Bull. NewYork Acad. Med.*, no. 48, pp. 452–458, 1972.
- [29] H. Murakawa, H. Kikura, and M. Aritomi, “Application of Ultrasonic Multi-wave Method for Two-phase Flow,” in *International Symposium on Ultrasonic Doppler Methods for Fluid Mechanics and Fluid Engineering*, 2013, pp. 23–26.
- [30] Y. Wu, M. Almasri, and J. D. Benson, “MEMS Coulter counter for dynamic impedance measurement of cells,” *2011 IEEE SENSORS Proc.*, pp. 794–797, Oct. 2011.
- [31] D. Satake, H. Ebi, N. Oku, K. Matsuda, H. Takao, M. Ashiki, and M. Ishida, “A sensor for blood cell counter using MEMS technology,” *Sensors Actuators B Chem.*, vol. 83, no. 1–3, pp. 77–81, Mar. 2002.
- [32] S. Zheng, M. S. Nandra, and Y. Tai, “Human Blood Cell Sensing with Platinum Black Electroplated Impedance Sensor,” in *NEMS-07*, 2007, pp. 520–523.
- [33] K. Roberts, “A silicon microfabricated aperture for counting cells using the aperture impedance technique,” 1999.
- [34] Z. Mei, S. H. Cho, A. Zhang, J. Dai, T.-F. Wu, and Y.-H. Lo, “Counting leukocytes from whole blood using a lab-on-a-chip Coulter counter,” *Conf. Proc. IEEE Eng. Med. Biol. Soc.*, vol. 2012, pp. 6277–80, Jan. 2012.
- [35] Y. Wu, J. D. Benson, J. K. Critser, and M. Almasri, “Note: Microelectromechanical systems Coulter counter for cell monitoring and counting,” *Rev. Sci. Instrum.*, vol. 81, no. 7, p. 076103, Jul. 2010.

- [36] A. V Jagtiani, J. Zhe, J. Hu, and J. Carletta, "Detection and counting of micro-scale particles and pollen using a multi-aperture Coulter counter," *Meas. Sci. Technol.*, vol. 17, no. 7, pp. 1706–1714, Jul. 2006.
- [37] S. Murali, X. Xia, A. V Jagtiani, J. Carletta, and J. Zhe, "Capacitive Coulter counting: detection of metal wear particles in lubricant using a microfluidic device," *Smart Mater. Struct.*, vol. 18, no. 3, p. 037001, Mar. 2009.
- [38] L. L. Sohn, O. a Saleh, G. R. Facer, a J. Beavis, R. S. Allan, and D. a Notterman, "Capacitance cytometry: measuring biological cells one by one.," *Proc. Natl. Acad. Sci. U. S. A.*, vol. 97, no. 20, pp. 10687–90, Sep. 2000.
- [39] L. Du, J. Zhe, J. E. Carletta, and R. J. Veillette, "Inductive Coulter counting: detection and differentiation of metal wear particles in lubricant," *Smart Mater. Struct.*, vol. 19, no. 5, p. 057001, May 2010.
- [40] L. Du, J. Carletta, R. Veillette, and J. Zhe, "A magnetic Coulter counting device for wear debris detection in lubrication" in *IMECE'09*, 2014, pp. 1–5.
- [41] L. Du, J. Zhe, J. Carletta, R. Veillette, and F. Choy, "Real-time monitoring of wear debris in lubrication oil using a microfluidic inductive Coulter counting device," *Microfluid. Nanofluidics*, vol. 9, no. 6, pp. 1241–1245, May 2010.
- [42] K. Cheung, S. Gawad, and P. Renaud, "Impedance spectroscopy flow cytometry: on-chip label-free cell differentiation.," *Cytometry. A*, vol. 65, no. 2, pp. 124–32, Jun. 2005.
- [43] H. E. Ayliffe, A. B. Frazier, and R. D. Rabbitt, "Microchannels with Integrated Metal Electrodes," vol. 8, no. 1, pp. 50–57, 1999.
- [44] S. Gawad, L. Schild, and P. H. Renaud, "Micromachined impedance spectroscopy flow cytometer for cell analysis and particle sizing.," *R. Soc. Chem.*, vol. 1, no. 1, pp. 76–82, Sep. 2001.
- [45] C. Bernabini, D. Holmes, and H. Morgan, "Micro-impedance cytometry for detection and analysis of micron-sized particles and bacteria.," *Lab Chip*, vol. 11, no. 3, pp. 407–412, 2011.
- [46] R. DeBlois and C. Bean, "Counting and sizing of submicron particles by the resistive pulse technique," vol. di, no. October, pp. 1012–1014, 2013.
- [47] U. Larsen, "Microchip Coulter particle counter," in *Solid State Sensors and Actuators* 1997, pp. 1319–1322.

- [48] B. A. Koch, M. , Evans A. G. R., “Design and fabrication of a micromachined Coulter counter,” vol. 159, 1999.
- [49] O. A Saleh and L. L. Sohn, “Direct detection of antibody-antigen binding using an on-chip artificial pore.,” *Proc. Natl. Acad. Sci. U. S. A.*, vol. 100, no. 3, pp. 820–4, Feb. 2003.
- [50] O. A. Saleh and L. L. Sohn, “An artificial nanopore for molecular sensing,” *Nano Lett.*, vol. 3, no. 1, pp. 37–38, 2003.
- [51] S. M. Bezrukov, I. Vodyanoy, R. A. Brutyan, and J. J. Kasianowicz, “Dynamics and free energy of polymers partitioning into a nanoscale pore,” *Macromolecules*, vol. 29, no. 26, pp. 8517–8522, 1996.
- [52] J. J. Kasianowicz, E. Brandin, D. Branton, and D. W. Deamer, “Characterization of individual polynucleotide molecules using a membrane channel,” *Proc. Natl. Acad. Sci. U. S. A.*, vol. 93, no. 24, pp. 13770–13773, 1996.
- [53] M. Akeson, D. Branton, J. J. Kasianowicz, E. Brandin, and D. W. Deamer, “Microsecond time-scale discrimination among polycytidylic acid, polyadenylic acid, and polyuridylic acid as homopolymers or as segments within single RNA molecules.,” *Biophys. J.*, vol. 77, no. 6, pp. 3227–3233, 1999.
- [54] J. Guo, “Numerical Investigation of the Performance of CoulterCounter with Novel Structure,” *Int. J. Inf. Electron. Eng.*, vol. 2, no. 6, pp. 885–888, 2012.
- [55] J. H. Nieuwenhuis, F. Kohl, J. Bastemeijer, P. M. Sarro, and M. J. Vellekoop, “Integrated Coulter counter based on 2-dimensional liquid aperture control,” *Sensors Actuators B Chem.*, vol. 102, no. 1, pp. 44–50, Sep. 2004.
- [56] R. Rodriguez-Trujillo, C. A. Mills, J. Samitier, and G. Gomila, “Low cost micro-Coulter counter with hydrodynamic focusing,” *Microfluid. Nanofluidics*, vol. 3, no. 2, pp. 171–176, Sep. 2006.
- [57] R. Rodriguez-Trujillo, O. Castillo-Fernandez, M. Garrido, M. Arundell, A. Valencia, and G. Gomila, “High-speed particle detection in a micro-Coulter counter with two-dimensional adjustable aperture.,” *Biosens. Bioelectron.*, vol. 24, no. 2, pp. 290–6, Oct. 2008.
- [58] T. Stiles, R. Fallon, T. Vestad, J. Oakey, D. W. M. Marr, J. Squier, and R. Jimenez, “Hydrodynamic focusing for vacuum-pumped microfluidics,” *Microfluid. Nanofluidics*, vol. 1, no. 3, pp. 280–283, Mar. 2005.

- [59] R. Scott, P. Sethu, and C. K. Harnett, “Three-dimensional hydrodynamic focusing in a microfluidic Coulter counter.,” *Rev. Sci. Instrum.*, vol. 79, no. 4, p. 046104, Apr. 2008.
- [60] H. P. Schwan, “Electrode polarization impedance and measurements,” *Ann. N. Y. Acad. Sci.*, vol. 148, pp. 191–209, 1968.
- [61] Y. Wu, X. Han, J. D. Benson, and M. Almasri, “Micromachined Coulter counter for dynamic impedance study of time sensitive cells.,” *Biomed. Microdevices*, vol. 14, no. 4, pp. 739–50, Aug. 2012.
- [62] P. Zoltowski, “On the electrical capacitance of interfaces exhibiting constant phase element behaviour,” *J. Electroanal. Chem.*, vol. 443, no. 1, pp. 149–154, Feb. 1998.
- [63] E. Barsoukov and J. R. Macdonald, *Impedance Spectroscopy: Theory, Experiment, and Applications*. John Wiley & Sons, Inc., 2005, pp. 1–595.
- [64] J.-B. Jorcin, M. E. Orazem, N. Pébère, and B. Tribollet, “CPE analysis by local electrochemical impedance spectroscopy,” *Electrochimica Acta*, vol. 51, no. 8–9, pp. 1473–1479, 2006.
- [65] D. W. Lee, S. Yi, and Y.-H. Cho, “A flow-rate independent cell counter using a fixed control volume between double electrical sensing zone,” 2005, pp. 678–681.
- [66] R. Pethig, “Dielectrophoresis: Using Inhomogeneous AC Electrical Fields to Separate and Manipulate Cells,” *Critical Reviews in Biotechnology*, vol. 16, no. 4, pp. 331–348, 1996.
- [67] Y. Huang, X. B. Wang, R. Hölzel, F. F. Becker, and P. R. Gascoyne, “Electrorotational studies of the cytoplasmic dielectric properties of Friend murine erythroleukaemia cells.,” *Phys. Med. Biol.*, vol. 40, no. 11, pp. 1789–1806, 1995.
- [68] G. Tresset and S. Takeuchi, “A Microfluidic device for electrofusion of biological vesicles,” *Biomed. Microdevices*, vol. 6, no. 3, pp. 213–218, 2004.
- [69] K. C. Cheung, M. Di Berardino, G. Schade-Kampmann, M. Hebeisen, A. Pierzchalski, J. Bócsi, A. Mittag, and A. Tárnok, “Microfluidic impedance-based flow cytometry.,” *Cytometry. A*, vol. 77, no. 7, pp. 648–66, Jul. 2010.
- [70] L. Wang, L. Flanagan, and A. P. Lee, “Side-Wall Vertical Electrodes for Lateral Field Microfluidic Applications,” *J. Microelectromechanical Syst.*, vol. 16, no. 2, pp. 454–461, Apr. 2007.

- [71] S. Oh, J. S. Lee, K.-H. Jeong, and L. P. Lee, "Minimization of Electrode Polarization Effect by Nanogap Electrodes for Biosensor Applications," in *MEMS'03*, 2003, pp. 52–55.
- [72] Y. Wu, J. D. Benson, J. K. Critser, and M. Almasri, "MEMS-based Coulter counter for cell counting and sizing using multiple electrodes," *J. Micromechanics Microengineering*, vol. 20, no. 8, p. 085035, Aug. 2010.
- [73] A. L. Richards, M. D. Dickey, a S. Kennedy, and G. D. Buckner, "Design and demonstration of a novel micro-Coulter counter utilizing liquid metal electrodes," *J. Micromechanics Microengineering*, vol. 22, no. 11, p. 115012, Nov. 2012.
- [74] H. Choi, C. S. Jeon, H. K. Kim, T. D. Chung, and H. C. Kim, "A label-free size-based micro Coulter counter system for circulating rare tumor cells," in *μ TAS'13*, 2013, vol. di, no. October, pp. 1012–1014.
- [75] A. V. Jagtiani and J. Zhe, "AC Measurements and Multiplexed Detection of Microparticles Using Parallel Channel Coulter Counter," *2010 18th Bienn. Univ. Micro/Nano Symp.*, pp. 1–4, Jun. 2010.
- [76] G. Karp, *Cell and Molecular Biology: Concepts and Experiments*. 2008, pp. 662–682.
- [77] K. R. Foster and H. P. Schwan, "Dielectric properties of tissues and biological materials: a critical review.," *Crit. Rev. Biomed. Eng.*, vol. 17, no. 1, pp. 25–104, 1989.
- [78] M. A. Burns, B. N. Johnson, S. N. Brahmasandra, K. Handique, J. R. Webster, M. Krishnan, T. S. Sammarco, P. M. Man, D. Jones, D. Heldsinger, C. H. Mastrangelo, and D. T. Burke, "An integrated nanoliter DNA analysis device.," *Science*, vol. 282, no. 5388, pp. 484–487, 1998.
- [79] Y. Demircan, "Detection of imatinib and doxorubicin resistance in K562 leukemia cells by 3d-electrode contactless dielectrophoresis," 2013.

APPENDIX A

FABRICATION FLOW OF THE COULTER COUNTER DEVICES

Table A.1: Process Flow

	Glass wafer (4")
	Piranha + BHF cleaning
	Dehydration in oven at 110°C for 15 min
	4 gr of Parylene coating with silane
	Dehydration in oven at 90°C for 40 min (not needed if the wafers will be inserted into the BESTEC sputtering device directly after parylene coating)
	Ti sputtering (~20nm) with BESTEC
	300W T1:120s, T2:70s, Distance : 135mm, Flow: 2.5sccm
	Au sputtering (~400nm) with BESTEC
	300W T1:120s, T2:400s, Distance : 130mm, Flow: 6.2sccm
	Dehydration in oven at 90°C for 40 min
	1st lithography for Ti & Au etch
Mask1	HDMS coating at 500 rpm for 7s + 3000 rpm for 30s
	S1813 coating at 500 rpm for 7s + 4000 rpm for 30s
	Softbake at 95°C for 70s at hotplate
	Expose UV for 4.5s at hard contact
	PR develop with MF319 for 1 min (eye-control)
	Rinse with DI water for 1.5min + 1.5min
	Dry with N2
	Inspection
	Hardbake in oven at 95°C for 30min
	Dessicator for 5 – 10 min.
	Au etch
	Commercial Au etchant for 1.5 min
	Rinse with DI water for 3 cycles
	Dry by N2
Inspection	

Table A.1 (continued)

	Ti Etch
	10ml HF + 10ml H2O2 + 80ml DI water (very strong etchant)
	Ti etchant for 30s
	Photoresist strip
	Acetone for 30min
	Rinse with DI water for 3 cycles
	Dry by N2
	Inspection
	Dehydration in oven at 90°C for 40min
	2 nd lithography for electroplating step
Mask2	HDMS coating at 500 rpm for 7s + 1000 rpm 30s
	AZ9260 at 500rpm for 7s + 1500 rpm for 30s
	Edge Bead removal
	Wait for 15 min by putting the wafers in horizontal form into the wafer holder
	Prebake at 95°C for 3 min at hotplate
	Swing the wafer in the air for 1 min to release the heat on the wafer
	AZ9260 at 500rpm for 7s + 2000 rpm for 30s
	Edge bead removal
	Wait for 15 min by putting the wafers in horizontal form into the wafer holder
	Prebake at 95°C for 5 min at hotplate
	Wait for 15 min by putting the wafers in horizontal form into the wafer holder
	Hardbake in oven from 40°C to 95°C and wait at 95°C for 50 min.
	Cool down the wafers from 95°C to 70°C in oven
	Rehydration (4 pipettes of DI water in blue box for 4 hours)
	Expose UV for 40s vacuum+hard contact
	Develop photoresist in AZ 826 MIF for 10min (eye control)
	Rinse with DI water for 1.5min + 1.5min
	Dry with N2
	Expose UV for 20s vacuum+hard contact
	Develop photoresist in AZ 826 MIF for 10min (eye control)
	Dry with N2
	Inspection
	Cu electroplating
	100mA at 0.3-0.7 duty cycle for 65min for 26 μm thickness
	Photoresist strip
	Acetone for 120min
Rinse with DI water for 3 cycles	
Dry with N2	

Table A.1 (continued)

	Inspection
	O ₂ plasma for 5 min
	Inspection
	Dehydration in oven at 90°C for 40 min
	3rd lithography for constructing microchannel
Mask3	HDMS coating at 500rpm for 7s +1500 rpm for 30s
	AZ9260 coating at 300rpm for 7s + 1500 rpm for 30s
	Edge bead removal
	Wait for 15 min by putting the wafers in horizontal form into the wafer holder
	Prebake at 95°C for 3 min at hotplate
	Swing the wafer in the air for 1 min to release the heat on the wafer
	AZ9260 coating at 300rpm for 7s + 2000 rpm for 30s
	Edge bead removal
	Wait for 15 min by putting the wafers in horizontal form into the wafer holder
	Hardbake in oven from 40°C to 95°C and wait at 95°C for 50 min.
	Cool down the wafers from 95°C to 70°C in oven
	Rehydration with 4 pipettes of DI water in blue box for 4 hours
	Expose UV for 40s vacuum + hard contact
	Develop PR in AZ 826MIF for 10min
	Rinse with DI water for 1.5 min + 1.5 min
	Dry with N ₂
	Expose UV for 20s vacuum + hard contact
	Develop PR in AZ 826MIF for 10min
	Dry with N ₂
	Inspection
Thickness measurement with DEKTAK profilometer	
40 gr of parylene coating without silane	
	4th lithography for opening
Mask 4	HDMS coating at 500 rpm for 7s + 3000 rpm for 30s
	AZ 9260 coating at 500 rpm for 10s + 750 rpm for 20s
	Edge bead removal
	Wait for 15 min by putting the wafers in horizontal form into the wafer holder
	Prebake at 95°C for 3 min at hotplate
	Swing the wafer in the air for 1 min to release the heat on the wafer
	AZ 9260 coating at 500 rpm for 10s + 750 rpm for 20s

Table A.1 (continued)

	Wait for 15 min by putting the wafers in horizontal form into the wafer holder
	Hardbake in oven from 40°C to 95°C and wait at 95°C for 50 min.
	Cool down the wafers from 95°C to 70°C in oven
	Expose UV for 55s with vacuum+hard contact
	Develop PR in AZ 826 MIF for 30 min
	Rinse with DI water for 1.5 min + 1.5 min
	Dry with N ₂
	Expose UV for 55s with vacuum+hard contact
	Develop remaining PR in AZ 826MIF for 20 min
	Rinse with DI water for 1.5 min + 1.5 min
	Dry with N ₂
	Inspection
	Thickness measurement with DEKTAK profilometer
	Parylene etch with RIE
	In RIE (20 min + 20 min + 20min)
	Inspection
	Dicing
	Strip photoresist by Acetone in glass petri for 2 days
	Placing nanoports to inlet with white and yellow epoxy.

APPENDIX B

MATLAB CODE FOR COUNTING THE NEGATIVE PEAKS

```
clc, clear all, close all
signal = load('Peak.txt');
i=length(signal);

[n,fo,ao,w] = firpmord([1000 1200],[1 0],[0.01 0.1],200000);
b = firpm(n,fo,ao,w);
y1 = filter(b,1,signal);
y2 = filter(b,1,y1);
y3 = filter(b,1,y2);
y4 = filter(b,1,y3);
y5 = filter(b,1,y4);
y6 = filter(b,1,y5);

subplot(221),plot(signal);
subplot(222),plot(y1);axis
subplot(223),plot(y3);axis
subplot(224),
beat_count = 0;

for j = 0.1*10^5:1:1*10^6
if y6(j) < 0.0895 & y6(j) < y6(j-1) & y6(j) < y6(j+1)
    j;
    beat_count = beat_count+1;
end
end

plot(y6);
axis([2*10^5 2.5*10^6 0.086 0.094]);
```